Geology and Geotechnical Report

TELLUS

TELLUS

ATKINS

Preliminary assessment of the salt horizon geomechanics of Chandler salt mine

A report to Douglas Partners Pty Ltd
acting on behalf of Tellus Holdings Ltd

25 March 2016

Notice

This document and its contents have been prepared and are intended solely for Douglas Partners Pty Ltd.'s information, acting on behalf of Tellus Holdings Limited, and use in relation to the preliminary assessment of the salt horizon geomechanics of Chandler salt mine.

Atkins Energy assumes no responsibility to any other party in respect of or arising out of or in connection with this document and/or its contents.

This document has 64 pages including the cover.

Document history

Job number: SN0113126			**Document ref: SN0113126**			
Revision	Purpose description	Originated	Checked	Reviewed	Authorised	Date
Rev P0	First Issue for Comment	EP	DR	CMM	MC	16/02/16
Rev A1	Updated following client comments	EP	DR	CMM	MC	03/03/16
Rev A2	Updated following client comments	EP	DR	CMM	MC	11/03/16
Rev A3	Updated following client comments	EP	DR	CMM	MC	21/03/16
Rev A4	Updated following client comments	EP	DR	CMM	MC	24/03/16
Rev A5	Final report	EP	CMM	CMM	MC	25/03/16

Table of contents

Executive summary

A geomechanical evaluation of the salt horizon of Chandler salt mine, taking into consideration the time-dependent mechanical behaviour of the Chandler Halite formation, was carried out by implementing appropriate numerical investigations. The objective of the geomechanical studies of the planned Chandler mine was achieved by employing engineering judgement in analysing the results of the geomechanical modelling, by making use of established experience and knowledge in utilising appropriate parameters concerning the strength and the constitutive response of the Chandler Halite, and by realistically modelling the geometry, the *in situ* geostatic stresses and the boundary conditions that characterise the planned room and pillar mine layout.

The finite difference method was successfully used for the numerical simulation of the planned Chandler mine in investigating the development of the subsurface stress concentrations and creep response of the Chandler Halite that surrounds the planned room and pillar mine layout. With respect to the geomechanical response of the planned Chandler mine, a significant element is the Jay Creek Limestone strata that overlay the Chandler formation, which have an average thickness of more than 250 m. Provided that no major faults or prevalent systems of significant discontinuities exist, the Jay Creek Limestone will act as an enormous thick plate, with built-in-ends, that is expected to contribute significantly to the stability of the planned excavations.

Examination of the distribution of the principal stresses, for the first 23 years, indicates that the minor principal stress is essentially very close to the compressive regime. Consequently, during the first 23 years following the excavation of the panels, the possibility of developing in the roof of the rooms tensile stresses that may exceed the tensile strength of the Chandler Halite is almost unlikely. However, the excessive creep closure that has been identified in the roof of the rooms next to edge of the panels will, in all probability, result in the development of tensile cracks.

Calculation of the *Strength Factor* against shear failure for the salt pillars has shown that, even at the early life of the mine, the *Strength Factor* values indicate no shear failure. The identified *Strength Factor* values demonstrate that the Chandler Halite of the pillars, when subjected to the stress concentrations caused by the excavations, is able to endure shear stresses over a period of thirty years. Moreover, assessment of the distribution of the minor principal stress and the Von Mises stress above the salt mine provided evidence that the 20 m thickness of salt, which is left between the roof of the rooms and the top of the Chandler Halite, prevents the establishment of a pathway to the biosphere. Essentially, the roof salt above the underground excavations constitutes an adequate barrier that prevents the development of migration paths for potential contaminants (associated with the underground storage operations) towards the non-salt formations.

Practical experience from *in situ* measurements and observations concerning underground openings in salt formations, suggests that the identified order of magnitude of the rates of creep displacements, both along the vertical and horizontal directions, are excessive and they are expected to have a long term negative effect on the serviceability limit state of the underground excavations. The identified rates of room creep convergence are very high, indicating that the roof of the rooms (especially those rooms located near the edges of the panel) may be unstable in the long term.

In summary, the preliminary assessment of the geomechanical conditions of the planned Chandler mine indicates that, although the 15 m wide rib pillars are expected to accept the high stress concentrations while maintaining their long term stability, the 15 m width of the roof span of the rooms is considered to be too large and will potentially result in unacceptable creep convergence of the rooms. It is important of course to take into consideration that the derived preliminary conclusions are based on the use of assumed material parameters for the Chandler Halite which clearly have an effect both on the creep convergence of the rooms and the shear strength of the pillars. Although the assumed material parameters are based on well-established practical experience derived from designing and monitoring underground openings in salt formations, once laboratory test results from the Chandler Halite will be made available, there will be a need to re-evaluate the investigated geomechanical conditions.

Taking into consideration that the 15 m width of the roof span of the rooms is considered to be too large, it is recommended to undertake a series of parametric studies to determine the maximum permissible roof span that will provide the requisite long term stability while satisfying the requirements of the serviceability limit state.

The barrier pillars that form the boundaries of the panels, should be able to withstand all anticipated loading conditions encountered during panel development and also should provide adequate isolation to minimise the structural interaction of adjacent panels. The configuration of the planned barrier pillars, concerning their proposed width, is considered to be insufficient especially since there are plans to reduce their cross-sectional area by driving ventilation tunnels through them. It is recommended to investigate the geomechanical conditions of the central barrier pillar in addition to the other barrier pillars to optimise their required width.

Assessment of the stress distribution around the excavated rooms indicates high stress concentrations limited around the corners of the rooms. The adopted geomechanical model employed rectangular openings and the stress distribution plots are based on square corners. To minimise the effect of the square corners it is recommended to consider using a continuous miner equipped with a rotating drum cutting head system comprising specially designed cutter pick configuration that will allow the rooms to be excavated with rounded angles at the corners of the cut.

The identified stress gradients above the mine should be used as guide to decide the particular depths from which we should select core samples to be used for rock testing. Similarly, in planning the future rock mechanics laboratory test programme, the confining pressures that will be used in the triaxial compression tests and the deviatoric stresses that will be used in the required triaxial creep tests should be determined by considering the identified stress concentrations. As part of the future recommendations, consideration should also be given to investigate the influence of the sequence of the excavation operations on the long term stability of the room and pillar layout, by carrying out a series or parametric geomechanical numerical analyses.

The benefit of the active support, provided by the proposed post-tensioned resin grouted rockbolts, and also by the passive support, exerted both by the packaged and the hydraulically backfilled waste materials, is important since it is expected that these measures will bring under control the development of the identified tensile regime in the roof of the rooms and the shear stresses near the walls of the pillars. Another positive measure that is expected to contribute to the overall stability of the underground excavations is the plan to stow with crushed salt all the main access roads when they are no longer required for use.

1. Introduction

Atkins were commissioned by Douglas Partners Pty Ltd to undertake the geomechanical evaluation of the salt horizon of Chandler salt mine, taking into consideration the time-dependent mechanical behaviour of the Chandler Halite formation, by implementing appropriate numerical investigations. For this reason, we have investigated and assessed the influence of the geometry of the planned mine layout on the geomechanical stability of the salt horizon to allow us to draw the conclusions we have reached in this report.

This report presents the results of the numerical modelling of the planned mine layout, which was undertaken by making use of the following information that was provided by Douglas Partners:

- the geometry of the planned mine layout (i.e. corresponding depth, dimensions and shape of the room and pillar layout);
- the local geology as established from the available technical report by Douglas Partners (2016);
- the results of the analyses concerning the non-soluble material of the Chandler Halite (Terra Search, 2011); and
- the core photographs from the exploratory borehole CH001A (ErcosPlan, 2009).

In addition, use was made of salt mechanics data and results from *in situ* measurements, derived from previous geomechanical studies carried out by Atkins.

The stability assessment of underground excavations in salt formations, involves a number of components that require careful consideration. These include:

- physical and mechanical properties of the geological materials that surround the underground excavations;
- information on the geostatic stress field conditions to which the geological formations are subjected; and
- computational methods for predicting and/or evaluating the geomechanical performance of the underground excavations.

A mine layout in the Chandler Halite formation may be considered unfit for use for underground storage purposes when it reaches the limit state in which it infringes on one of the criteria governing its performance or use. Such limit states are directly associated with the salt excavations' ability or inability:

- to prevent the development of migration paths for potential contaminants (associated with the underground storage operations) towards the non-salt formations, and
- to contain the stored materials,

which typically depends on a number of factors. The significance and influence of these factors may be addressed by comparing the results of the applied geomechanical numerical modelling of the planned mine layout with the appropriate relevant criteria.

Following a holistic approach for the geomechanical analysis of the planned mine layout in the Chandler Halite formation, the implemented numerical modelling employed its site-specific geomechanical characterisation incorporating:

- the proposed depth and geometrical configuration of the planned room and pillar mine layout;
- the geological formations involving the stratigraphy and geology of the Chandler mine location;
- the *in situ* geostatic stress parameters in relation to the respective gradient of the vertical and horizontal components; and
- the physical and mechanical characteristics of the geological materials that surround the underground excavations (including the shear and tensile strength as well as the creep behaviour, in the case of salt)

2. Geological succession

The successful development of an underground excavation is crucially dependent on knowing the geological environment. A good understanding of the stratigraphy and geological structure is therefore essential.

The generalised geological succession that is used in the geomechanical modelling of the planned mine layout was based on the information given in Appendix C of the report by Douglas Partners (2016) from which a description of the identified strata, ranging between 502 m bgl and 825 m bgl, is summarised in Table 2-1. Moreover, concerning the geological formations encountered from 825 m bgl and below, additional information, shown also in Table 2-1, was taken from the report produced by Wakelin-King et al. (1992).

Table 2-1 Stratigraphic column and description of the geological formations in the Chandler mine location from a depth of 502 m bgl

Depth range [m bgl]	Description	Stratigraphic interpretation
502 - 607	SILTSTONE: banded/laminated multi-coloured (brown, green, blue, grey, yellow) siltstone. The initial finely laminated siltstone beds are calcareous- probably calcitic cement. Intermittent fine to medium grained sandstone beds. Becoming weakly to non-calcareous with depth- probably becoming dolomitic as cement is hard and carbonitic in appearance. Interbedded dark red brown clastic siltstone with paler grey/green/blue dolostone/dolomitic siltstone - paler units are harder. Minor bioturbation in places. Dolomite patches, blebs and nodules appear at approximately 572.5 m bgl, narrow veins concordant with bedding also begin. Occasional discordant dolomite veins. From approximately 555 m bgl crystalline dolomite becomes apparent.	Jay Creel Limestone
607-772	SILTSTONE: Interbedded red brown and pale bluish grey units. Red brown is siltstone and pale unit is dolostone. Only occasional multi-coloured laminae- predominantly dm scale and repetitive beds. Common dolomite blotches, veins (discordant) and laminae (concordant), probably 1-5% of core mass. Red brown clastic siltstone grades to very fine grained siltstone in parts. Minor calcareous laminae in parts. Chert nodules appear at 672.5 m bgl. Natural breaks/fractures occur along narrow stylolites in dolostone. Dolostone beds become hard/partially silicified with depth. At approximately 728 m bgl fractured dolostone with chert and dolomite fracture fill. Fairly homogeneous red brown siltstone 720.5 m bgl – 725 m bgl.	
772-780	SILTY CLAYSTONE: Dark grey to medium grey finely laminated claystone very similar in texture and colour to 720 m bgl -726 m bgl interval in borehole CH003. Anhydrite blotches to 20 mm diameter abundant in final 1.5 m. Secondary gypsum growth post drilling.	Chandler Formation
780-825	SILSTONE: red brown to dark brown laminated siltstone grading to silty claystone; micaceous in part. Interbedded with pale grey dolostone- homogeneous and finely bedded In parts- some coarse anhydrite crystal clusters/aggregates visible in dolostone 100 mm chert at 799.8 m bgl - fractured; also a large nodule at 807.4 m bgl. Appearance of vughy fractures in dolostone at 807.4 m bgl, halite appears as fracture fill at 811.5 m bgl. Vughy red siltstone with halite matrix In parts 818 m bgl - 825.3 m bgl.	
825-1,090	HALITE: The target halite horizon is between the depths of 825 m bgl and 860 m bgl. The halite is light pink, coarsely crystalline with interbedded reddish, clayey siltstone and scattered quartz, potassium feldspar and some green biotite grains. Some of the quartz grains have reddish iron coatings. Very fine anhydrite and carbonate crystals occur throughout the salt. Mudstone, siltstone and dolomite are interbedded with the salt units. The mudstone is haematitic. The siltstone is halitic and anhydritic with angular to rounded coarse grained ferruginous clastics. The dolomite is ferruginous, cryptocrystalline and slightly calcareous.	
1,090 – 1,540 estimated	SILTSTONE, SANDSTONE: The Winnall Beds are a monotonous sequence of greenish-grey to reddish brown shale and siltstone interlaminated with very thin sandstone streaks. Rare dolomite bands occur near the contact with the Bitter Springs Formation. Green biotite and muscovite are aligned parallel to bedding planes. Grains are cemented by chlorite, limonite, haematite, and pyrite. Very fine dolomite crystals occur throughout the Formation. Sandstone is present in fine laminations grading to shale and siltstone. The sandstone is composed of fine to very fine grained, angular, well sorted quartz, some potassium feldspar, very rare albite, igneous and sericitised rock grains and muscovite. Authigenic or autochthonous glauconite occurs in grains, pellets, in irregular aggregates moulded around quartz particles and as staining in the matrix. The glauconite is associated with phosphatic grains. Heavy minerals form the accessories. The cement is chlorite, as well as some kaolinite, sericite, intergranular quartz and a very small amount of dolomite.	Winnall Beds

3. The geostatic stress field

The *in situ* geostatic stresses in the earth's crust have been widely recognised as a basic parameter necessary in the engineering design of underground structures. More specifically, the analysis of the geomechanical stability of excavations in salt beds is greatly dependent upon the magnitudes of these primitive, otherwise known as geostatic stresses, naturally existing in the underground formations before the caverns were leached. In general, the larger these geostatic stresses are, the larger are the induced stress concentrations to which the geological materials are subjected.

The geostatic state of stress within an undisturbed and continuous geological formation is expected to depend on two stress fields:

- the lithostatic or gravitational stress field, which may be defined in terms of its principal stress components σ_v, σ_H and σ_h, acting approximately along the vertical and the two horizontal directions respectively (see sketch below), and
- the stress field related to the possible presence of tectonic forces or locked-in stresses that may act in any direction.

Stresses due to tectonic loading are superimposed on the lithostatic stress field, and will lead in general to a change in magnitude and direction of the principal stresses. In areas which are tectonically inactive and in the absence of any specific knowledge on the magnitude and direction of the tectonic stresses, which is usually the case, it is acceptable to assume for design purposes that the geostatic stress field is simply lithostatic.

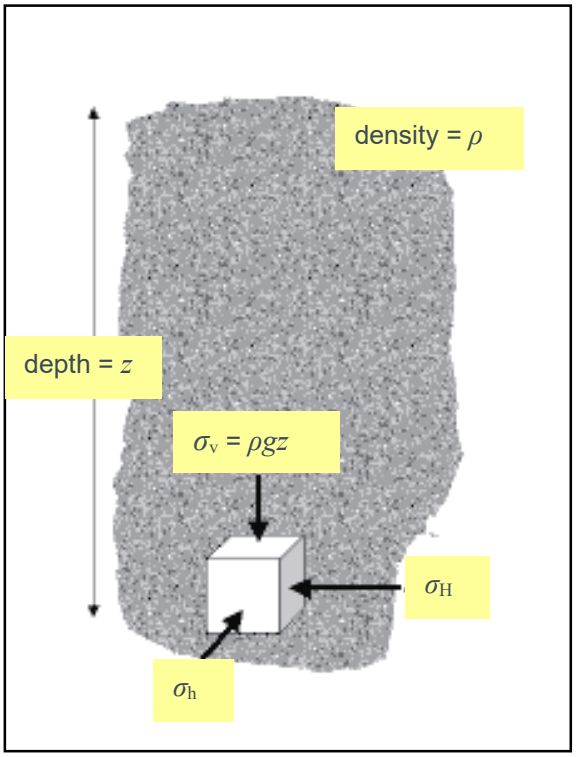

The vertical stress component σ_v resulting from the weight of the superincumbent strata increases linearly with vertical depth. If there are n layers of geological formations overlying an underground excavation, each of thickness t_i and density ρ_i then the compressive (i.e. negative) vertical stress may be estimated using the following relationship:

$$\sigma_v = -g\sum_{i=1}^{n}\rho_i t_i$$

Equation 1

where g = 9.80665 m/s^2 is the standard gravitational acceleration.

Measurements of vertical stress around the world (as published by Brown & Hoek, 1978) confirm that this relationship is valid although, as illustrated in Figure 3-1, there is a significant amount of scatter in the measurements.

The geostatic vertical stress gradient of 0.027 MPa/m, shown in Figure 3-1, corresponds to an average overburden density of 2,750 kg/m^3. Nevertheless, a value of 0.025 MPa/m has been used in the geomechanical modelling of the Chandler salt mine, as recommended by Douglas Partners.

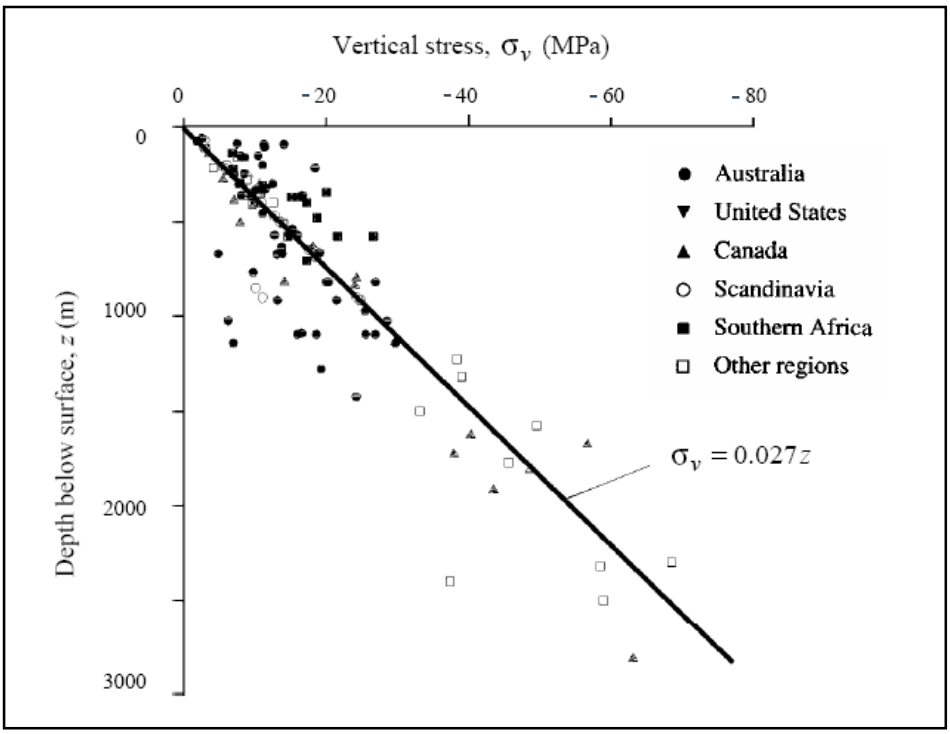

Figure 3-1 Vertical geostatic stress measurements from various projects around the world (after Brown & Hoek, 1978)

Moreover, an estimate of the geostatic stress components σ_H and σ_h, from rock strength and tele-viewer breakout, as identified in the exploratory borehole CH001A by Douglas Partners (2016), suggests that the horizontal geostatic stresses may be calculated (in MPa) by the following relationships:

$$\sigma_h = 0.75\ \sigma_H \qquad \textbf{Equation 2}$$

$$\sigma_H = 1.5\ \sigma_v + 0.5 \qquad \textbf{Equation 3}$$

On the other hand, the assumption that the *in situ* stress state in salt is isotropic (i.e. $\sigma_{h\,(max)} = \sigma_{h\,(min)} = \sigma_v$) is generally accepted since it is well established that salt is a geological material characterised by a time dependent deformational response. Results from more than 200 laboratory creep experiments (Hunsche, 1981), using salt samples taken from a number of localities, confirmed that the steady state creep strain ($\dot{\varepsilon}_S$) is related to the differential stress ($\sigma_1 - \sigma_3$) by the following Arrhenius' relationship:

$$\dot{\varepsilon}_S = A \exp\left(-\frac{Q}{RT}\right)(\sigma_1 - \sigma_3)^n \qquad \textbf{Equation 4}$$

Where σ_1 and σ_3 are the major and minor effective principal stresses (expressed in MPa), A is creep constant (expressed in $MPa^{-n}\ d^{-1}$), Q is the activation energy (expressed in cal/mol), R = 1.987 cal/(mol K) is the universal gas constant and n is a dimensionless stress exponent.

Equation 4 indicates that the salt will have a non-zero strain rate as long as $\sigma_1 \neq \sigma_3$. Thus, over long times, especially geological times, creep will continue until $\sigma_1 = \sigma_3$ (i.e. the *in situ* stress is isotropic). This effect, that long-term creep has in removing any differences in the horizontal and vertical stress components, has been confirmed by *in situ* investigations (Arnold et al., 1975). For this reason, in the Chandler Halite formation that ranges between 825 m bgl and 1,090 m bgl the geostatic stress have been modelled to be isotropic, while in the non-salt formations Equations 2 and 3 are considered to be valid.

4. Modelling of the geological materials

4.1. The Drucker-Prager plasticity model

The Drucker-Prager model (Drucker & Prager, 1952) is used for geological materials that yield when subjected to shear loading and the corresponding shear failure envelope is expressed by the following relationship:

$$f^s = \sqrt{J_2} + \frac{q_\varphi}{3} I_1 - k_\varphi \qquad \textbf{Equation 5}$$

while the tensile failure is given by the following tension yield function:

$$f^s = \sigma_t - \sigma_3 \qquad \textbf{Equation 6}$$

where σ_t is the tensile strength.

Examination of Equation 5 indicates that that the yield stress depends on the two stress invariants:

- the first invariant (I_1) of the Cauchy stress tensor equal to:

$$I_1 = \sigma_1 + \sigma_2 + \sigma_3 \qquad \textbf{Equation 7}$$

and

- the second invariant (J_2) of the deviatoric stress tensor equal to

$$J_2 = \frac{1}{6}\left[(\sigma_1 - \sigma_2)^2 + (\sigma_1 - \sigma_3)^2 + (\sigma_2 - \sigma_3)^2\right] \qquad \textbf{Equation 8}$$

where: σ_1, σ_2 and σ_3 are the major, intermediate and minor principal stresses respectively and where q_φ and k_φ are constant material properties. The parameter q_φ corresponds to ⅓ of the slope of the Drucker-Prager failure envelope and the parameter k_φ is the intercept of the Drucker-Prager failure envelope with the $\sqrt{J_2}$ axis.

The Drucker-Prager model belongs to the family of the plastic models which potentially involve some degree of permanent, path-dependent deformation (failure): a consequence of the nonlinearity of the stress-strain relation that governs its constitutive response. The model is characterised by its yield function, hardening/softening functions and flow rule. The yield function defines the stress combination for which plastic flow takes place and is represented by a combination of limiting surfaces in a generalised stress space with points below or on the surface being characterised by an incremental elastic or plastic behaviour, respectively. The adopted plastic flow formulation rests on basic assumptions from plasticity theory that the total strain increment may be decomposed into elastic and plastic parts, with only the elastic part contributing to the stress increment by means of an elastic law. In addition, both plastic and elastic strain increments are taken to be coaxial with the current principal axes of the stresses (this is only valid if elastic strains are small compared to plastic strains during plastic flow). The flow rule specifies the direction of the plastic strain increment vector as that normal to the potential surface - it is called associated if the potential and yield functions coincide, and non-associated otherwise. For the Drucker-Prager model a shear yield function and a non-associated shear flow rule are used. In addition, the failure envelope is characterised by a tensile yield function with associated flow rule.

In the implemented numerical analysis the out-of-plane stress is taken into consideration in the formulation that is expressed in three-dimensional terms. In the numerical implementation of the model, an elastic trial (or "elastic guess") for the stress increment is first computed from the total strain increment using the incremental form of Hooke's law. The corresponding stresses are then evaluated. If they violate the yield criterion (i.e., the stress point representation lies above the yield function in the generalised stress space), plastic deformations take place. In this case, only the elastic part of the strain increment can contribute to the stress increment; the latter is corrected by using the plastic flow rule to ensure that the stresses lie on the composite yield function.

4.2. The Hoek-Brown failure criterion

Reliable estimates of the strength and deformation characteristics of rock masses are required for almost any form of analysis used for the design of underground excavations. Hoek & Brown (1980a, 1980b) proposed a method for obtaining estimates of the strength of rock masses, based upon an assessment of the interlocking

of rock blocks and the condition of the surfaces between these blocks. This method was modified over the years in order to meet the needs of users who were applying it to problems that were not considered when the original criterion was developed (Hoek 1983, Hoek & Brown 1988).

The Hoek-Brown failure criterion is an empirical relation that characterises the stress conditions that lead to failure in intact rock and rock masses and has been used very successfully in design approaches that use limit equilibrium solutions. The "generalised" Hoek-Brown criterion (Hoek & Brown, 1980a and 1998) that has been used in modelling the shear strength of the non-salt geological materials encountered in the Chandler mine location - adopting the convention of positive compressive stress - is:

$$\sigma_1 = \sigma_3 + \sigma_{ci}\left\{ m_b \frac{\sigma_3}{\sigma_{ci}} + s \right\}^a \qquad \textbf{Equation 9}$$

where σ_1 and σ_3 are the major and minor effective principal stresses at failure, m_b is the value of the Hoek-Brown constant for the rock mass, s and a are constants which depend upon the rock mass characteristics and can be related to the Geological Strength Index and rock damage (Hoek et al., 2002), and σ_{ci} is the uniaxial compressive strength of the intact rock.

Note that the criterion shown in Equation 9, does not depend on the intermediate principal stress, σ_2, implying that the failure envelope is not isotropic.

4.3. The concept of the *Strength Factor* for the Chandler Halite

To evaluate whether or not salt fracturing is likely to occur around the investigated underground excavations, the available strength of the modelled Chandler Halite must be compared to the induced stresses on a point-by-point basis around the openings. In general, the ratio of available strength to induced stress is referred to as the 'factor of safety'.

The traditional method of calculating the *Factor of Safety* has been to express the ratio of the peak strength (i.e. maximum permitted value of the major principal stress, σ_1) to the calculated value of σ_1, at a point as determined from the model. The maximum permitted value of σ_1 is calculated from the employed strength criterion, based on the calculated value of the confining stress, σ_3, at the same point.

The *Strength Factor*, on the other hand, is a ratio which expresses available strength and induced stress in terms of deviatoric stress. That is, the allowable maximum shear stress divided by existing shear stress at a point.

As is evident from the example shown in Figure 4-1, in assessing the loading of a pillar there is a subtle difference between the calculated *Factor of Safety* and *Strength Factor*. Further deliberations on the difference between factor of safety and *Strength Factor* may be found in the publication by McCreath & Diederichs (1994).

To assess the geomechanical stability of the investigated room and pillar layout, use was made of the *Strength Factors* corresponding to the Drucker-Prager failure criterion for shear and tensile strength as specified respectively by Equations 5 and 6. In particular, if the minor principal stress σ_3 is greater or equal than the positive stress, that corresponds to the tensile strength of the geological material, (i.e. if $\sigma_3 \geq \sigma_t$) then the *Strength Factor* is set equal to -1 indicating that tensile failure has occurred. If on the other hand $\sigma_3 < \sigma_t$ then the *Strength Factor* is calculated by dividing the shear strength of the geological material by the induced shear stress expressed in terms of $\sqrt{J_2}$, i.e.:

$$Strength\ Factor = \frac{k_\varphi + q_\varphi \frac{I_1}{3}}{\sqrt{J_2}} \qquad \textbf{Equation 10}$$

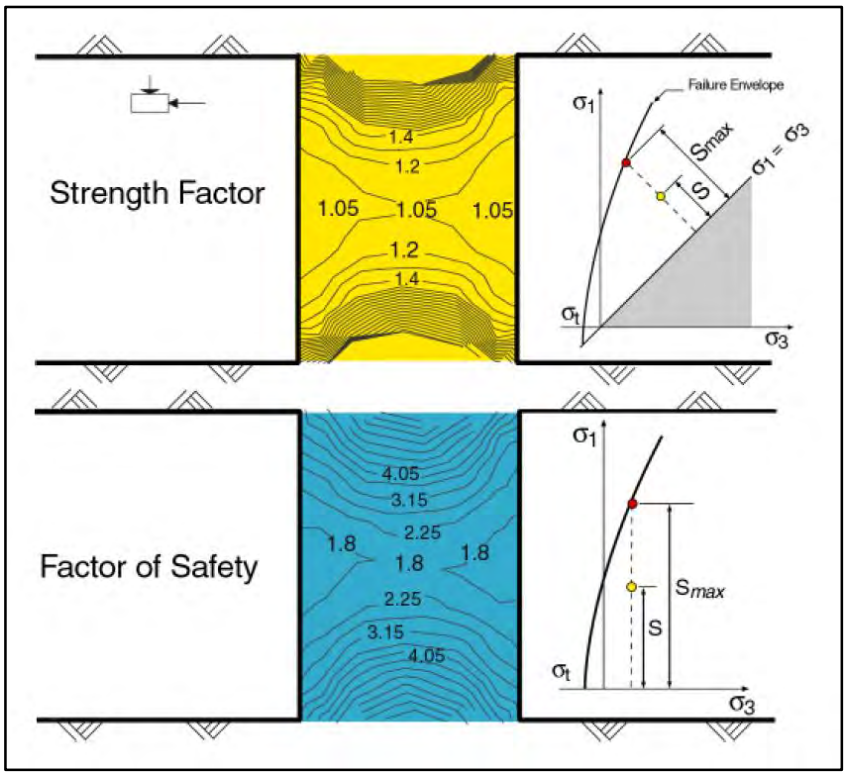

Figure 4-1 ***Strength Factor*** **vs** ***Factor of Safety*** **(after Kaiser et al., 2002)**

If the *Strength Factor* is greater than 1, this indicates that the salt's shear strength is greater than the induced shear stress and as such no shear failure occurs. However, if 0 < *Strength Factor* ≤ 1, this indicates that the shear stress in the Chandler Halite exceeds the salt's shear strength signifying that shear failure occurs. Since all three principal stresses (σ_1, σ_2 and σ_3) have an influence on the *Strength Factor*, the calculated *Strength Factor* can be considered three dimensional.

4.4. The WIPP-creep viscoplastic model

Appraisal of the safety of underground structures in rock salt formations requires a constitutive law that accurately models the time-dependent mechanical behaviour of rock salt. Rock salt is characterised by a distinctive creep response which is manifested by the fact that it is capable of deforming with time even if the applied stress remains constant.

Creep typically occurs in three stages: primary, or Stage I; secondary, or Stage II and tertiary, or Stage III (see Figure 4-2). At first, as the load is applied the initial elastic strain occurs (virtually instantaneously) but as time passes, under constant stress, the rate of strain reduces. Initially, the strain rate is relatively high but it slows with increasing strain and this period of decelerating strain-rate is identified as primary creep. Resistance to creep increases as the strain rate eventually reaches a minimum and becomes near constant when the secondary creep phase is reached. The rate of creep during the secondary creep phase becomes roughly steady and for this reason this stage is often referred to as steady state creep.

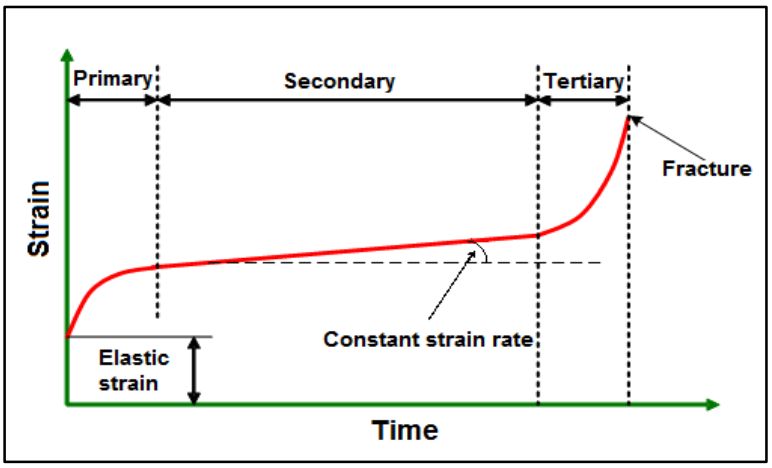

Figure 4-2 The idealised strain-time curve for a creep test

At the end of Stage II, as the strain rate exponentially increases with strain, the creep rate begins to accelerate resulting in the initiation of a creep fracture process. This final stage of accelerating deformation that leads to a rapid material failure is called Stage III, or tertiary creep.

The creep law that describes the behaviour of rock salt should be valid for wide ranges of stress states, stress magnitude and time, and also for complex stress histories and temperature histories. For this reason the time-dependent behaviour of rock salt in this report has been modelled by combining the non-linear visco-elastic WIPP model (Herrmann et al., 1980a, 1980b) with the Drucker-Prager plasticity model. Of the available plasticity models the Drucker-Prager model is the most compatible with the WIPP-reference creep law, because both models are formulated in terms of the second invariant of the deviatoric stress tensor (J_2).

The WIPP creep law is based in the exponential function of Arrhenius according to the following mathematical configuration:

$$\varepsilon = A\sigma^n \exp\left(-\frac{Q}{RT}\right) t + \varepsilon_a (1 - exp[-B\dot{\varepsilon}_{ss} t]) \quad \text{for} \quad \dot{\varepsilon}_{ss} \geq \dot{\varepsilon}^*_{ss} \qquad \textbf{Equation 11}$$

$$\varepsilon = A\sigma^n \exp\left(-\frac{Q}{RT}\right) t + \varepsilon_a \left(\dot{\varepsilon}_{ss} / \dot{\varepsilon}^*_{ss}\right)\left(1 - exp[-B\dot{\varepsilon}^*_{ss} t]\right) \quad \text{for} \quad \dot{\varepsilon}_{ss} \leq \dot{\varepsilon}^*_{ss} \qquad \textbf{Equation 12}$$

where:

ε = creep strain expressed in [m/m],

t = time expressed in [d]

T = temperature expressed in [K],

σ = applied stress (stress difference) expressed in [MPa],

Q = activation energy for rock salt expressed in [cal/mol],

R = 1.987 cal/(mol K) is the universal gas constant,

n = dimensionless stress exponent,

A = creep constant expressed in [MPa^{-n} d^{-1}],

B = dimensionless empirical material parameter relating the creep rate parameters to the steady-state creep rate,

$\dot{\varepsilon}^*_{ss}$ = the critical steady-state creep rate expressed in [(m/m) d^{-1}], and

ε_α = the asymptotic transient strain parameter expressed in [m/m].

In Equations 11 and 12, which express mathematically the WIPP creep law, the first part i.e. the expression:

$$\varepsilon = A\sigma^n \exp\left(-\frac{Q}{RT}\right)t$$

represents the secondary creep, while the remaining terms correspond to the primary creep.

5. Properties of the geological materials

5.1. Non-salt materials

By employing the available descriptive categories of rock mass structure and the respective discontinuities surface conditions, it was possible to estimate the Geological Strength Index (GSI) in accordance with the chart (shown in Figure 5-1), produced by Hoek et al. (2013), by assigning to the non-salt formations respective characteristic GSI ranges. GSI is a system of rock mass characterisation that was developed in engineering rock mechanics to meet the need for reliable input data related to rock mass properties required as input for numerical analysis for designing rocks structures. Different colours have been used in Figure 5-1 to define the GSI range for the:

- Jay Creek Limestone upper formation (502 m bgl – 607 m bgl);
- Jay Creek Limestone lower formation (607 m bgl – 772 m bgl);
- Chandler Silty Claystone and Siltstone formation (772 m bgl – 825 m bgl); and
- Winnall Beds (1,090 m bgl – 1,540 m bgl estimated)

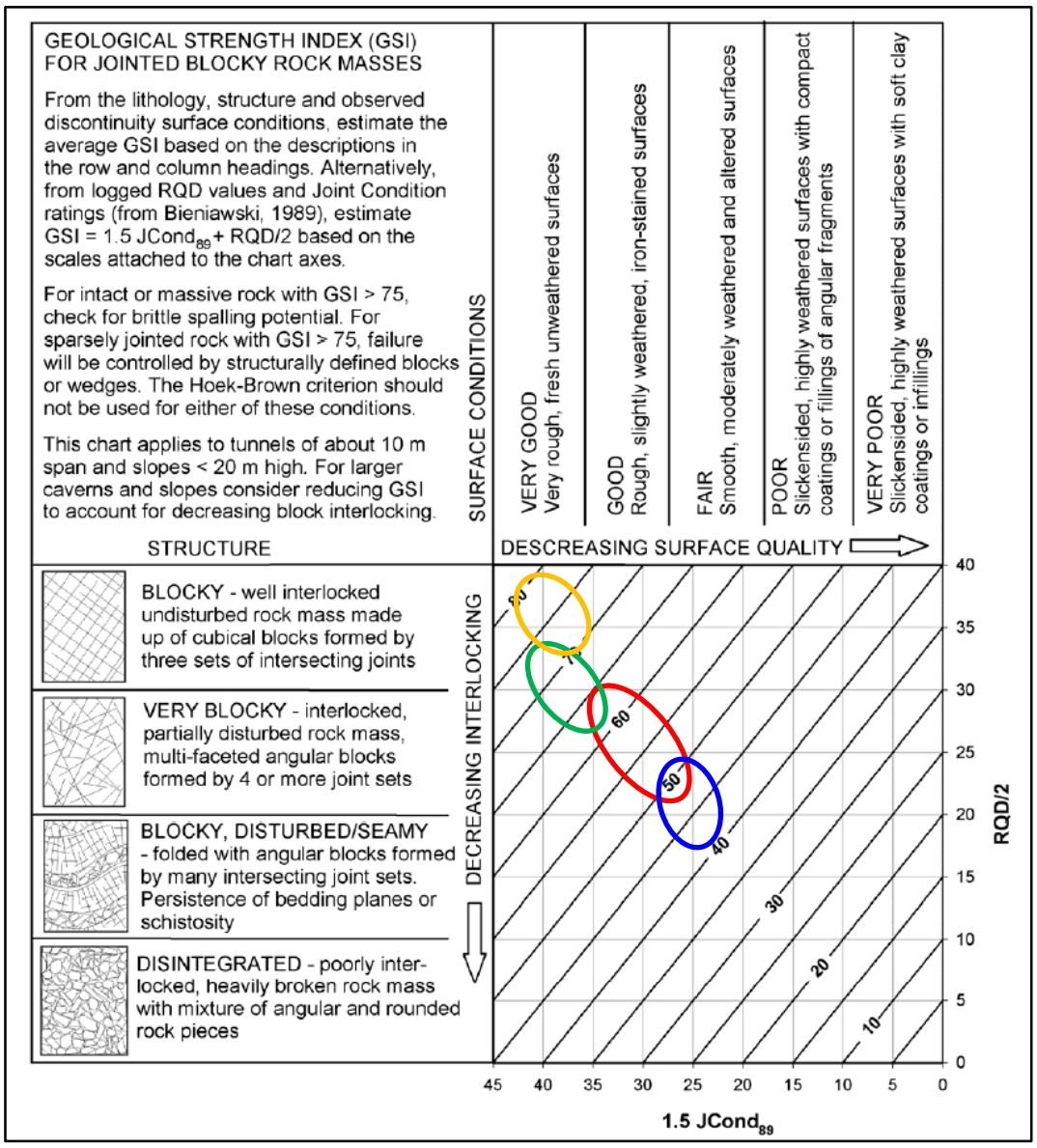

Figure 5-1 Quantification of GSI by Joint Condition and RQD (after Hoek et al., 2013) for Winnall Beds, Jay Creek Limestone (lower layer), Jay Creek Limestone (upper layer), and Chandler Silty Claystone and Siltstone.

By making use of the rock materials databases incorporated in the programs RocLab (Rocscience, 2004a) and RocSupport (Rocscience, 2004b), besides the identified GSI ranges, the following assumed material properties were assigned to the non-salt formations:

Jay Creek Limestone upper formation

Density: 2.56 Mg/m^3, Uniaxial compressive strength of the intact rock: 52 MPa, Hoek-Brown material constant m_i: 14, Hoek-Brown reduced material constant m_b: 3.36, Hoek-Brown rock mass constant s: 0.0117, Hoek-Brown rock mass constant a: 0.503, Hoek-Brown upper limit of confining stress over which the material no longer dilates σ_3^{cv}: 16.5 MPa, Young's modulus: 33.3 GPa, Poisson's ratio: 0.15.

Jay Creek Limestone lower formation

Density: 2.62 Mg/m^3, Uniaxial compressive strength of the intact rock: 65 MPa, Hoek-Brown material constant m_i: 16, Hoek-Brown reduced material constant m_b: 5.48, Hoek-Brown rock mass constant s: 0.0357, Hoek-Brown rock mass constant a: 0.501, Hoek-Brown upper limit of confining stress over which the material no longer dilates σ_3^{cv}: 27.5 MPa, Young's modulus: 48 GPa, Poisson's ratio: 0.16.

Chandler Silty Claystone and Siltstone formation

Density: 2.59 Mg/m^3, Uniaxial compressive strength of the intact rock: 58 MPa, Hoek-Brown material constant m_i: 16, Hoek-Brown reduced material constant m_b: 5.48, Hoek-Brown rock mass constant s: 0.0067, Hoek-Brown rock mass constant a: 0.504, Hoek-Brown upper limit of confining stress over which the material no longer dilates σ_3^{cv}: 17 MPa, Young's modulus: 42 GPa, Poisson's ratio: 0.17.

Winnall Beds

Density: 2.71 Mg/m^3, Uniaxial compressive strength of the intact rock: 70 MPa, Hoek-Brown material constant m_i: 17, Hoek-Brown reduced material constant m_b: 8.32, Hoek-Brown rock mass constant s: 0.1084, Hoek-Brown rock mass constant a: 0.501, Hoek-Brown upper limit of confining stress over which the material no longer dilates σ_3^{cv}: 39.6 MPa, Young's modulus: 86 GPa, Poisson's ratio: 0.18.

5.2. Chandler Halite

The derivation of the assumed material parameters for the Chandler Halite was based on our well-established practical experience in the testing and characterisation of salt formations and the identified average percentage of the non-soluble material as well as the inspection of the core photographs from the exploratory borehole CH001A.

The Chandler Halite was modelled as a WIPP-creep visco-plastic material whose plastic constitutive response conforms to the Drucker-Prager elasto-plastic model. The corresponding physical and mechanical properties that refer to the time-independent mechanical response of the halite were taken to be:

- Density: ρ = 2.37 Mg/m^3
- Young's modulus: E = 33,000 MPa
- Poisson's ratio: ν = 0.225
- Uniaxial tensile strength: σ_t = 1.83 MPa
- Drucker-Prager constants: q_φ = 0.116, k_φ = 15.38 MPa and q_ψ = 0.001

The non-linear visco-elastic characteristics of the halite conformed to the WIPP creep law and the corresponding mechanical properties that refer to the time-dependent mechanical response of the Chandler halite were taken to be:

- Activation energy: Q = 14,070 cal/mol

- Universal gas constant: R = 1.987 cal/(mol K)
- Dimensionless stress exponent: n = 2.71
- Creep constant: A = 256.8 MPa^{-n} d^{-1}
- Dimensionless empirical material parameter relating the creep rate parameters to the steady-state creep rate: B = 569.8
- Critical steady-state creep rate: $\dot{\varepsilon}_{ss}^{*}$ = 1.4×10^{-5} (m/m) d^{-1}
- Asymptotic transient strain parameter: ε_{α} = 0.067 m/m
- Temperature at depth of salt horizon: T = 27°C

6. Geomechanical numerical analysis

6.1. Introduction

In the design of underground excavations in salt formations, numerical tools such as the finite element and finite difference techniques play an increasingly important role. However, in order to successfully employ geomechanical numerical modelling for such a purpose, simulation approaches must fulfil strong requirements. An essential demand is that the geomechanical analyses are efficient and lead to accurate and reliable results. This in turn will depend upon the mathematical model of the physical structure of the salt caverns under investigation, which should be undertaken:

- using appropriate numerical tools;
- adopting realistic material properties;
- applying rational assumptions about the caverns' loading conditions; and
- specifying suitable boundary conditions.

Before commencing the stability analysis of the planned salt mine, it is necessary to develop a meaningful geomechanical ground model and to identify which constitutive law and which failure criteria best match the prevailing geological conditions. This issue has been addressed in Section 4 of this report where it was specified that the plastic behaviour of the modelled geological materials is best simulated by the Hoek-Brown criterion with the exception of the Chandler Halite which was modelled by combining the non-linear viscoelastic WIPP model with the Drucker-Prager plasticity model. Moreover, prior to any geomechanical numerical modelling of room and pillar layouts, it is useful to make a cursory evaluation of the loading conditions that are expected to develop in the pillars by making use of appropriate pillar strength equations. Such a pillar-design equation was used as a basic tool for the calculation of the average stresses in the investigated salt pillars and the resulting findings are presented in Appendix E.

This section provides a description of the finite difference analysis that was employed to investigate the geomechanical stability and creep convergence of the room and pillar mine layout over a period of thirty years.

The computer aided numerical technique, employed to model the geomechanical response of the geologic materials, was the finite difference method and the particular code used was the Fast Lagrangian Analysis of Continua (*FLAC*) developed by Itasca Consulting Group, Inc. *FLAC* is the most well-known stress analysis computer code for engineering problems that employs the finite difference technique, and is based upon a 'Lagrangian' calculation scheme which is well suited for modelling large distortions, primarily encountered in geomechanical applications in salt formations. The finite difference method is one of the oldest numerical techniques used for the solution of sets of differential equations, given initial values and/or boundary values and allows the implementation of complicated loading paths and highly non-linear constitutive behaviour without requiring the complex iterative procedure of a standard implicit code. The finite difference method can be used to discretise both time and space; it provides easy error estimation techniques and is particularly suitable for large, non-linear problems which may involve creep deformation or progressive failure. The ability of *FLAC* to employ successfully the WIPP creep model (Munson, 1997) in the modelling of Chandler Halite was verified with known close form solution (Passaris & Horseman, 1982) for an externally pressurised cylindrical cavity.

6.2. System configuration for analysis

In order to set up the finite difference model for the geomechanical numerical simulation of the investigated room and pillar mine layout, three fundamental components were specified:

- the constitutive behaviour, the strength characteristics and the physical properties of the geological materials,
- a model grid, and
- the boundary and initial conditions.

The constitutive behaviour and the associated material properties dictate the type of reaction the model will have upon the imposed disturbances such as the deformational response due to the excavation of the rooms. The grid defines the geometry of the problem and the boundary and the initial conditions define the *in situ* state (i.e. the condition before a change or disturbance in problem state was introduced).

During the implementation of the finite difference code, the modelled structure of the virgin ground needs to be pre-stressed in conformance with the *in situ* geostatic stress field before an alteration can be introduced in the model by the excavation of the rooms.

The applied geostatic stresses may be derived employing the relationships specified in Section 3 of this report, by which way the vertical geostatic component is a function of the body forces that correspond to the weight of the geological material surrounding each grid-point. If no initial stresses are present, the forces will cause the material to move (during stepping) in the direction of the forces until equal and opposite forces are generated by zone stresses. Given the appropriate boundary conditions (e.g., fixed bottom, roller side boundaries), the model will, in fact, generate extrinsically its own gravitational stresses that are compatible with the applied gravity. However, this process is inefficient, and the pre-stressing of the modelled ground has been incorporated intrinsically by using the INITIAL command of *FLAC* that sets all stresses to the given values. When employing this approach it is possible that the pre-stressing of the ground could lead to unrealistic stress profiles caused by the stress redistribution that may take place as a result of the large deformations that could occur. For this reason, during the pre-stressing of the ground model, the mechanical parameters of the geological materials were artificially increased to prevent any excessive deformations while still embodying the applied geostatic stresses. Following the pre-stressing of the ground and before any modelling actions are taking place, the material parameters were reinstated to their original values.

The distribution of the geostatic stresses for the modelled mine, following the pre-stressing phase, are shown in Figures 6-1 and 6-2 for the vertical (σ_{yy}) and horizontal (σ_{xx}) geostatic stress components respectively.

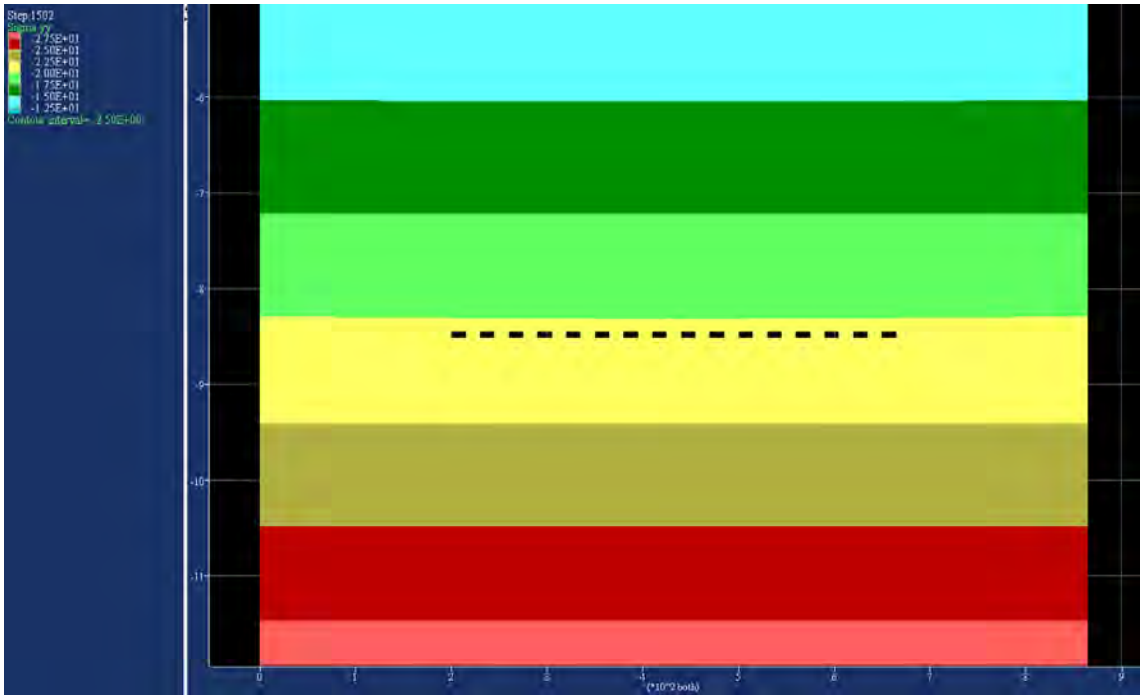

Figure 6-1 Distribution of the vertical geostatic stress component σ_{yy}, resulting from the pre-stressing of the ground model

The vertical geostatic stress (σ_{yy}) distribution, shown in Figure 6-1, reflects a linear gradient with depth. However, the linearity of the horizontal geostatic stress (σ_{xx}), shown in Figure 6-2, is disrupted at the location of the Chandler Halite (which ranges between 825 m bgl and 1,090 m bgl) where the stress regime has been modelled by assuming a hydrostatic configuration (in accordance with Section 3 of this report). This is made clear in Figure 6-3, where the profile of σ_{xx}, along the vertical direction, is plotted against depth.

It is important to clarify here that, during the numerical analysis that was carried out for the preliminary assessment of the salt horizon geomechanics, the excavation of the rooms was modelled by instantaneously by creating all the rooms at the same time. Clearly, this modelling process will result in a significant overestimate of the stress concentration during the early part of the time-dependent analysis and this need to

be considered in interpreting the numerical results. Future geomechanical modelling should investigate the influence of the sequence of the excavation operations on the long term stability of the room and pillar layout, by carrying out a series or parametric numerical analyses.

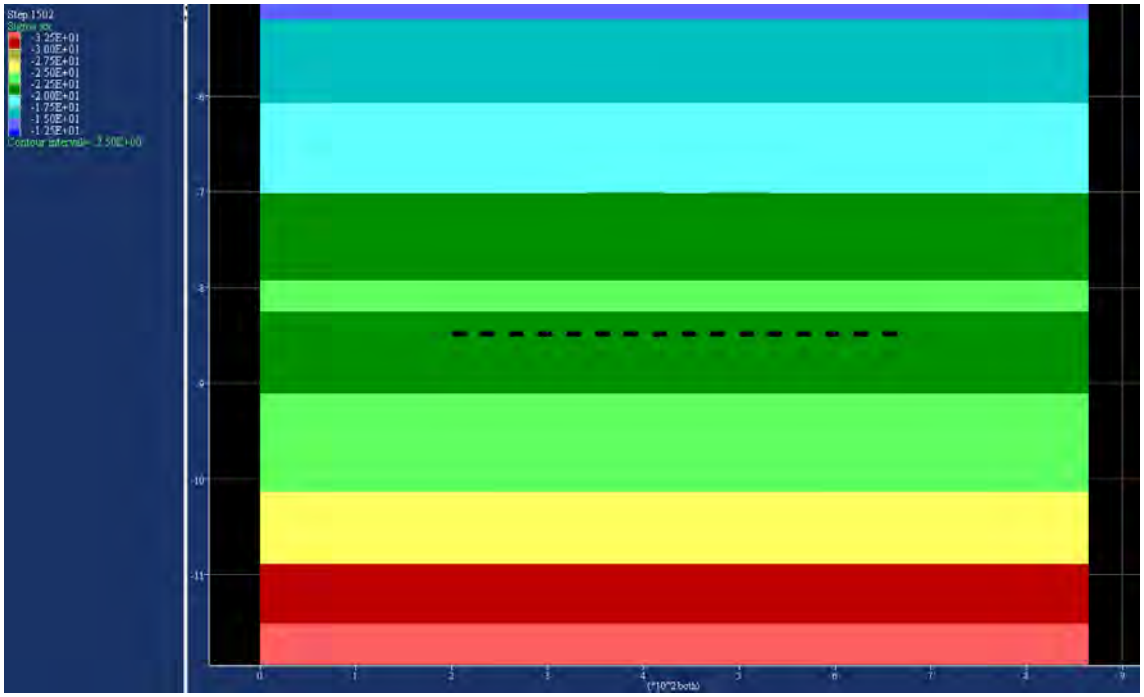

Figure 6-2 Distribution of the horizontal geostatic stress component σ_{xx}, resulting from the pre-stressing of the ground model

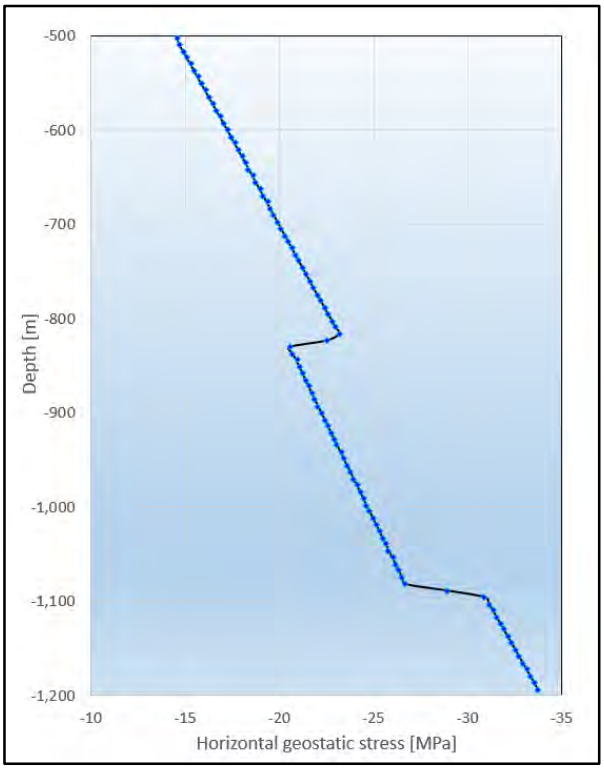

Figure 6-3 Profile of the horizontal geostatic stress σ_{xx} vs depth, along the vertical direction, resulting from the pre-stressing of the ground model

In assessing the deformational response of the modelled underground excavations to the geostatic pre-stressing, it is necessary to recognise the development of the displacements caused only by the excavation of the rooms and to distinguish them from the displacements that resulted from the previously applied gravitational pre-stressing. For this reason, the horizontal and vertical displacement components are zeroed before the creation of the underground excavations is modelled. In this way only the deformational response caused by the excavations is recorded. This technique does not affect the calculations since the finite difference modelling of *FLAC* does not require displacements in the calculation sequence. They are kept simply as a convenience to the user.

The geometrical details of the room and pillar layout were derived from Drawing 4 of Appendix B of the technical report by Douglas Partners (2016), which is reproduced accordingly in Appendix D of this report with appropriate “cloud mark-up” annotations. The planned room and pillar mine layout involves a number of panels (separated by barrier pillars) that comprise 16 rooms, each with a length of 240 m, which alternate with rib pillars (i.e. pillars whose length is large compared with their cross-sectional dimensions). Both the rooms and the pillars have a height of 6 m and a width of 15 m. The width of the ordinary barrier pillars is 45 m, while the central barrier pillar (which is aligned with the bottom of the shaft) is characterised by a width of 95 m.

Taking into consideration that the dimension of the investigated mine layout in one direction is very large in comparison with the respective dimensions in the other two directions, the geomechanical modelling of the pillar layout was realised by employing a two dimensional plane strain analysis of a vertical transverse cross-section (Obert and Duvall, 1967). Since one of the tasks of the geomechanical analysis was to investigate the structural adequacy of the planned barrier pillars, the modelled pillars were purposely configured by employing a width larger than 45 m to help in the identification of the extent of the penetration of the high stress concentrations caused by the underground excavations.

6.3. Results of the geomechanical numerical analysis

The potential development of tensile stresses at the roof of the excavated rooms is typically assessed by evaluating the distribution of the minor principal stress σ_3, while the shear stresses that are expected to develop in the pillars are investigated by considering the Von Mises stress components. The likelihood of shear failure, as a consequence of the potential occurrence of high compressive stresses, cannot be evaluated by simply considering the individual values of σ_1 and σ_3. Instead, the shear stress intensity is typically assessed by employing the Von Mises stress component defined by the following expression:

$$\sigma_{vm} = \sqrt{3J_2} \qquad \textbf{Equation 13}$$

where J_2 is the second invariant of the deviatoric stress tensor specified in Equation 8.

The interpretation of the numerical modelling results is best accomplished by presenting the analysis output graphically in the form of a series of relevant contour plots. The contour plots comprise the major, intermediate and minor principal stress components σ_1, σ_2 and σ_3 as well as the Von Mises stress component. In addition, graphs are presented of the time-dependent development over a span of thirty years for:

- the average Von Mises stress of the pillars,
- the vertical displacements of the roof and the floor of the rooms,
- the horizontal displacements of the walls of the rooms,
- the differential creep vertical convergence of the rooms,
- the average σ_3 at the roof of the excavated rooms, and
- the average Von Mises stress at the upper corner of the room at the centre of the panel,

Moreover, graphs were produced showing the distribution of the stress components and the respective *Strength Factor*, across the width of the pillar at the centre of panel, after one, five and thirty years following the excavation of the panel.

To minimise any boundary effects, the cross-section that was used in geomechanical analysis extended 200 m in the horizontal direction and 340 m in the vertical direction above and below the mining level (as shown in Figure 6-4).

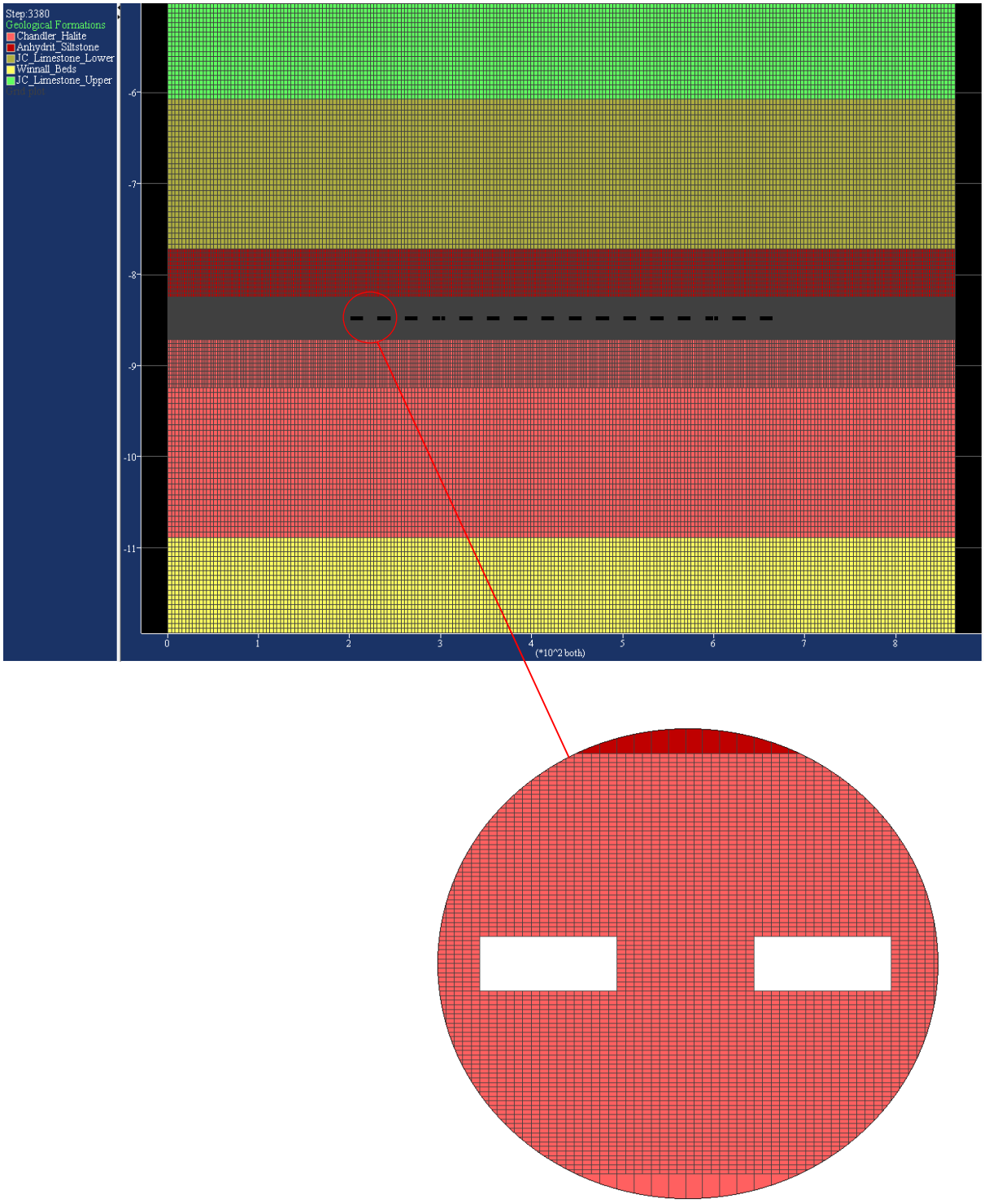

Figure 6-4 Finite difference model used in the geomechanical analysis of Chandler mine

Furthermore, to model the existing geologic formations in a satisfactory manner and to improve the accuracy of the finite difference calculations, a relatively fine grid was used 20 m above and below the excavated rooms. The grid was composed of 151,470 grid-points resulting in a total number of 150,640 zones, corresponding to 561 zones along the x-axis and 269 zones along the y-axis.

In addition to the initialisation of the geostatic stresses (in accordance with Section 3 of this report) suitable displacement constraints were also specified along the edges of the grid. The kinematic boundary conditions specified along the sides of the model were:

- no horizontal displacement along the vertical sides (i.e. roller side boundaries), and
- no vertical displacement along the top and bottom horizontal boundaries (i.e. fixed top and bottom).

The results of the finite difference analysis, in the form of contour diagrams showing the distribution of the three principal stresses, the Von Mises stress, and the vertical and horizontal stress components are presented in:

- Appendix A, for the conditions corresponding to one year after the excavation of the rooms;
- Appendix B, for the conditions corresponding to five years after the excavation of the rooms; and
- Appendix C, for the conditions corresponding to thirty years after the excavation of the rooms.

Assessment of the Von Mises stress concentrations in the pillars (as shown in Figures A-4, B-4 and C-4 included in Appendices A, B and C respectively) indicates that the pillar in the centre of the panel is subjected to a higher loading than the one exerted to the pillars at the edge of the panel. This is evident from the time graphs shown in Figure 6-5, where is shown that (although the difference is relatively small) the pillar at the centre of the panel is not subjected to the same stress relief with time as the pillar at the edge of the panel.

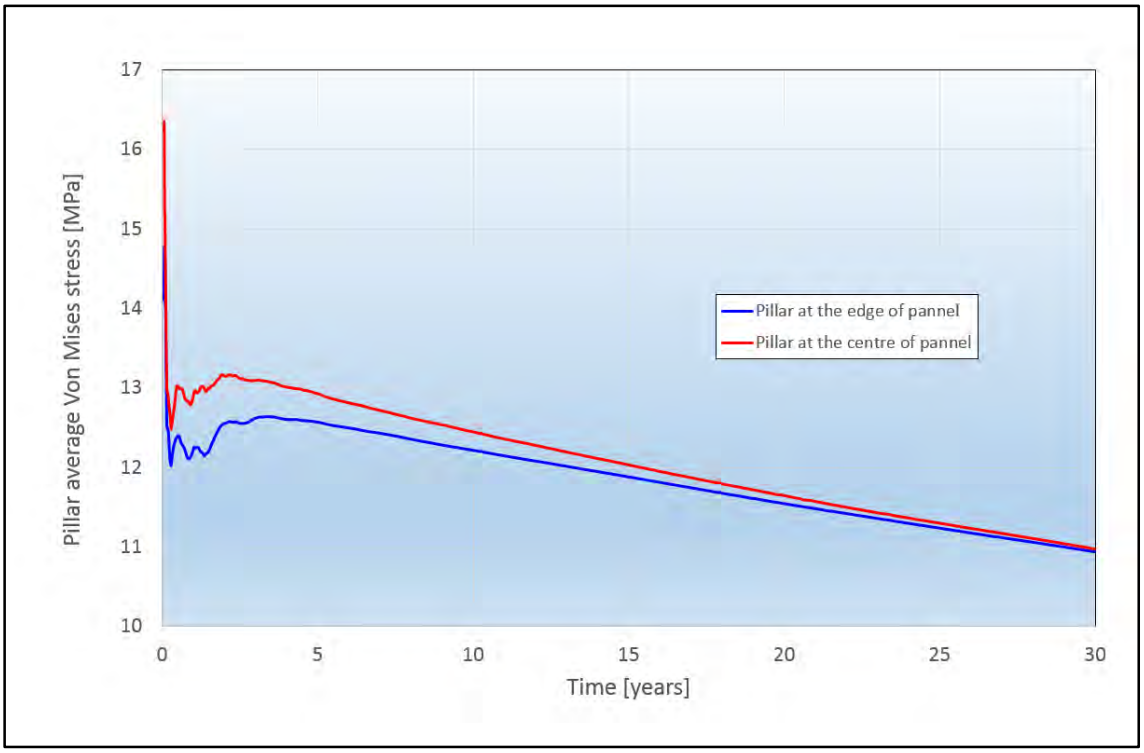

Figure 6-5 Reduction with time of the pillar average Von Mises stress

Examination of the displacements resulting from the creep deformation of the room at the edge of the panel (as shown in Figure 6-6), indicate that the rate of the roof's mid-span vertical convergence is approximately 72.0 mm/year while the floor's vertical displacement is characterised by a time-dependent heave with an approximate rate of 46.6 mm/year. Concerning the horizontal displacements of the walls (at mid-height) the wall nearer to the barrier pillar (i.e. left wall) converges at a rate of approximately 71.0 mm/year while at the anti-diametric location the wall converges at an approximate rate of 33.8 mm/year. The proximity of the barrier pillar provides a potential explanation for the difference in the horizontal deformation of the walls, since the left wall is affected by the stress concentrations that develop near the edge of the panel resulting in higher lateral displacements when compared with the right wall.

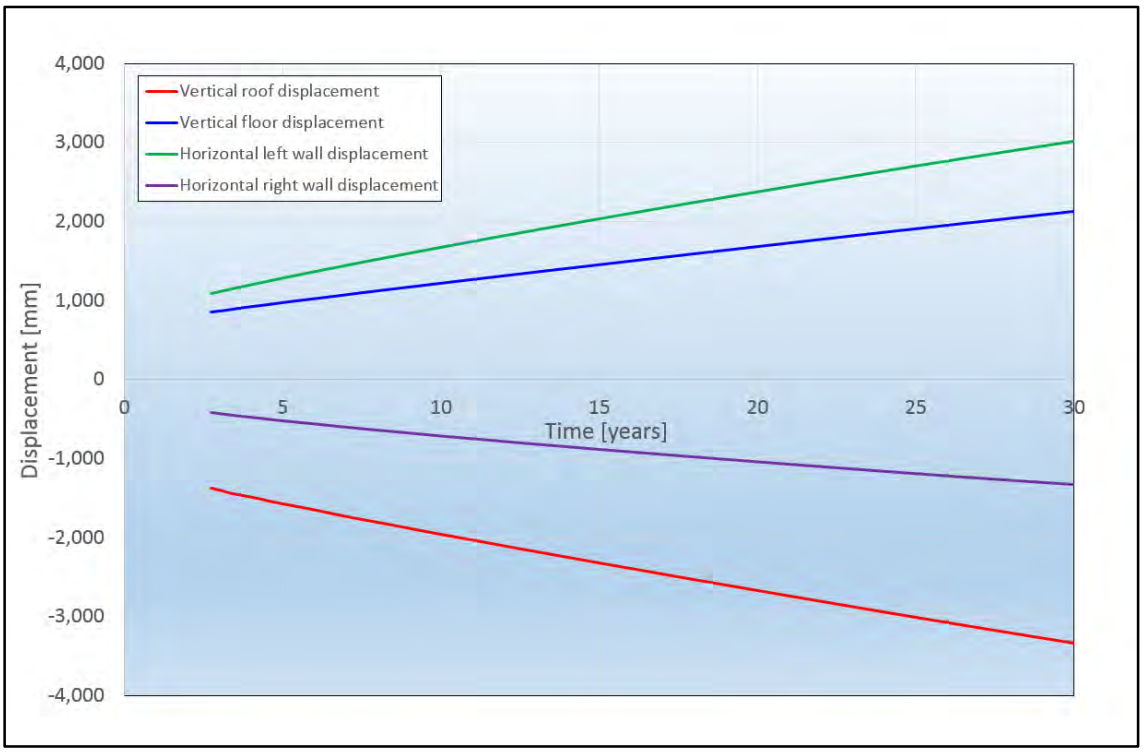

Figure 6-6 Development of creep displacements of the room nearer to the barrier pillar

Inspection of the displacements resulting from the creep deformation of the room at the centre of the panel (as shown in Figure 6-7), indicate that the rate of the roof's mid-span vertical convergence is approximately 59.5 mm/year while the floor's vertical displacement is characterised by a time-dependent heave with an approximate rate of 52.8 mm/year. In a similar way to the room at the edge of the panel, once more the roof displacement is larger than the respective floor vertical displacement. However, this time the difference between roof and floor is smaller since the loading of the pillars at the centre of the panel is more uniform than the loading of the pillars adjacent to the edge of the panel.

Concerning the horizontal displacements of the walls (at mid-height), as expected, the difference in the convergence of the wall is very small. The left wall converges at a rate of approximately 53.9 mm/year while at the anti-diametric location the right wall converges at an approximate rate of 51.8 mm/year.

The identified differences in the rate of the displacements along the vertical direction between the roof and floor for the two rooms (i.e. at the centre of the panel and next to the barrier pillar) are shown in the time graphs of Figure 6-8 that present the differential vertical convergence that the rooms are experiencing.

As already mentioned, the room at the edge of the panel exhibits a higher rate of differential creep convergence than the room near the centre of the panel. In particular, the room at the edge of the panel is characterised by a differential creep convergence of 25.6 mm/year while the room near the centre of the panel, is only subjected to a differential creep convergence rate of approximately 6.7 mm/year.

Practical experience from *in situ* measurements and observations concerning underground openings in salt formations, suggests that the identified order of magnitude of the rates of creep displacements, both along the vertical and horizontal directions, are very high and they are expected to have a negative effect on the serviceability limit state of the underground excavations. An encouraging sign, but not significant enough to ameliorate the identified excessive creep convergence, is the very slightly concave nature of the creep convergence displacement curves (shown in Figures 6-6 and 6-7). This behaviour indicates that the creep closure is decelerating, providing evidence that the creep response remains within the primary creep stage, implying that the creep closure has not entered the constant strain rate stage.

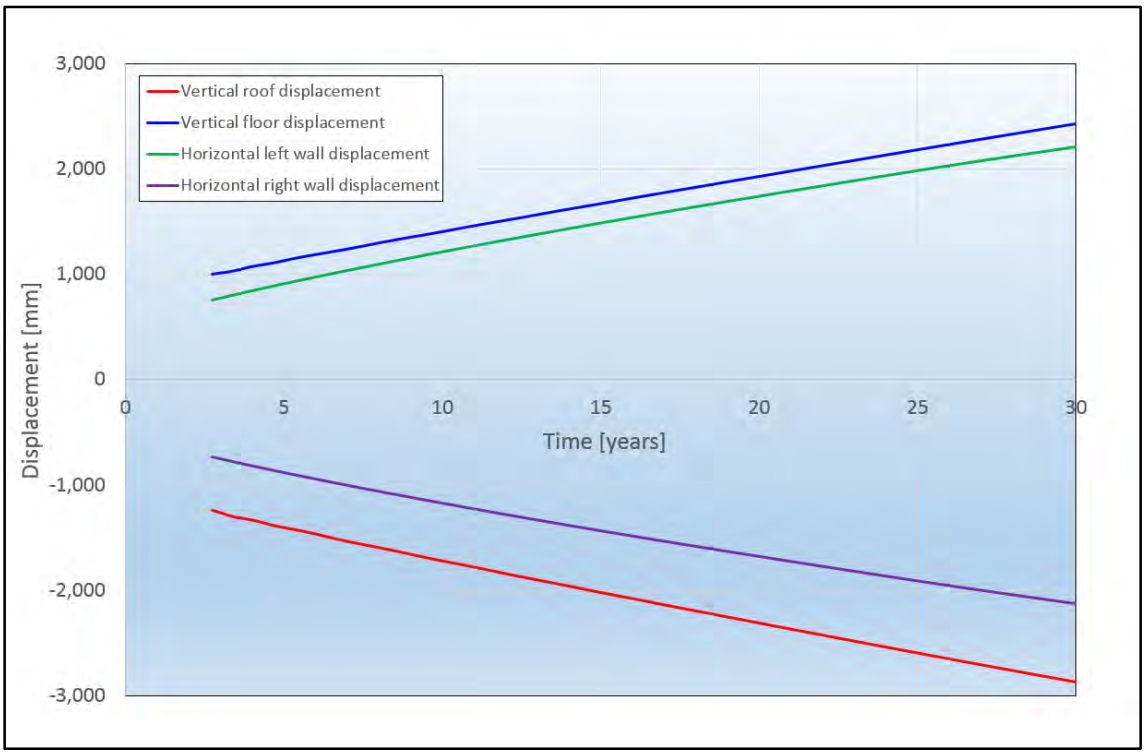

Figure 6-7 Development of creep displacements of the room at the centre of the panel

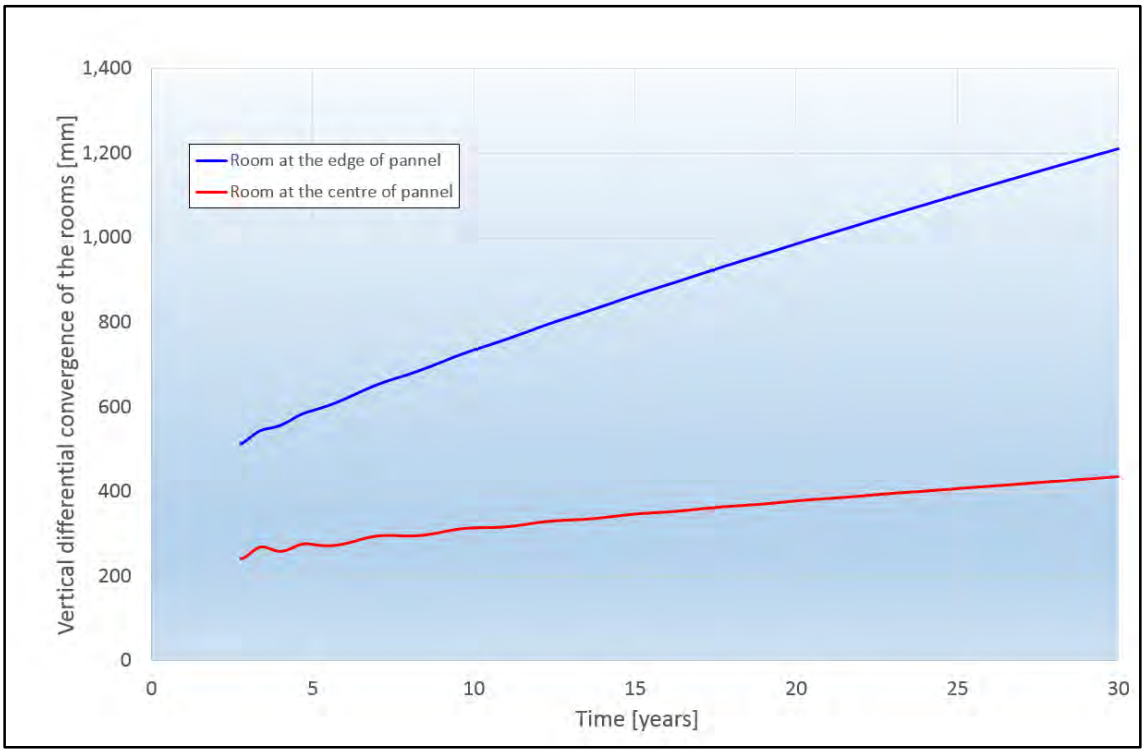

Figure 6-8 Development of the vertical differential creep closure of the rooms

Evaluation of the development, with time, of the average minor principal stress at the roof of the rooms (shown in Figure 6-9) indicates that, up to 23 years following the excavation of the panel, although the σ_3 is slightly tensile, the corresponding *Strength Factor* against tensile failure for both rooms is of the order of 13, implying

that the development of any tensile cracks is practically unattainable. However, as shown in Figure 6-9, after 23 years from the excavation of the panel, the minor principal stress at the roof of the room at the edge of the panel becomes more and more tensile and towards the end of 30 years the *Strength Factor*, against tensile failure, drops to about 1.04 which signifies potential tensile failure.

The distribution of the Von Mises stress, across the width of the pillar located at the centre of panel (i.e. the pillar with the most severe load), at one year, five years and thirty years after the excavation of the panel (shown in Figure 6-10) follows the same trend shown in Figure 6-5 whereby the shear stress loading of the pillars reduces with time. It is interesting to note that (as expected) this reduction with time does not affect significantly the core of the pillar (see the curves for year 1 and year 5 in Figure 6-10).

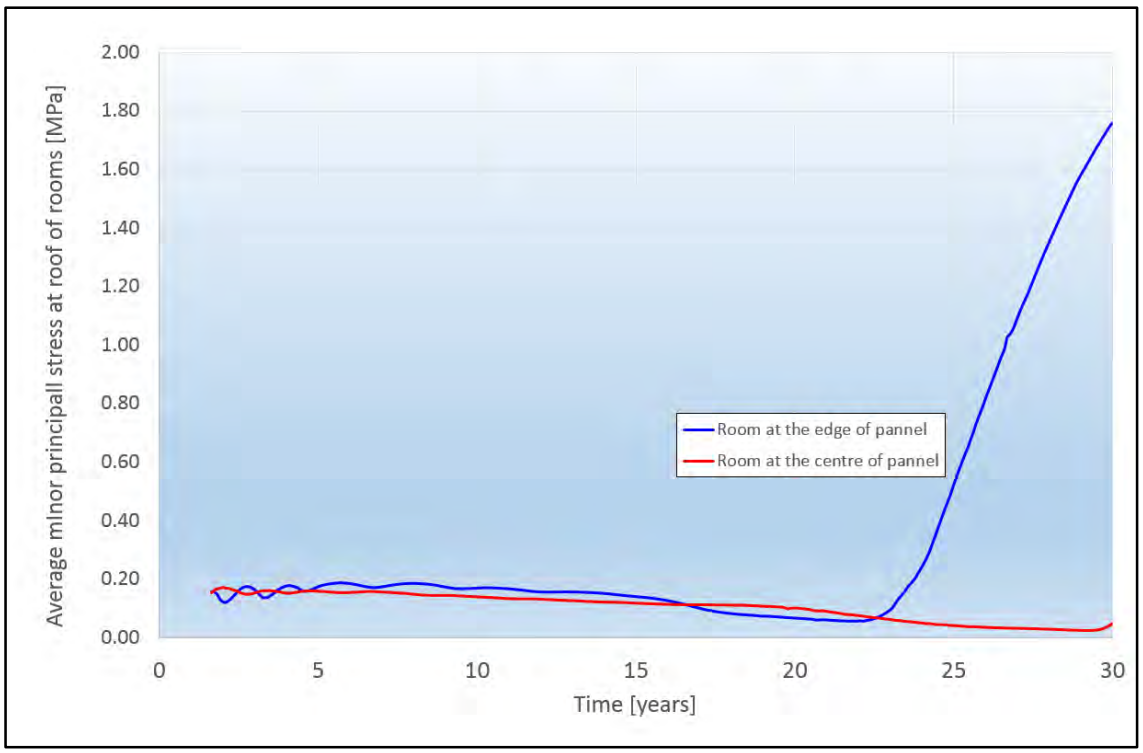

Figure 6-9 Development of the average minor principal stress at the roof of the rooms

Examination of the of the time-dependent development of the stress concentrations that develop, following the excavation of the room, at the upper corner of the room located at the centre of the panel, indicates a relatively high Von Mises stress of the order of 26 MPa. Evidently, within a very short time (as shown in Figure 6-11), the Von Mises stress reduces drastically to approximately 16 MPa and after that, its time-dependent reduction follows an asymptotic trend towards an approximate value of 12.8 MPa.

Clearly, these high stress concentrations around the corners of the rooms are the result of the geometry of the adopted geomechanical model which employed rectangular openings with square corners. To minimise the unwanted effect of the square corners, consideration should be given in employing a continuous miner equipped with a rotating drum cutting head system comprising specially designed cutter pick configuration that will allow the rooms to be cut with rounded angles at the corners of the cut.

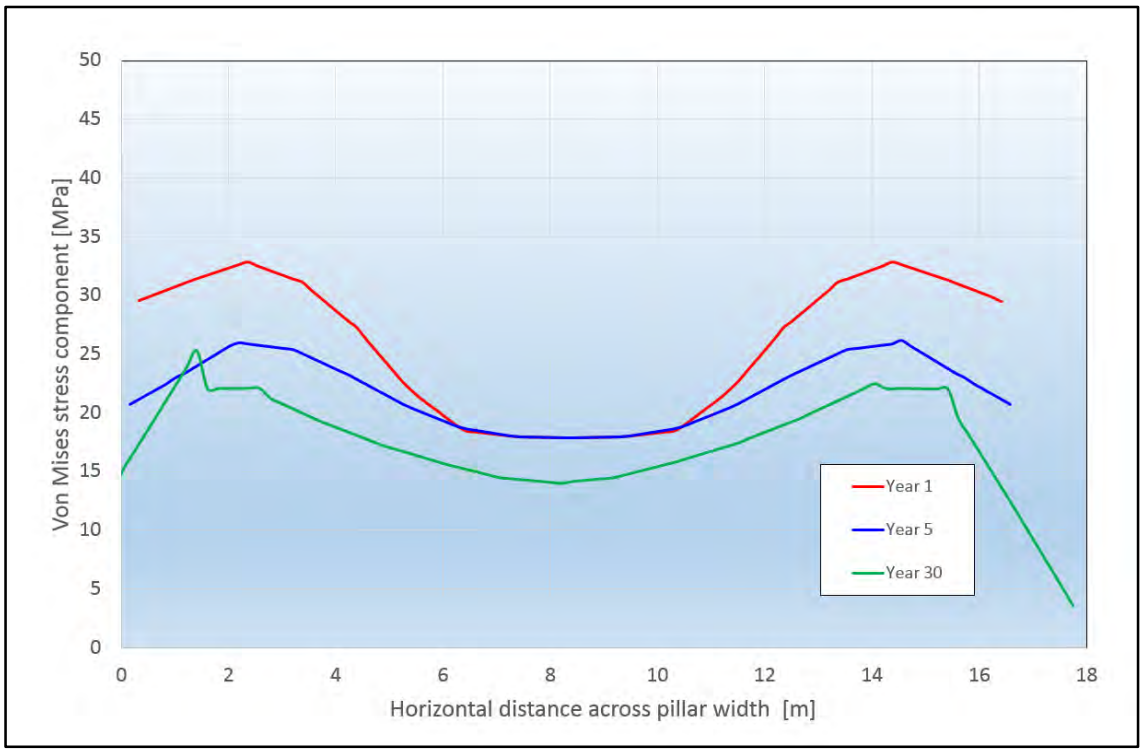

Figure 6-10 Distribution of the Von Mises stress, across the width of the pillar at the centre of panel, after 1 year, 5 years and 30 years following the excavation of the panel

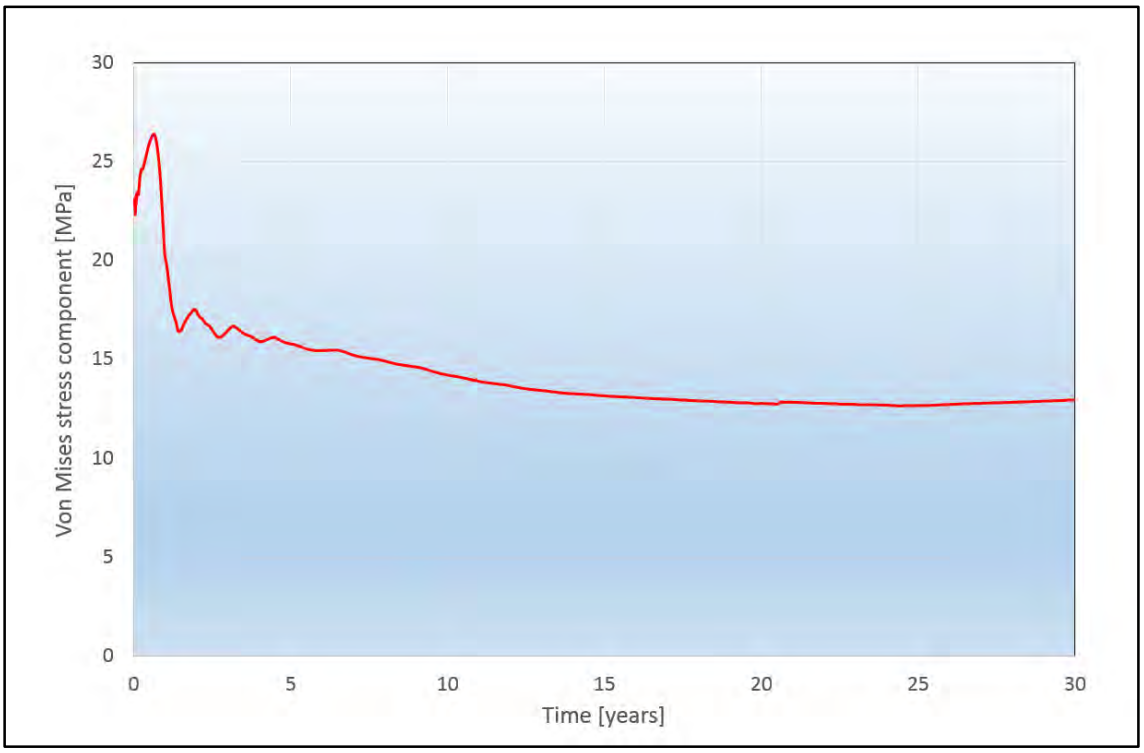

Figure 6-11 Reduction with time of the average Von Mises stress that develops at the upper corner of the room at the centre of the panel

6.3.1. Results after one year following the excavation of the rooms

The distribution of the major principal stress after one year, at the centre of the panel, is shown in Figure 6-12 where it is evident that the highest stress concentrations develop at the corners of the excavated rooms. Similar trends are also noticeable when the distribution of the intermediate principal stress at the centre of the panel, is plotted in Figure 6-13.

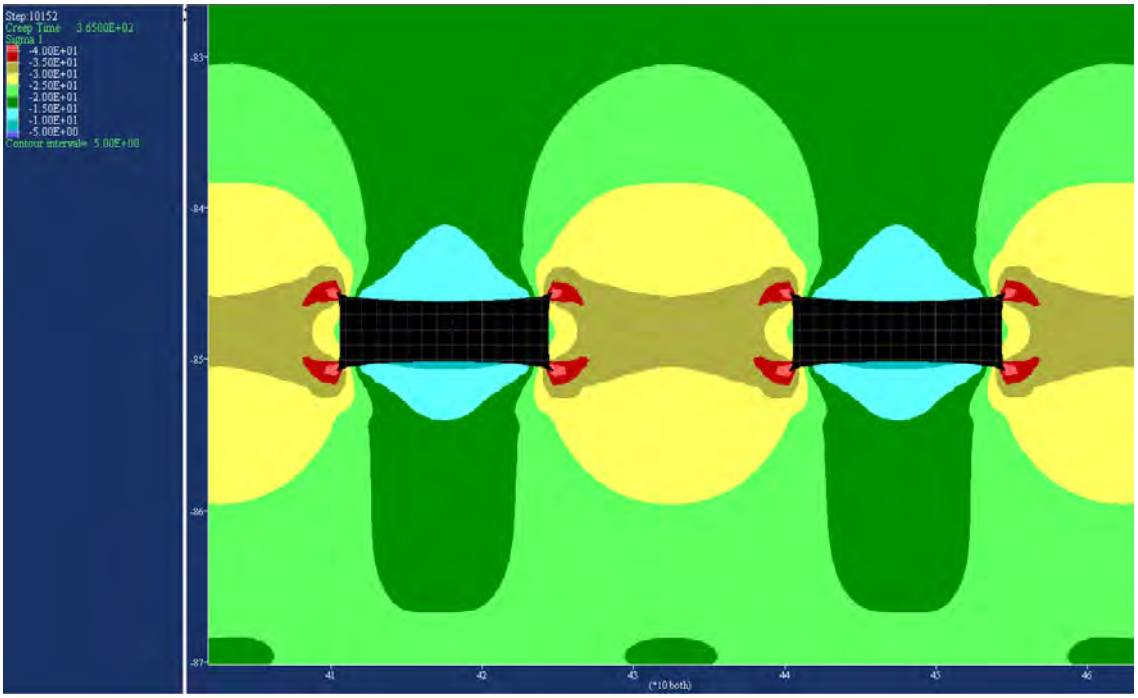

Figure 6-12 Distribution of major principal stress component σ_1, at the end of one year

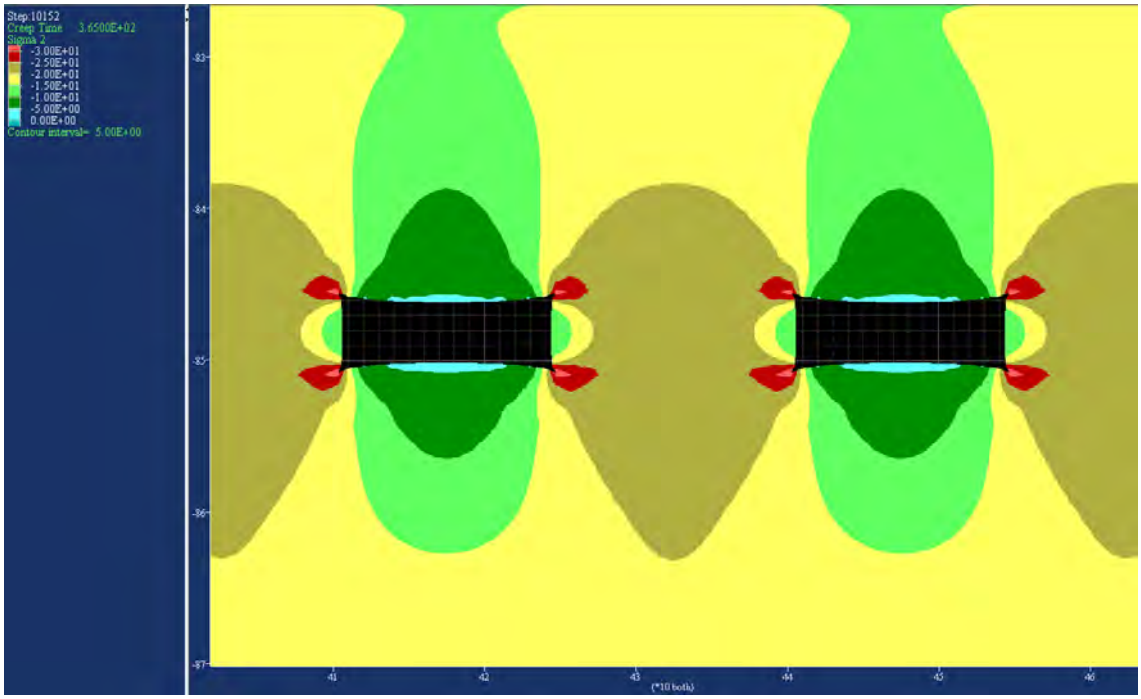

Figure 6-13 Distribution of intermediate principal stress component σ_2, at the end of one year

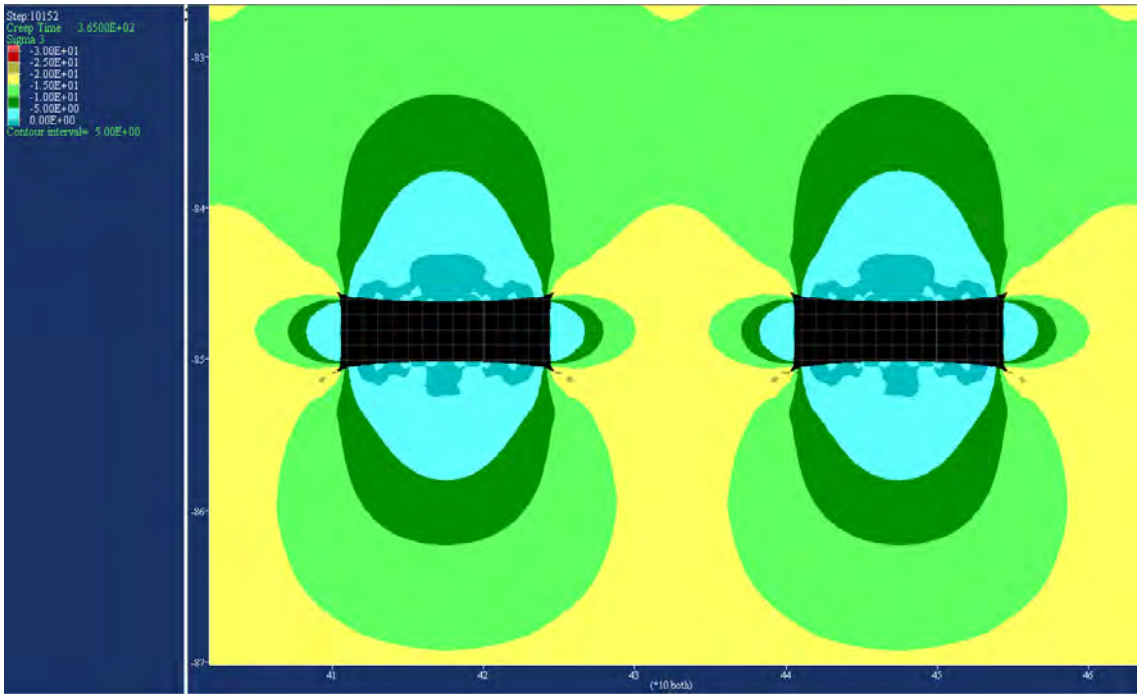

Figure 6-14 Distribution of minor principal stress component σ_3, at the end of one year

With respect to the distribution of the minor principal stress, at the centre of the panel shown in Figure 6-14, the roof of the rooms are primarily in compression with only pockets of insignificant tensile stresses. As for the sides of the pillars, the tensile stresses are absent as is also verified by the green curve shown in Figure 6-16.

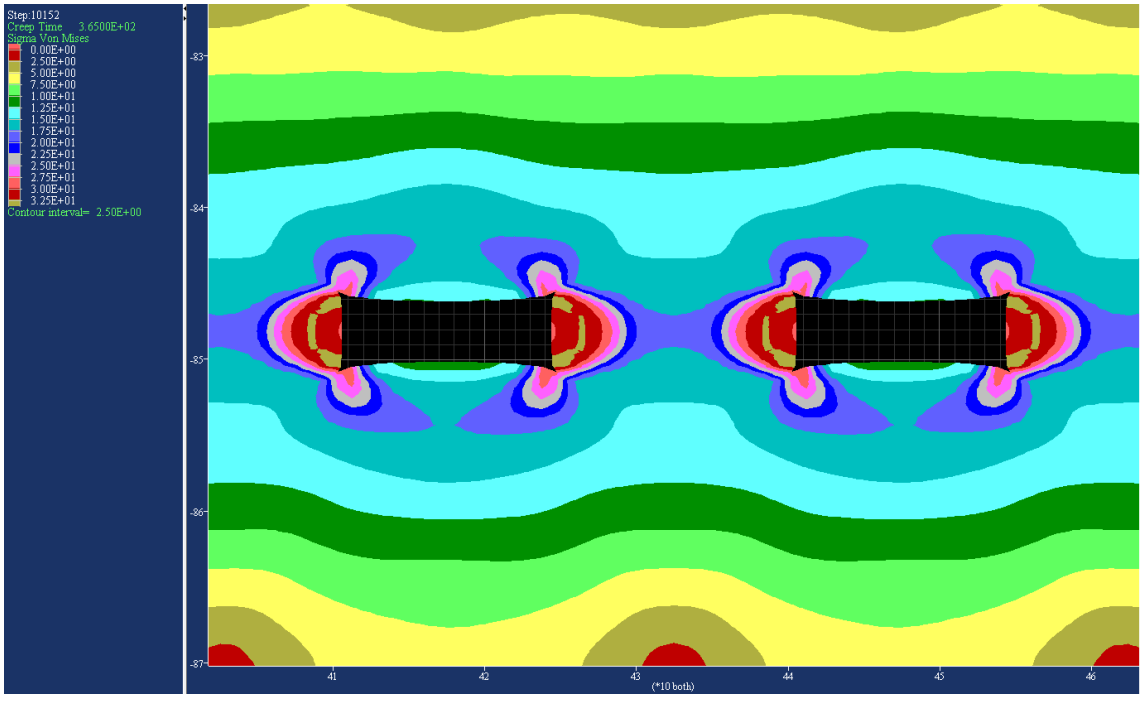

Figure 6-15 Distribution of Von Mises stress component σ_{vm}, at the end of one year

The distribution of the Von Mises stress, at the centre of the panel, one year after the panel was excavated is shown in Figure 6-15 where it is evident that the highest stress concentrations develop at the sides of the pillars.

The distribution of σ_1, σ_2, σ_3 and Von Mises stress, across the width of the pillar located at the centre of panel (i.e. the pillar with the most severe load), one year after the excavation of the panel is shown in Figure 6-16.

Moreover, the respective distribution of the *Strength Factor* against shear failure, is also plotted in the same figure, providing significant evidence that the pillars are capable of accepting the shear stresses that develop as the panel is excavated.

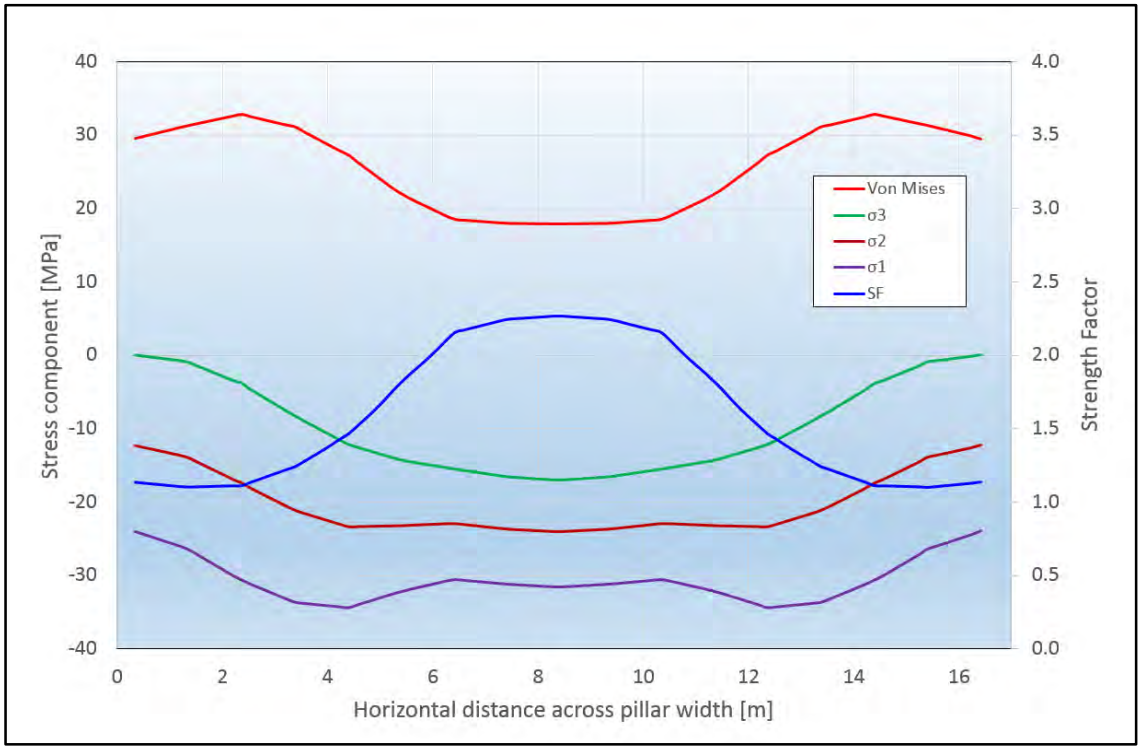

Figure 6-16 Distribution of the stress components, across the width of the pillar at the centre of panel, after 1 year following the excavation of the panel

6.3.2. Results after five years following the excavation of the rooms

The distribution of the major principal stress after five years, at the centre of the panel, is shown in Figure 6-17 where it is evident that, as was the case of one year, high stress concentrations develop at the corners of the excavated rooms.

Furthermore, similar trends are also noticeable when the distribution of the intermediate principal stress at the centre of the panel, is plotted in Figure 6-18.

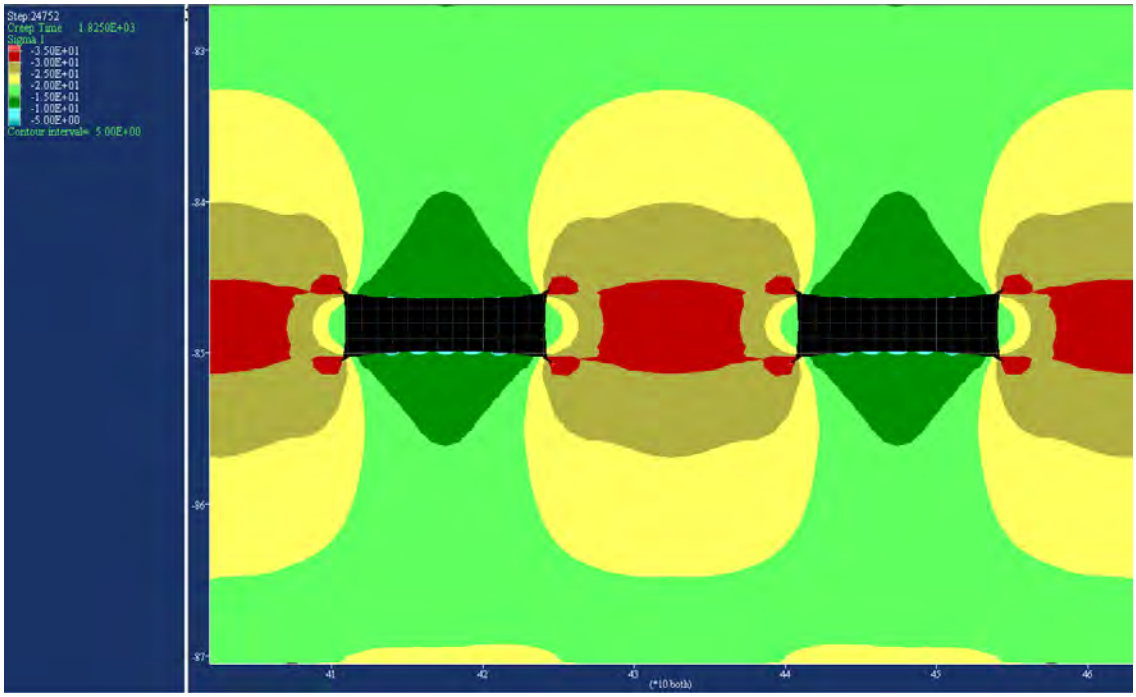

Figure 6-17 Distribution of major principal stress component σ_1, at the end of five years

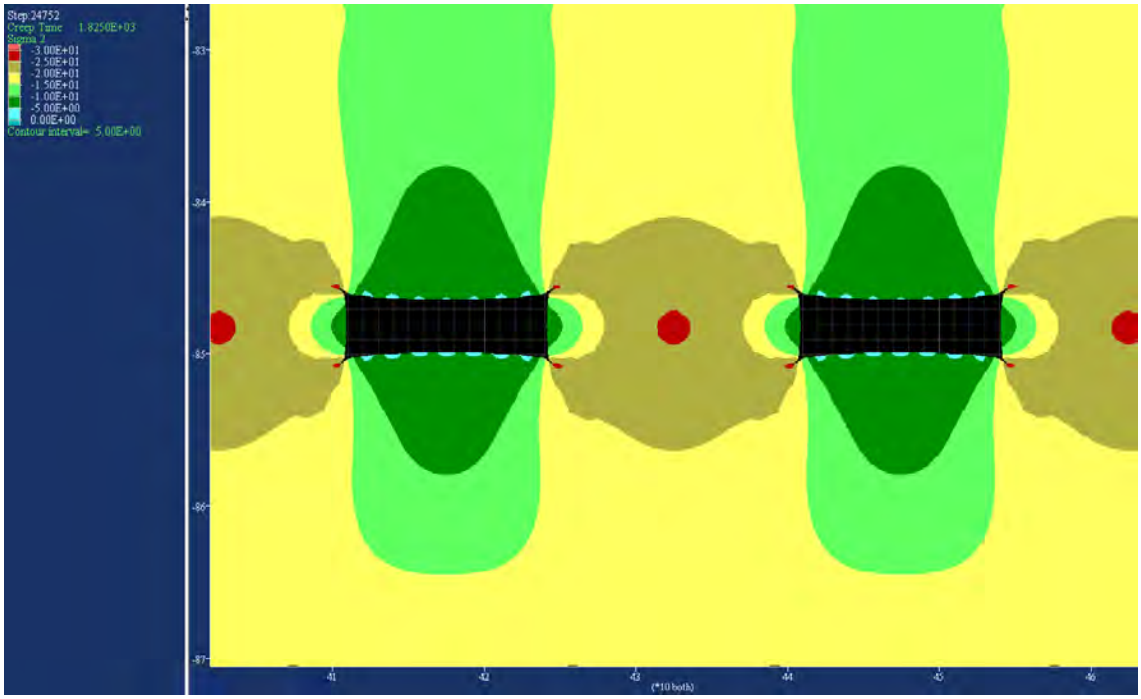

Figure 6-18 Distribution of intermediate principal stress component σ_2, at the end of five years

Figure 6-19 shows the distribution of the minor principal stress, at the centre of the panel, where the roof of the rooms are essentially in compression with only inconsequential pockets of trivial tensile stresses. Following a similar pattern, to the one we have seen for the year 1, in the sides of the pillars the tensile stresses are absent as is also verified by the green curve shown in Figure 6-21.

The distribution of the Von Mises stress, at the centre of the panel, five years after the panel was excavated is shown in Figure 6-20 where it is evident that the highest stress concentrations develop at the sides of the

pillars. Figure 6-21 shows the distribution of σ_1, σ_2, σ_3 and Von Mises stress, across the width of the pillar located at the centre of panel (i.e. the pillar with the most severe load), five years after the excavation of the panel. Furthermore, the respective distribution of the *Strength Factor* against shear failure, shown also in the same figure, indicates clearly that the pillars are capable of accepting the shear stresses that develop as the panel is excavated. If anything, as a result of the creep deformation of the pillars, the shear stresses have relaxed with time.

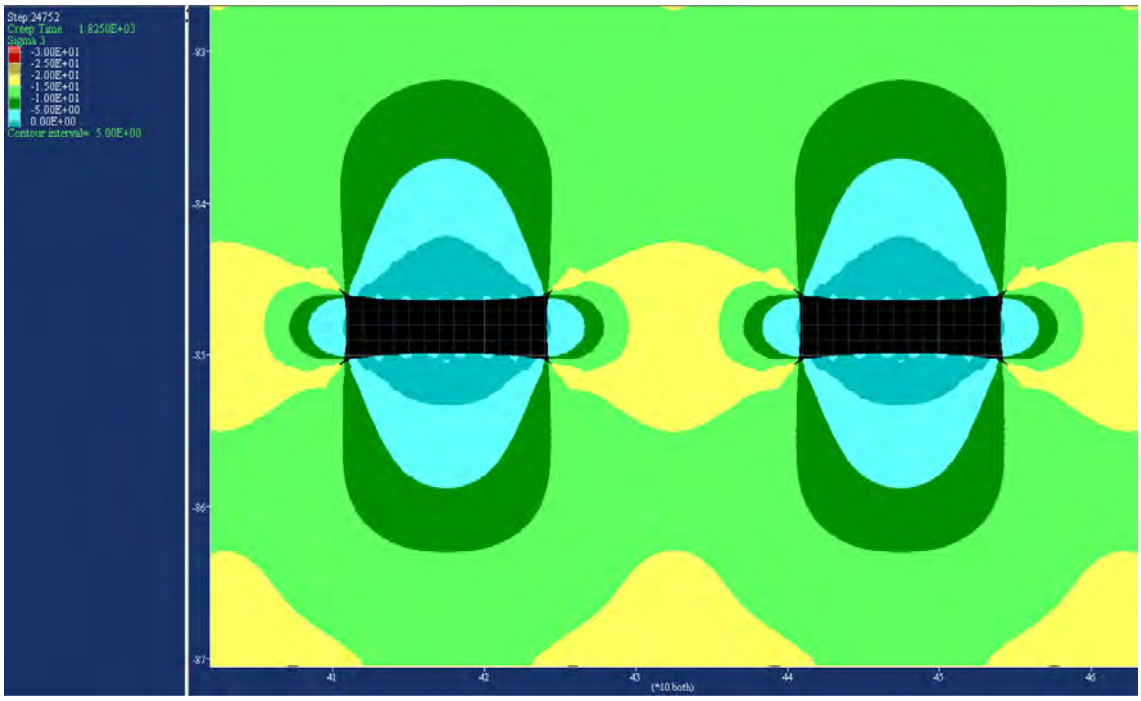

Figure 6-19 Distribution of minor principal stress component σ_3, at the end of five years

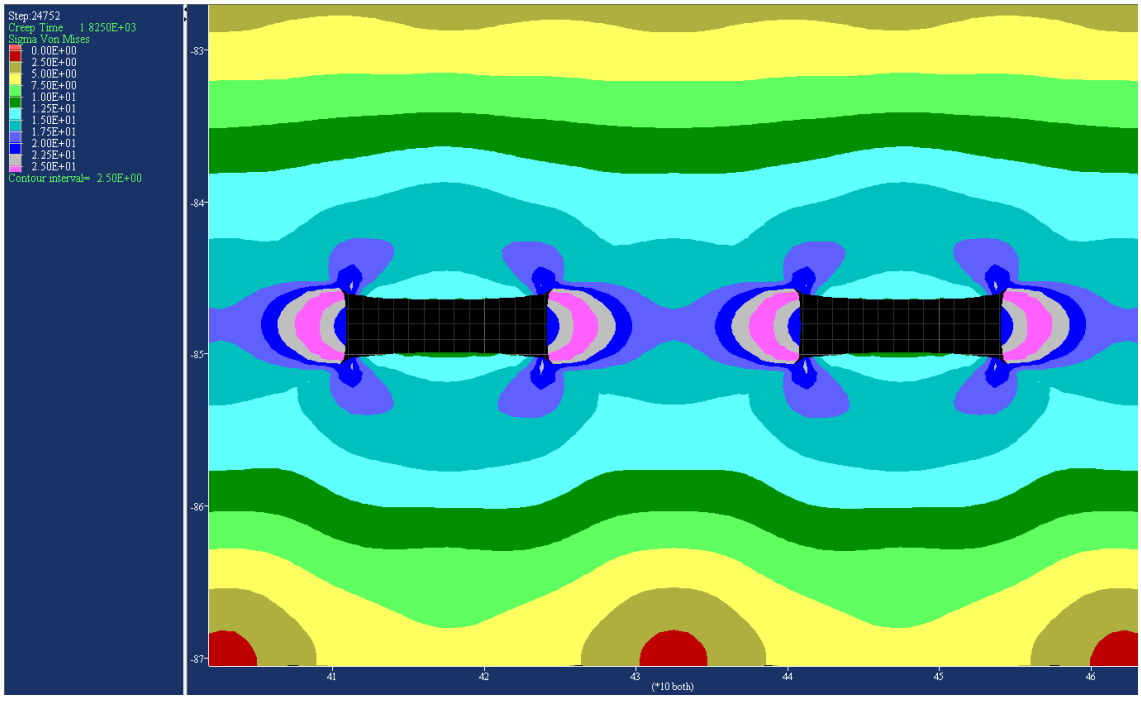

Figure 6-20 Distribution of Von Mises stress component σ_{vm}, at the end of five years

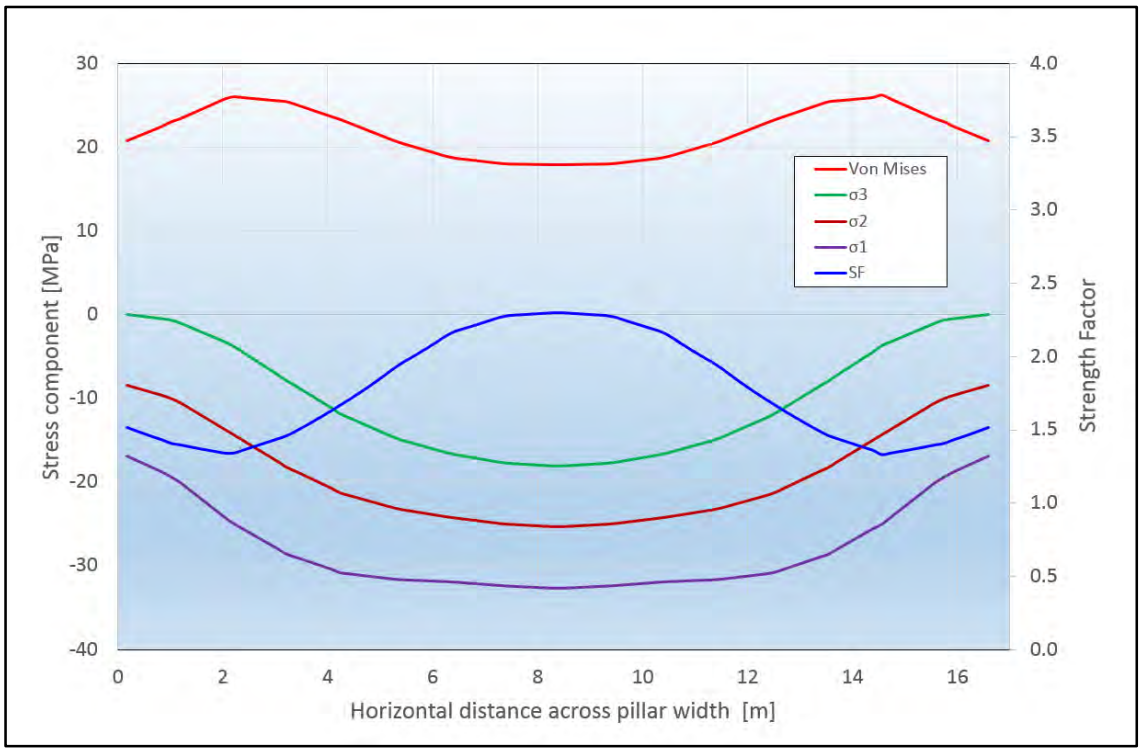

Figure 6-21 Distribution of the stress components, across the width of the pillar at the centre of panel, after five years following the excavation of the panel

6.3.3. Results after thirty years following the excavation of the rooms

Figure 6-22 shows the distribution of the major principal stress, at the centre of the panel, after thirty years have elapsed from the excavation of the rooms.

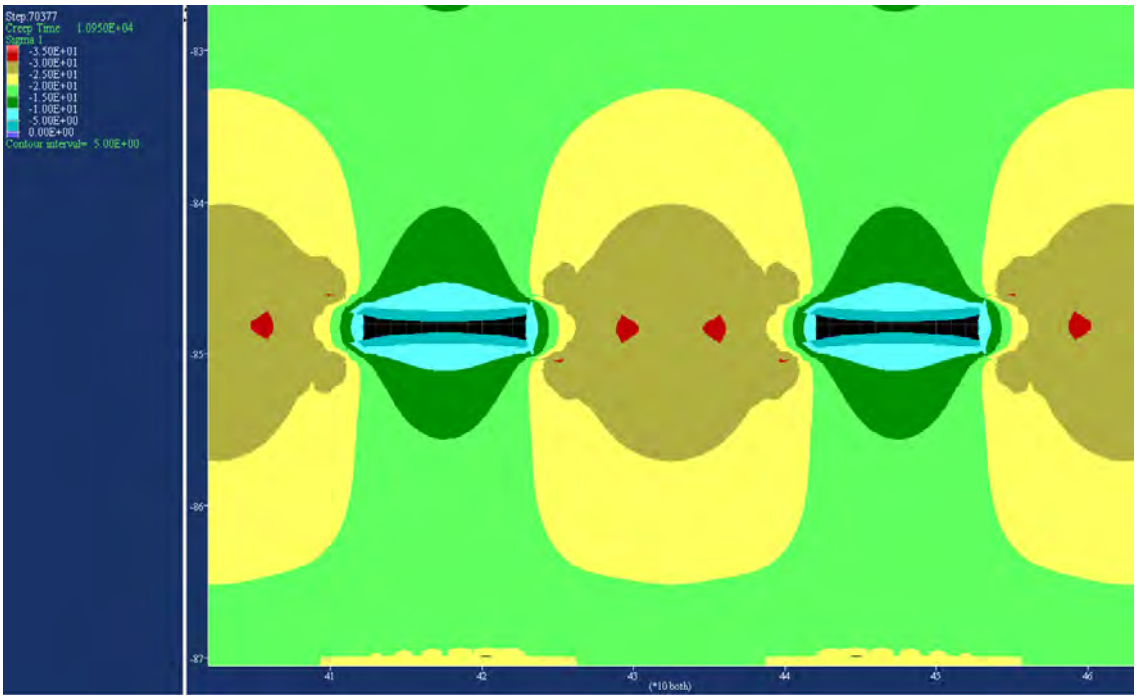

Figure 6-22 Distribution of major principal stress component σ_1, at the end of thirty years

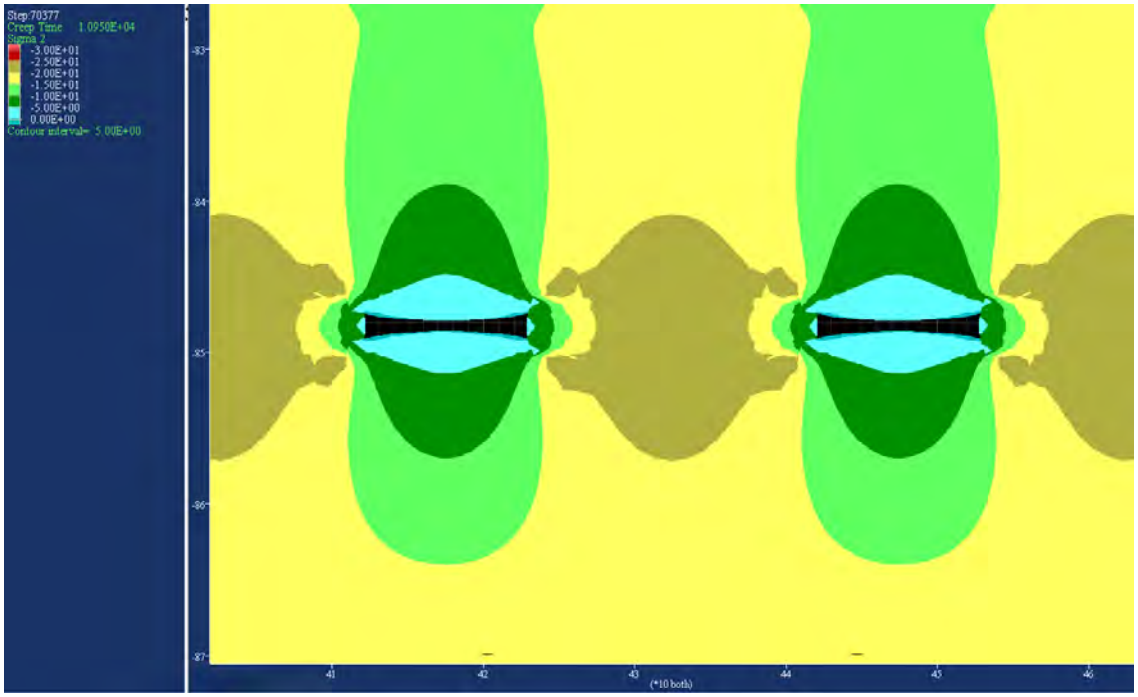

Figure 6-23 Distribution of intermediate principal stress component σ_2, at the end of thirty years

The distribution of σ_1 provides evidence that, although high stress concentrations develop in the main body of the pillars, the roof and floor of the rooms have relatively low stress concentrations resulting from the identified creep convergence. Furthermore, Figure 6-23 shows similar trends concerning the distribution of the intermediate principal stress at the centre of the panel, which also shows a relaxed stress regime in the roof and the floor of the rooms.

The distribution of the minor principal stress at the centre of the panel, shown in Figure 6-24, indicates that the roof of the rooms are in low compression. The same applies for the sides of the pillars, where we may see evidence of the stress relaxation that developed at the end of thirty years. The high creep convergence of the rooms that contributed in the relaxation of the stresses, is also evident from the distorted shape of the excavated rooms shown in Figures 6-22 to 6-24.

The distribution of the Von Mises stress at the centre of the panel, thirty years after the panel was excavated, indicates that the highest stress concentrations arise in zones that develop in the pillars approximately 3 m inside from the sides of the excavations (see Figure 6-25).

Figure 6-26 presents the distribution of the principal stresses and the Von Mises stress, across the width of the pillar located at the centre of panel, thirty years after the excavation of the rooms. Moreover, the distribution of the *Strength Factor* against the potential shear failure of the salt pillars provides evidence that the pillars are capable of accepting the shear stresses that develop as the panel is excavated (the lowest value of the calculated *Strength Factor* at a depth of approximately 3 m from the sides of the excavation, is 1.4).

Figure 6-27 shows the distribution of the minor principal stress σ_3 and the Von Mises stress σ_{vm}, above the centre of the roof of the central room, thirty years after the excavation of the rooms. This figure provides evidence, of the reduction of σ_{vm} and of the shift of σ_3 towards more compression, as we progress from the roof of the room (at 845 m bgl) towards the top of the salt (at 825 m bgl).

Clearly, the 20 m thickness of salt, which is left between the roof of the rooms and the top of the Chandler Halite, provides an adequate buffer that prevents the development of migration paths for potential contaminants (associated with the underground storage operations) towards the non-salt formations.

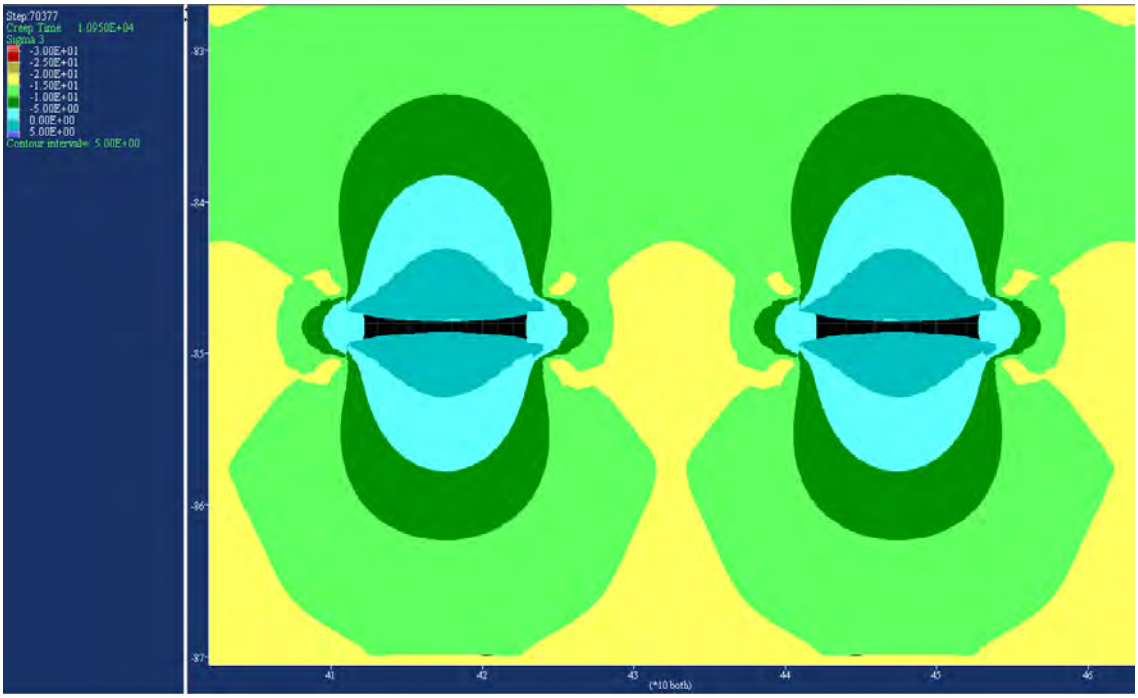

Figure 6-24 Distribution of minor principal stress component σ_3, at the end of thirty years

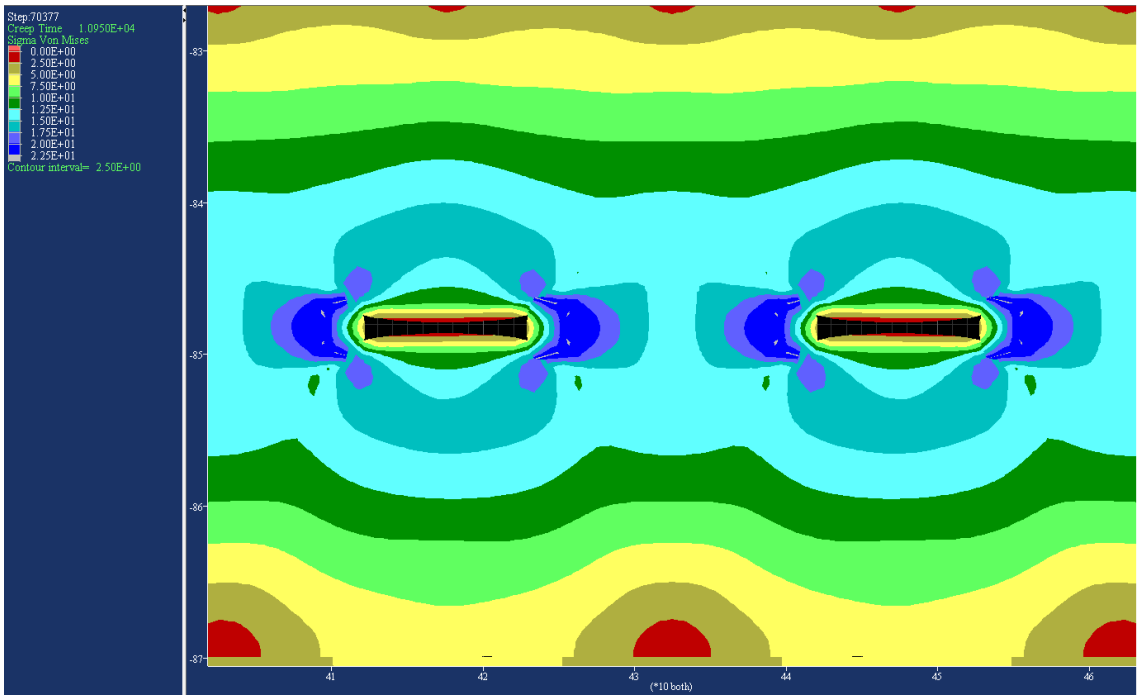

Figure 6-25 Distribution of Von Mises stress component σ_{vm}, at the end of thirty years

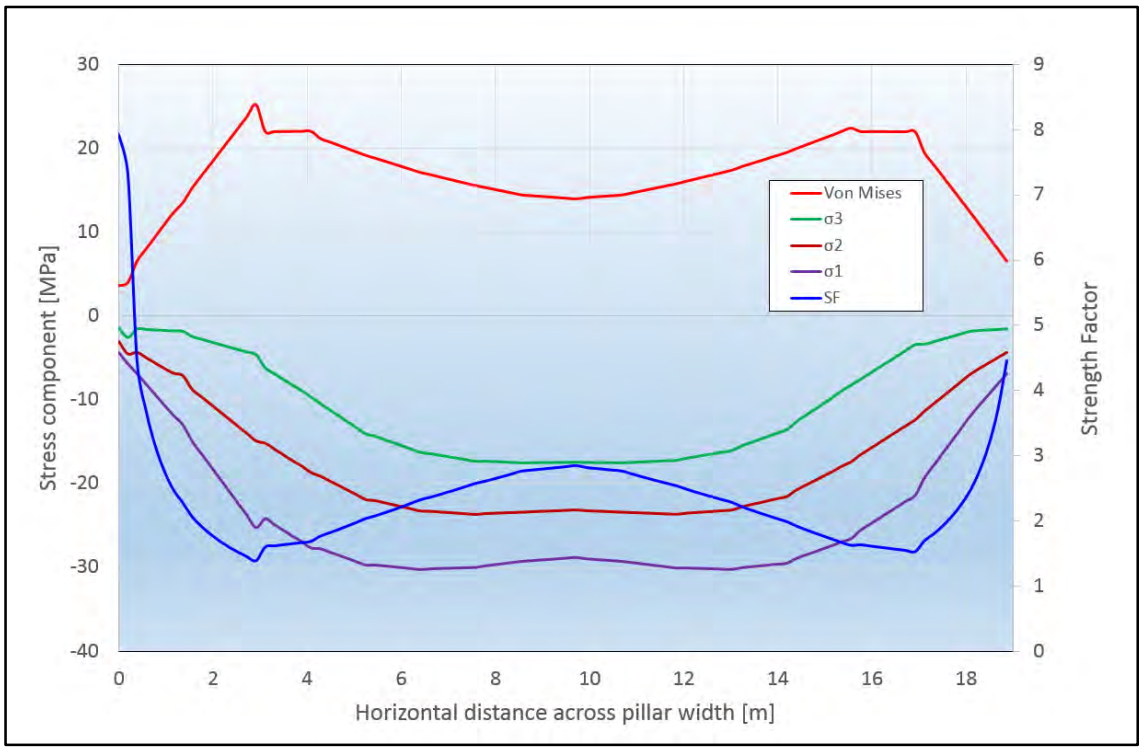

Figure 6-26 Distribution of the stress components, across the width of the pillar at the centre of panel, after thirty years following the excavation of the panel

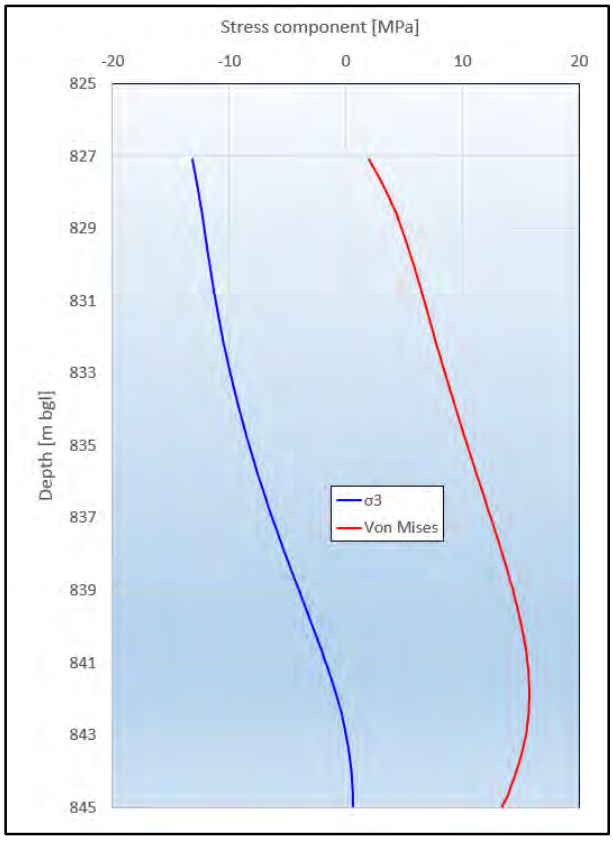

Figure 6-27 Distribution of minor principal stress and Von Mises stress above the roof of the room at the centre of panel, after thirty years following the excavation of the panel

6.3.4. The need for support of the excavated underground openings

6.3.4.1. Active support provided by rockbolts

To bring under control the development of the identified:

- tensile stresses in the roof of the rooms, and
- high shear stresses near the walls of the pillars,

it is recommended to provide appropriate rock reinforcement by means of post-tensioned, resin grouted rockbolts.

The proposed rock reinforcement should be active (whereby an active force is applied to the Halite formation) by employing 4 m length bolts with a grouted length of 2 m. Since the effectiveness of a post-tensioned rockbolt depends on its free length, the anchor force shall act in ground that is sufficiently distant from the anchored structure such that no additional force is applied on it (British Standard Institution, 2014). It is recommended, therefore, to ensure that each bolt should have a free length of 2 m in accordance with British Standard Institution (2015).

Until such time as we have practical experience from the potential development of localised small scale spalling at the roof of the excavated rooms, it is not recommended to incorporate in the roof support measures the use of mesh. Although mesh provides little structural support, it does however prevent small pieces of rock falling out from the space between rockbolts.

The post-tensioned loadings applied to any bolt shall not exceed 75% of the ultimate tensile strength or 90% of the yield stress of the steel bar. All rockbolt reinforcement should be Dywidag Gewi Steel Grade 500/600 high yield fully threaded bar or approved equivalent. The recommended rockbolt sizes and properties are shown in Table 6-1:

Table 6-1 Specifications for the proposed rockbolt active support

Nominal bar diameter (mm)	25
Steel grade (N/mm^2)	500/600
Diameter over threads (mm)	29
Mass per unit length (kg/m)	3.85
Cross sectional area (mm2)	491
Characteristic yield load (kN)	245
Maximum ultimate tensile load (kN)	295

All rock bolts are to be galvanized with a 325 g/m^2 coating in accordance with British Standard Institution (2009).

The density of the rockbolts used in the roof should be approximately 1 rockbolt/4 m^2 while the configuration of the rockbolts used in the side of the pillars should be approximately equal to 1 rockbolt/10 m^2.

It is important to take into consideration that the specified dimensioning and properties of the post-tensioned rockbolts are in essence indicative. Consequently, there will be a need at later stage to carry out an appropriate geomechanical analysis in which the timing of the support installation and the Halite-rockbolt structural interaction should be included.

6.3.4.2. Passive support provided by the stored waste acting as backfill material

Hazardous wastes including mercury contaminated solid wastes have been deposited in underground salt mines for several decades in Europe. Therefore, an extensive knowledge base on all repository relevant properties of rock salt and salt formations is available. In the European Union, salt mines are currently authorised for the underground disposal of hazardous waste only in Germany and the UK. Poland is currently considering using specific salt mines for the disposal of hazardous waste (European Commission, 2010).

The stored waste, in confined compression, is expected to exhibit a consolidation resulting from the compaction caused by room creep closure and therefore its behaviour may be expressed by a series of tangential slopes corresponding to stress versus volumetric plastic strain segments. Consequently, modelling of the constitutive response of the stored waste may be undertaken by adopting the classic double yield model (Rizkalla & Mitri, 1969).

Backfilling of the excavated rooms with waste will reduce the convergence rate and prevent long-term convergence, provided that the stored waste is placed in a suitable manner. The tighter the backfill of the waste (to the mine roof), the lower the convergence rate and the faster the rate of the storage operations, the better will be the control of the anticipated room convergence. This suggests that, when flowable waste materials are used they could be hydraulically backfilled in such a way as to minimise void space at the roof level and improve significantly the support provided by the stored waste.

In the absence of any actual backfill parameters, assuming a worst possible case scenario, we may consider that the packaged waste material, which is furthermore expected to have fine salt pneumatically placed around it, has poor compressibility characteristics. In this case, the packaged backfilled waste material will be capable of accepting reasonable compressive loads only once its plastic volumetric strain has exceeded a limit of approximately 15%. As a result, the anticipated reduction of the rate of closure of the excavated rooms is expected to range between 20% and 25%. For the case of well compacted hydraulically backfilled flowable waste materials, the rate of closure of the excavated rooms is expected to improve reaching an anticipated reduction ranging between 35% and 40%. Moreover, taking into consideration that all of the main access roads will be stowed with crushed salt, when they are no longer required for use, there will be a further reduction of the rate of the creep convergence. The identified creep convergence for both types of wastes, will cease to progress as soon as the reaction forces in the waste and the acting compressive loading (exerted by the room closure) reach an equilibrium.

In assessing the positive contribution of the passive support provided by the stored waste, it is important to take into consideration that the quoted anticipated reductions of the rate of closure of the excavated rooms, are indicative. As a result, there will be a need, at a later stage, to carry out an appropriate geomechanical analysis in which the timing of the placement of the waste and the Halite-waste material structural interaction should be included.

6.3.5. Reduction in room width to improve the stability of the roof

The development of the salt mine was modelled by employing an ‘instantaneous’ full excavation of the entire panel (which comprises 16 rooms), whereby the full width of 15 m and the entire height of 6 m of each room was generated suddenly. As a result, the identified stresses after one year remain at a relatively high level, corresponding to the lowest *Strength Factor* being 1.1 in the pillar sidewalls (see Figures 6-15 and 6-16). However, taking into consideration that each panel will require at least three years for its full development, the creep deformation of the Chandler Halite is expected to increase the *Strength Factor* in the pillars by approximately 35%, which will reduce accordingly the identified high stress concentrations in the pillars’ walls thus preventing the development of potentially unacceptable sidewall spalling.

To ensure that the required stress relaxation occurs, it will be necessary to determine the appropriate sequencing of the excavations by means of geomechanical modelling incorporating a series of a parametric analyses in which the timing of the excavations should correspond to the expected rate of development.

The roof span of the rooms, currently set at 15 m, encourages the development of relatively large rate of vertical creep converge mid-width of the excavated room, which is expected to have an undesirable influence on the respective serviceability limit state conditions and may have a negative effect on the long term stability of the roof.

In considering the reduction of the maximum permissible roof span of the rooms, it is suggested that at least two adjacent rooms located near each edge of the panel, should have their width reduced down to 12 m. In reducing the width of the rooms by 3m, although the resulting convergence mid-width of the excavated room will be reduced accordingly, the loading of the respective pillars is not expected to change in any appreciative manner. On the other hand, the proposed change in the room geometry will reduce slightly the overall span of the panel by more than 2.5%, which is expected to have a marginal positive effect on the loading of all the pillars.

6.3.6. Deductions derived from the assessment of the geomechanical numerical analysis

On the basis of the assumed properties of the geological materials and the anticipated geostatic loading conditions, the roof of the excavated rooms is expected to converge at relatively high rate but will remain intact and provide an appropriate geological barrier. Concerning the identified high stress concentration in the walls of the pillars, the expected stress relaxation associated with the creep deformation of the Chandler Halite is expected to contribute in the prevention of the development of potentially unacceptable sidewall spalling.

The width of the rooms, away from the edges of the panels, is acceptable at 15m wide, but there is a need to narrow down to 12 m at least two adjacent rooms located near each edge of the panels.

Concerning the barrier pillars (i.e. the inter-panel pillars) that provide support at the edges of the panels, there is a requirement to increase their width to improve the overall stability of the panels and to reduce the potential structural interaction of adjacent panels by providing appropriate load isolation conditions.

The benefit of the active support, provided by the proposed post-tensioned resin grouted rockbolts, and also by the passive support, exerted both by the packaged and the hydraulically backfilled waste materials, is important since it is expected that these measures will bring under control the development of the identified tensile regime in the roof of the rooms and the shear stresses near the walls of the pillars. Another positive measure that is expected to contribute to the overall stability of the underground excavations is the plan to stow, with crushed salt, all the main access roads when they are no longer required for use.

7. Conclusions and recommendations

The objective of the geomechanical studies of the planned Chandler mine was achieved by employing:

- engineering judgement in analysing the results of the geomechanical modelling;
- established experience and knowledge in utilising appropriate parameters concerning the strength and the constitutive response of the Chandler Halite; and
- realistic modelling of the geometry, the *in situ* geostatic stresses and the boundary conditions that characterise the room and pillar mine layout.

7.1. Conclusions

The following conclusions outline the results generated from the geomechanical numerical analysis:

1. The finite difference method was successfully used for the numerical simulation of the planned Chandler mine in investigating the development of the subsurface stress concentrations and creep response of the Chandler Halite that surrounds the room and pillar mine layout.

2. With respect to the geomechanical response of the planned Chandler mine, a significant element is the Jay Creek Limestone strata that overlay the Chandler formation, which have an average thickness of more than 250 m. Provided that no major faults or prevalent systems of significant discontinuities exist, the Jay Creek Limestone will act as an enormous thick plate, with built-in-ends, that is expected to contribute significantly to the stability of the planned excavations.

3. Examination of the distribution of the minor principal stresses, determined in the numerical modelling for the first 23 years, indicates that σ_3 is essentially very close to the compressive regime. Consequently, during the first 23 years following the excavation of the panels, the possibility of developing in the roof of the rooms tensile stresses that may exceed the tensile strength of the Chandler Halite is almost unlikely. However, the excessive creep closure that has been identified in the roof of the rooms next to edge of the panels will, in all probability, result in the development of tensile cracks.

4. Calculation of the *Strength Factor* against shear failure for the salt pillars has shown that, even at the early life of the mine, the *Strength Factor* values indicate no shear failure. The identified *Strength Factor* values demonstrate that the Chandler Halite of the pillars, when subjected to the stress concentrations caused by the excavations, is able to endure shear stresses over a period of thirty years.

5. Assessment of the distribution of the minor principal stress and the Von Mises stress above the salt mine provided evidence that the 20 m thickness of salt, which is left between the roof of the rooms and the top of the Chandler Halite, prevents the establishment of a pathway to the biosphere. Essentially, the roof salt above the underground excavations constitutes an adequate barrier that prevents the development of migration paths for potential contaminants (associated with the underground storage operations) towards the non-salt formations.

6. Practical experience from *in situ* measurements and observations concerning underground openings in salt formations, suggests that the identified order of magnitude of the rates of creep displacements, both along the vertical and horizontal directions, are excessive and they are expected to have a long term negative effect on the serviceability limit state of the underground excavations. An encouraging sign, but not significant enough to ameliorate the identified excessive creep convergence, is the very slightly concave nature of the creep convergence displacement curves. This behaviour indicates that the creep closure is decelerating, providing evidence that the creep response remains within the primary creep stage, implying that the creep closure has not entered the constant strain rate stage. Nevertheless, the identified rates of room creep convergence are very high, indicating that the roof of the rooms (especially those rooms located near the edges of the panel) may be unstable in the long term.

7. Backfilling of the excavated rooms with waste will reduce the convergence rate and prevent long-term convergence, provided that the stored waste is placed in a suitable manner. The tighter the backfill of the waste (to the mine roof), the lower the convergence rate and the faster is the rate of the storage operations, the better will be the control of the anticipated room convergence. This suggests that, when flowable waste

materials are used they could be hydraulically backfilled in such a way as to minimise unfilled spaces at the roof level and improve significantly the support provided by the stored waste. For packaged backfilled waste material the anticipated reduction of the rate of closure of the excavated rooms is expected to range between 20% and 25%. For the case of well compacted hydraulically backfilled waste materials, the rate of closure of the excavated rooms is expected to improve reaching an anticipated reduction ranging between 35% and 40%.

8. The benefit of the active support, provided by the proposed post-tensioned resin grouted rockbolts, and also by the passive support, exerted both by the packaged and the hydraulically backfilled waste materials, is important since it is expected that these measures will bring under control the development of the identified tensile regime in the roof of the rooms and the shear stresses near the walls of the pillars. Moreover, taking into consideration that all of the main access roads will be stowed with salt when they are no longer required for use, the anticipated reduction in the creep convergence will further increase accordingly.

9. In summary, on the basis of the assumed properties of the geological materials and the anticipated geostatic loading conditions, the roof of the excavated rooms is expected to converge at relatively high rate but will remain intact and provide an appropriate geological barrier. Moreover, the preliminary assessment of the geomechanical conditions of the planned Chandler mine indicates that, although the 15 m wide rib pillars are expected to accept the high stress concentrations while maintaining their long term stability, the 15 m width of the roof span of the rooms is considered to be too large and will potentially result in unacceptable creep convergence of the rooms. It is suggested therefore, to narrow down to 12 m at least two adjacent rooms located near each edge of the panels. Concerning the identified high stress concentration in the walls of the pillars, the expected stress relaxation associated with the creep deformation of the Chandler Halite is expected to contribute in the prevention of the development of potentially unacceptable sidewall spalling.

10. It is important to take into consideration that the derived preliminary conclusions are based on the use of assumed material parameters for the Chandler Halite which clearly have an effect both on the creep convergence of the rooms and the shear strength of the pillars. Although the assumed material parameters are based on well-established practical experience derived from designing and monitoring underground openings in salt formations, once laboratory test results from the Chandler Halite will be made available, there will be a need to re-evaluate the investigated geomechanical conditions.

11. The following practical limitations of the resources used, must be noted:
    - the assumed mechanical and physical parameters of the modelled geological materials;
    - the assumed simultaneous excavation of all the rooms in the modelled panel;
    - the assumptions made in determining the geostatic components; and
    - the introduced idealised configuration whereby a three-dimensional structure has been analysed by a two-dimensional model.

7.2. Recommendations

1. Taking into consideration that the 15 m width of the roof span of the rooms is considered to be too large, it is recommended to undertake a series of parametric studies to determine the maximum permissible roof span that will provide the requisite long term stability while satisfying the requirements of the serviceability limit state.

2. The barrier pillars that form the boundaries of the panels, should be able to withstand all anticipated loading conditions encountered during panel development and also should provide adequate isolation to minimise the structural interaction of adjacent panels. The configuration of the planned barrier pillars, concerning their proposed width, is considered to be insufficient especially since there are plans to reduce their cross-sectional area by driving ventilation tunnels through them. It is recommended to optimise the required width by investigating (using a numerical model that would comprise at least two panels) the geomechanical conditions of the central barrier pillar (i.e. the one which is in line with the bottom of the shaft) and of the ordinary barrier pillars.

3. Assessment of the stress distribution around the excavated rooms indicates high stress concentrations limited around the corners of the rooms. The adopted geomechanical model employed rectangular

openings and the stress distribution plots are based on square corners. To minimise the effect of the square corners it is recommended to consider using a continuous miner equipped with a rotating drum cutting head system comprising specially designed cutter pick configuration that will allow the rooms to be excavated with rounded angles at the corners of the cut.

4. To bring under control the development of the identified tensile stresses in the roof of the rooms, and the high shear stresses near the walls of the pillars, it is recommended to provide appropriate rock reinforcement by means of post-tensioned, resin grouted rockbolts. It is suggested, as an indicative measure, that the density of the rockbolts used in the roof should be approximately 1 rockbolt/4 m^2 while the configuration of the rockbolts used in the side of the pillars should be approximately equal to 1 rockbolt/10 m^2.

5. The identified stress gradients above the mine should be used as guide to decide the particular depths from which we should select core samples to be used for rock testing.

6. Similarly, in planning the future rock mechanics laboratory test programme, the confining pressures that should be used in the triaxial compression tests and the deviatoric stresses that should be used in the required triaxial creep tests, must be determined by considering the identified stress concentrations.

7. Any future geomechanical numerical modelling should incorporate a series or parametric analyses to investigate the influence of the sequence of the excavation operations on the long term stability of the room and pillar layout.

8. References

Arnold, W., Forster, S. & Menzel, W. 1975. In situ investigations of fracturing in salt cavities for determining stress components. *9th World Petroleum Congress, 11-16 May, Tokyo, Japan. PD 21(3)*: 89-96.

Bieniawski, Z.T. 1968. The effect of specimen size on the compressive strength of coal. *Intnl. J. Rock Mechanics & Min. Sci*. 5: 325-335.

British Standard Institution 2015. Code of practice for grouted anchors, *BS 8081:2015, August 2015,* BSI Standards Limited.

British Standard Institution 2009. Hot dip galvanized coatings on fabricated iron and steel articles - Specifications and test methods, *BS EN ISO 1461:2009, May 2009,* BSI Standards Limited.

British Standard Institution 2014. Eurocode 7: Geotechnical design - Part 1: General rules, *BS EN 1997-1:2004+A1:2013, July 2014,* BSI Standards Limited.

Brown, E.T. & Hoek, E. 1978. Trends in relationships between measured rock in-situ stresses at depth. *Int. J. Rock Mech. Min. Sci.* 15: 211-215.

Douglas Partners. 2016. Report on geotechnical assessment, Chandler salt mine, Maryvale Hills. Prepared for Tellus Holdings Ltd. Project 73204.02, February 2016.

Drucker, D.C. & Prager, W. 1952. Soil mechanics and plastic analysis on limit design. *Quarterly Appl. Math.* 10(2): 157-165.

Ercosplan Ingenieurgesellschaft Geotechnik und Bergbau mbH. 2014. Core photographs from the exploratory borehole CH001A. Taken from Appendix 1 of the report to Tellus Holdings Ltd.

European Commission 2010. Requirements for facilities and acceptance criteria for the disposal of metallic mercury, *Final report no. 07.0307/2009/530302, 16 April 2010,* Brussels: Beratungsgesellschaft für integrierte Problemlösungen.

Frayne, M.A. & Van Sambeek, L.L. 1999. Three-dimensional verification of salt pillar design equation. In N.D. Cristescu, H.R. Hardy, R.O. Simionescu (eds), *5th Conference on the Mechanical Behaviour of Salt, Bucharest, Romania, August 9-11*: 405-410.

Greewald, H.P., Howarth, H.W. & Hartman, I. 1939. Experiments on the strength of small pillars of coal in the Attsburg bed, *U.S. Bureau of Mines Tech. Rep. 605*.

Herrmann, W., Wawersik, W.R. & Lauson, H.S. 1980a. Analysis of steady state creep of Southeastern New Mexico bedded salt. *Sandia National Laboratories, report no. SAND80-0558*.

Herrmann, W., Wawersik, W.R. & Lauson, H.S. 1980b. Creep curves and fitting parameters for Southeastern New Mexico rock salt. *Sandia National Laboratories, report no. SAND80-0087*.

Hoek, E. 1983. Strength of jointed rock masses. 23rd. Rankine Lecture. *Géotechnique* 33(3): 187-223.

Hoek, E., & Brown, E.T. 1980a. Underground excavations in rock. *London: Instn. Min. Metall*.

Hoek, E., & Brown, E.T. 1980b. Empirical strength criterion for rock masses. *J. Geotech. Engng Div., ASCE* 106(GT9): 1013-1035.

Hoek, E., & Brown, E.T. 1988. The Hoek-Brown failure criterion - a 1988 update. In J.C. Curran (ed.) *Rock engineering for underground excavations, proc. 15th Canadian rock mech. symp., Toronto: Dept. Civ. Engineering, University of Toronto*: 31-38.

Hoek, E., & Brown, E.T. 1998. Practical estimates of rock mass strength. *Int. J. Rock Mech. Min. Sci.* 34(8): 1165-1186.

Hoek, E., Carranza-Torres, C. & Corkum, B. 2002. Hoek-Brown failure criterion - 2002 Edition, In R. Hammah, W. Bawden, J. Curran and M. Telesnicki, (*eds*.) *Proceedings of NARMS-TAC 2002, 5th North American Rock Mechanics Symposium and 17th Tunnelling Association of Canada Conference - Toronto, Canada - July 7 to 10 2002.* (1): 267-271. Toronto: University of Toronto Press.

Hoek, E., Carter, T.G. & Diederichs, M.S. 2013. Quantification of the Geological Strength Index Chart. *Proceedings of 47th US Rock Mechanics /Geomechanics Symposium, San Francisco, CA, USA, June 23-26*.

Holland, C.T. & Gaddy, F.L. 1957. Some aspects of permanent support of overburden on coal beds. *Proc. W. Virginia Coal Mining Institute*: 43-66.

Hunsche, U. 1981. Results and interpretation of creep experiments on rock salt. In H. R. Hardy, Jr. & M. Langer (eds). *First conference on the mechanical behaviour of salt. The Pennsylvania State University, November 9-11*: 159-167. Clausthal-Zellerfeld:Trans Tech Publications.

Kaiser P.K., Loew S. & Martin, C.D. 2002. Brittle rock failure and tunnelling in highly stressed rock. Special short course organised by the Chair of Engineering Geology, ETH Zurich. Switzerland: Swiss Federal Institute of Technology Zurich.

McCreath, D.R. & Diederichs M.S. 1994. Assessment of near-field rock mass fracturing around a potential nuclear fuel waste repository in the Canadian Shield. *Int. J. Rock Mech. Min. Sci. & Geomech. Abstr.* 31(5): 457-470.

Munson, D.E. 1997. Constitutive model of creep in rock salt applied to underground room closure. *Int. J. Rock Mech. Min. Sci.* 34(2): 233-247.

Obert, L. & Duvall, W.I. 1967. Rock mechanics and the design of structures in rock. New York: John Wiley & Sons, Inc.

Passaris, E.K.S. 1982. Rock engineering studies with reference to the in-situ strength of bauxite pillars. In I.W. Farmer (ed.) *Strata Mechanics, Proceedings of the Symposium on Strata Mechanics, Newcastle upon Tyne, 5-7 April, 1982*:274-282. Amsterdam: Elsevier.

Passaris, E.K.S. & Horseman, S.T. 1982. Creep closure of caverns in rock salt. In I.W. Farmer (ed.) *Strata Mechanics, Proceedings of the Symposium on Strata Mechanics, Newcastle upon Tyne, 5-7 April, 1982*:178-183. Amsterdam: Elsevier.

Rizkalla, M.K. & Mitri H.S. 1969. Time dependent modelling of fill and cable bolts in soft rock mines, Rock mechanics tools and techniques, In M. Auberti, F. Hassani & H. Mitri (eds), *Proc. NARMS'96 , 2nd North American Rock Mechanics Symposium, ISRM Regional Conference, Canada 19-21 June 1996*: 139-146, Rotterdam: Balkema.

Rocscience Inc. 2004a. RocLab: Rock mass strength analysis using the Hoek-Brown failure criterion, User's Guide, Version 1.010.

Rocscience Inc. 2004b. RocSupport: Rock support interaction and deformation analysis for tunnels in weak rock, User's Guide, Version 3.002.

Salamon, M.D.G. & Munro, A.H. 1967. A study of the strength of coal pillars. *J. South African Inst. of Mining & Metallurgy*. 68(2):55-67.

Steart, F.A. 1954. Strength and stability of pillars in coal mines, *J. Chem. Metall. Min. Soc. South Africa*. 54: 309-325.

Terra Search. 2011. Review of prospectivity of evaporite units, 3D modelling of Chandler formation, Overall resource potential of EL27972 (Charlotte), South East Amadeus basin, NT, a report to Tellus Holdings Ltd, September 2011.

Van Sambeek, L.L. 1996. Salt pillar design equation. In M. Aubertin and H. R. Hardy Jr. (eds.), *4th Conference on the Mechanical Behaviour of Salt, Ecole Poly technique de Montreal, Mineral Engineering Department, Quebec, Canada, June 17-18*: 495-508, Penn State University, Trans Tech Publications, Clausthal, Germany.

Wakelin-King, G. J., Westman, W.J. & Austin, L.A. 1992. Well proposal, Magee 1 EP38, Amadeus basin, report no. 304654 by Pacific Oil & Gas Pty Limited, September 1992.

Appendices

Appendix A. Results of the finite difference analysis for the conditions corresponding to one year after the excavation of the rooms

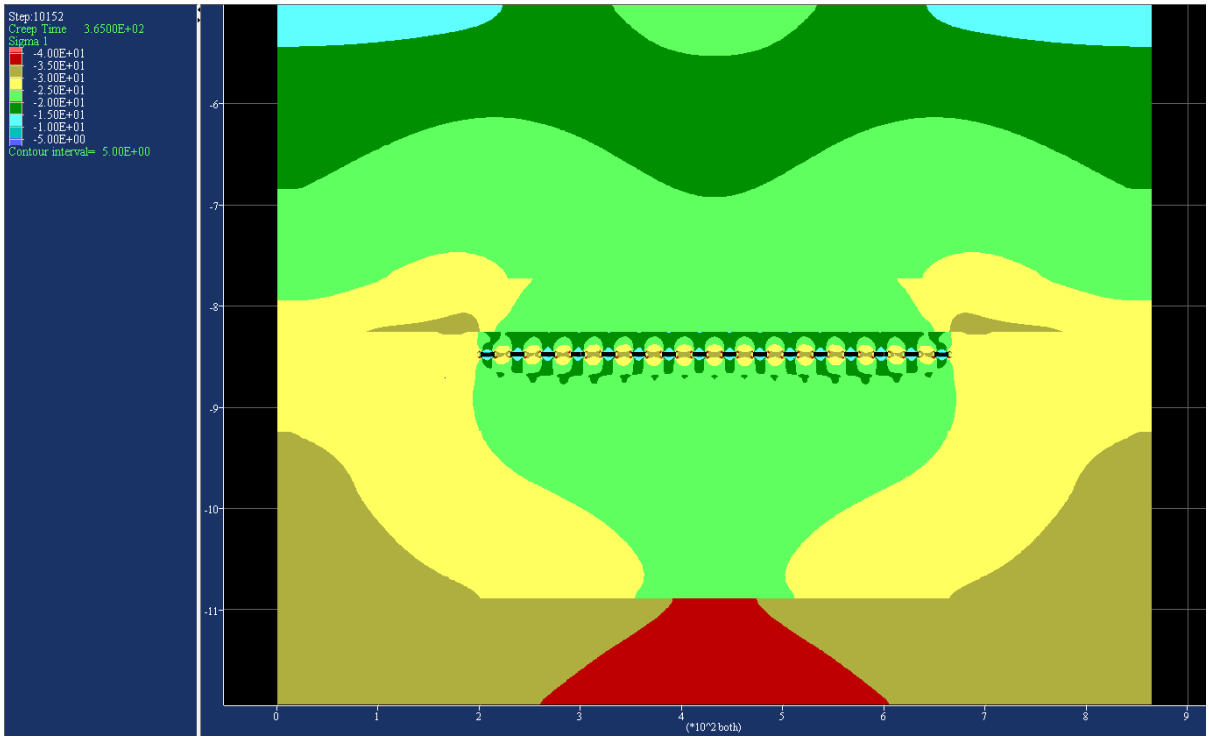

Figure A-1 Distribution of major principal stress component σ_1, at the end of one year

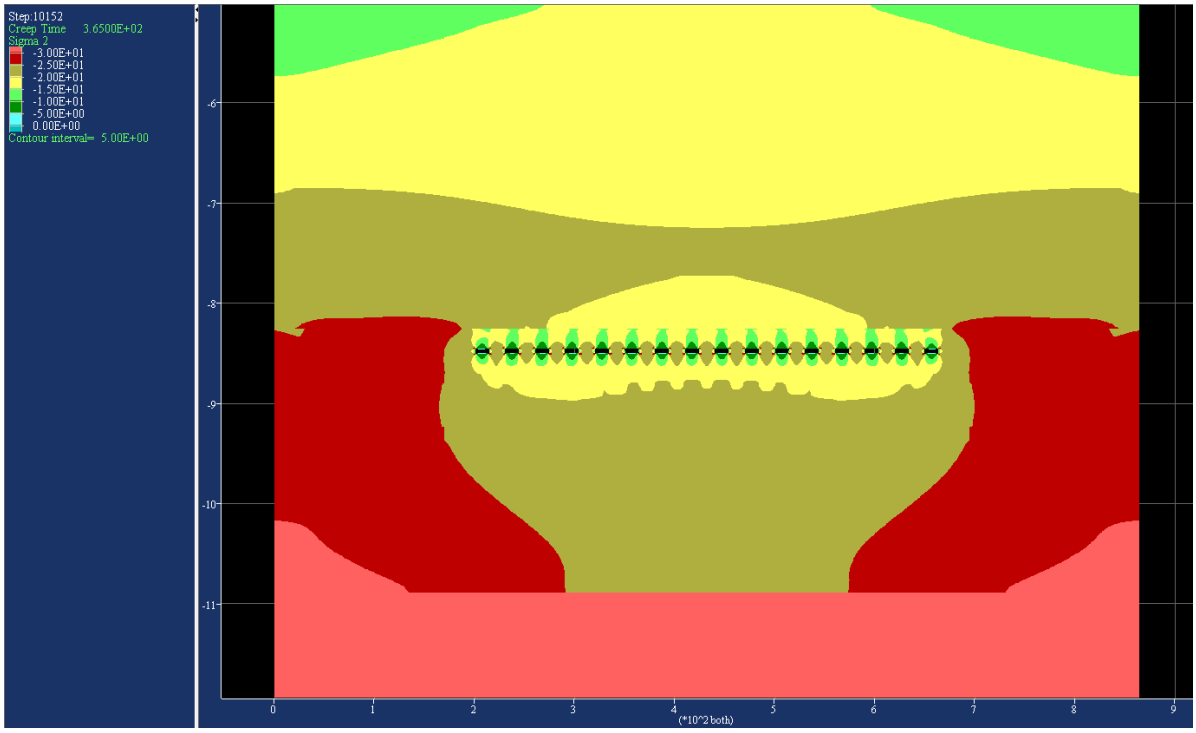

Figure A-2 Distribution of intermediate principal stress component σ_2, at the end of one year

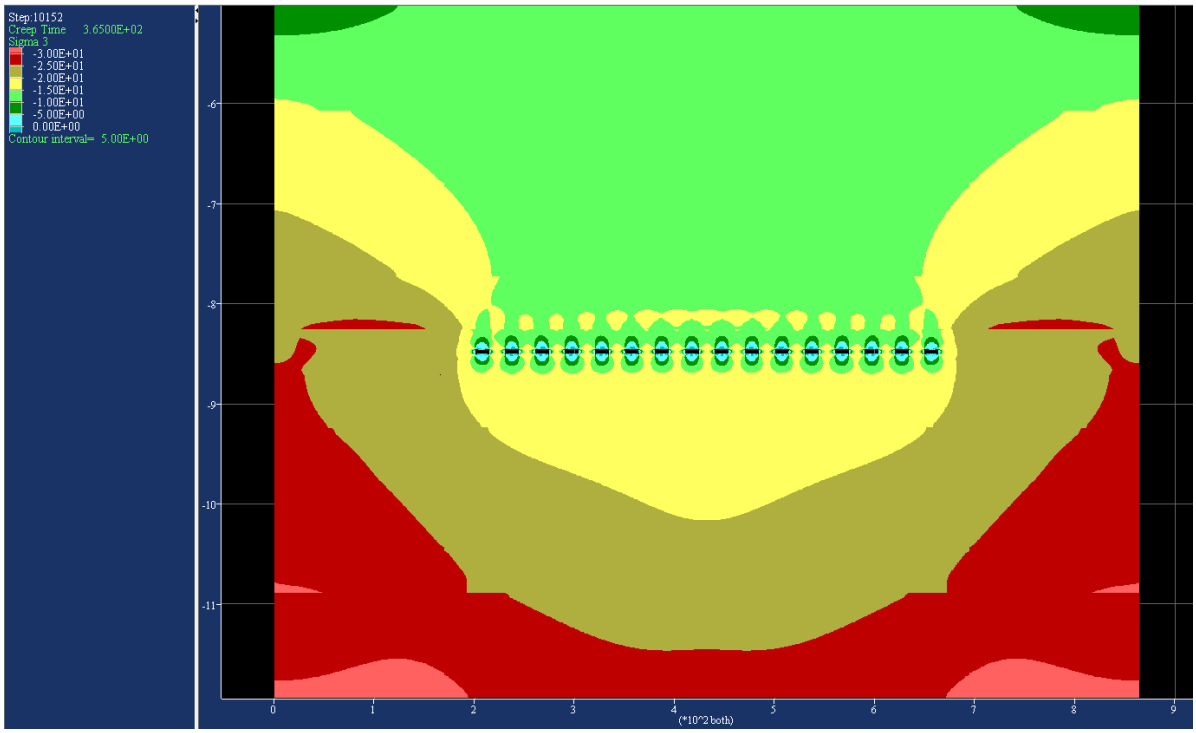

Figure A-3 **Distribution of minor principal stress component σ_3, at the end of one year**

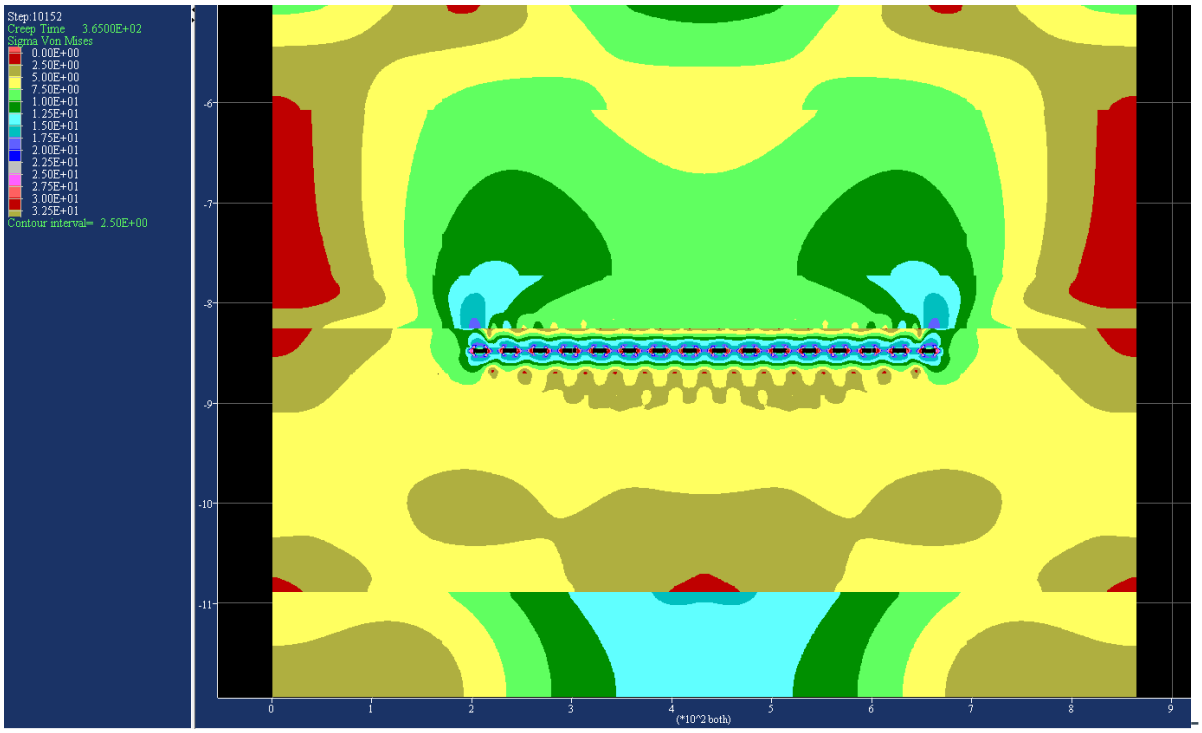

Figure A-4 **Distribution of Von Mises stress component σ_{vm}, at the end of one year**

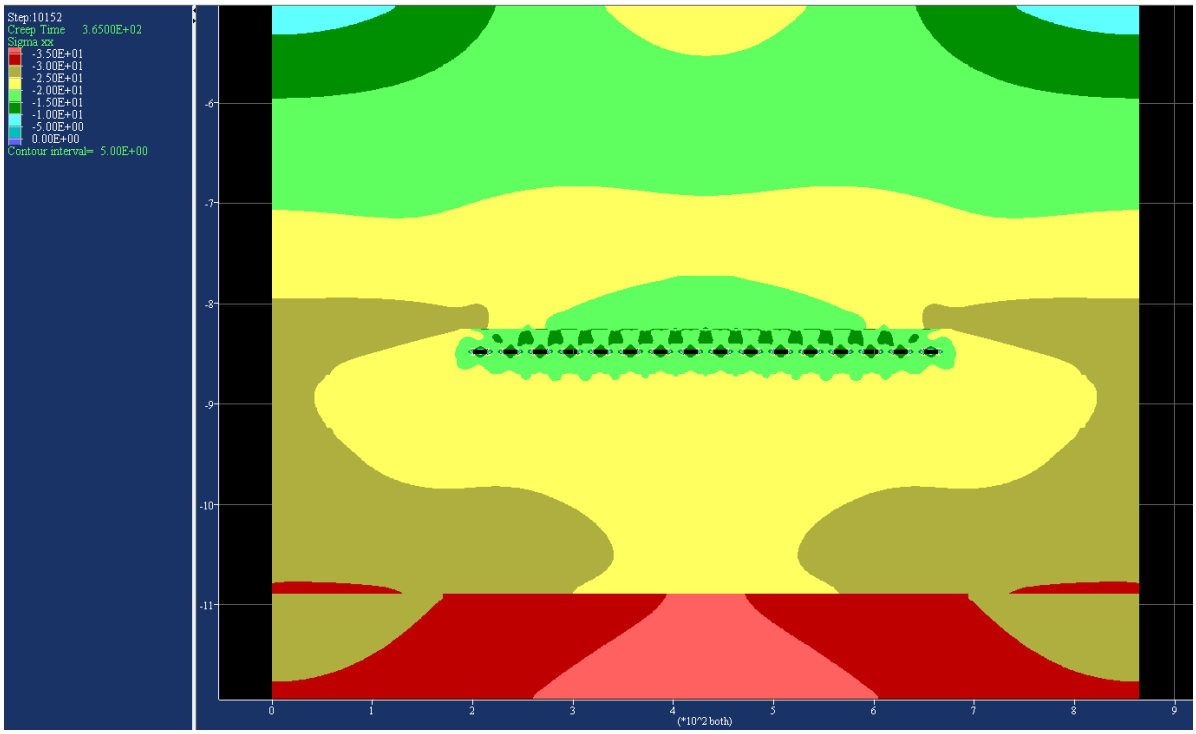

Figure A-5 Distribution of horizontal stress component σ_{xx}, at the end of one year

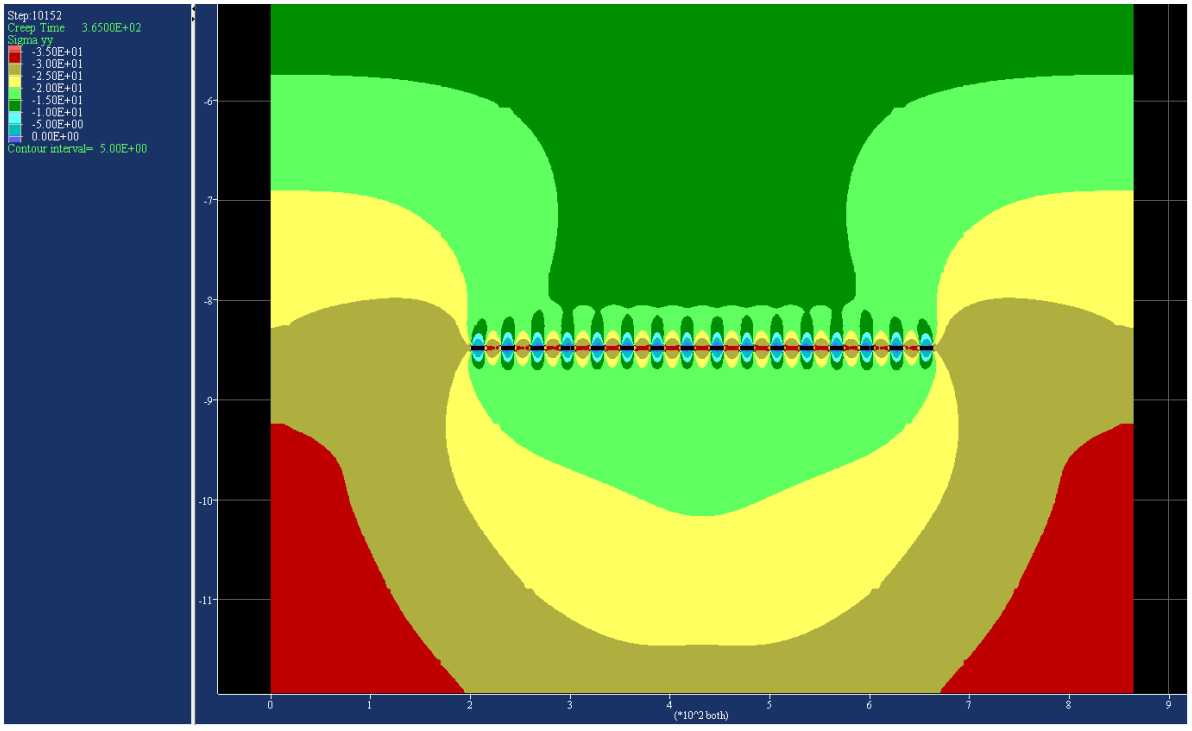

Figure A-6 Distribution of vertical stress component σ_{yy}, at the end of one year

Appendix B. Results of the finite difference analysis for the conditions corresponding to five years after the excavation of the rooms

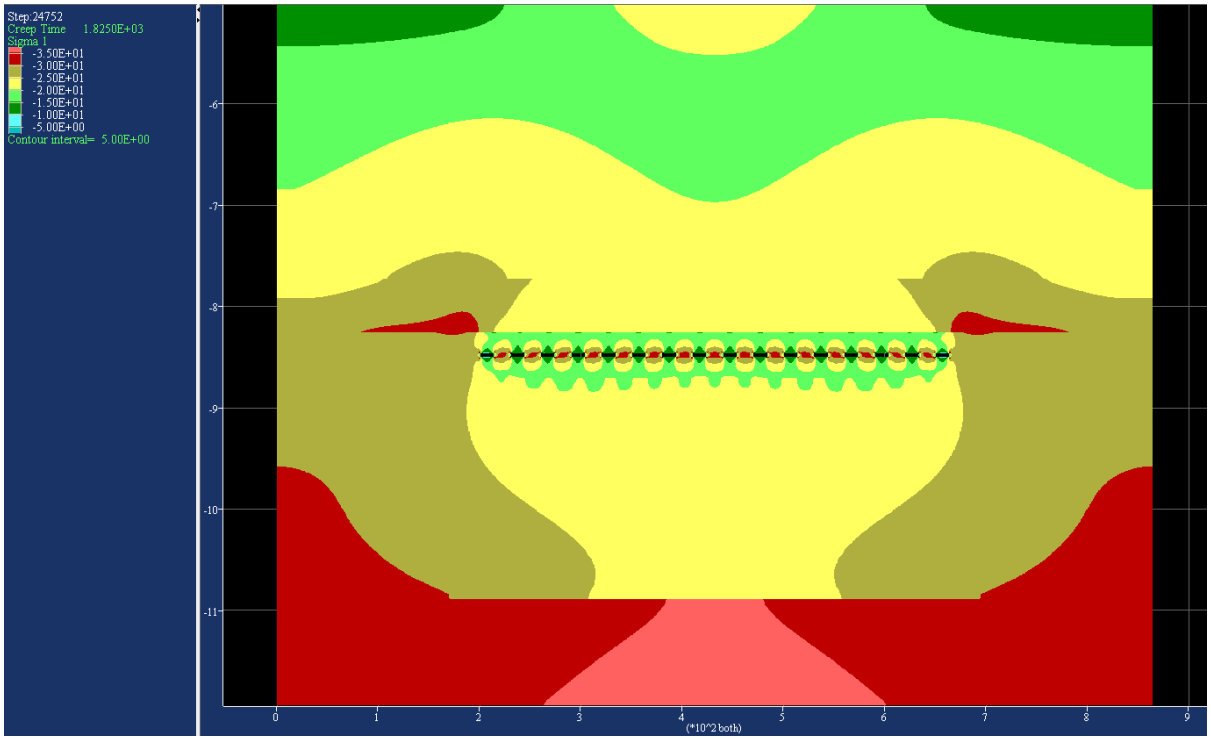

Figure B-1 Distribution of major principal stress component σ_1, at the end of five years

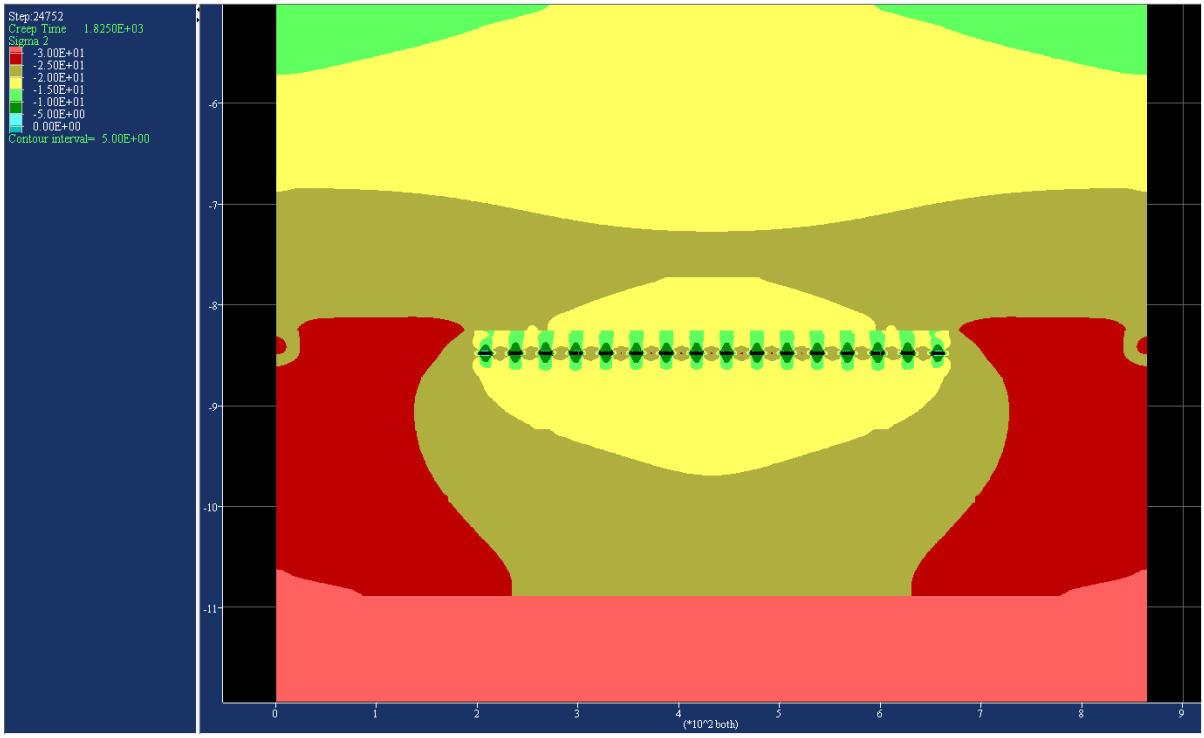

Figure B-2 Distribution of intermediate principal stress component σ_2, at the end of five years

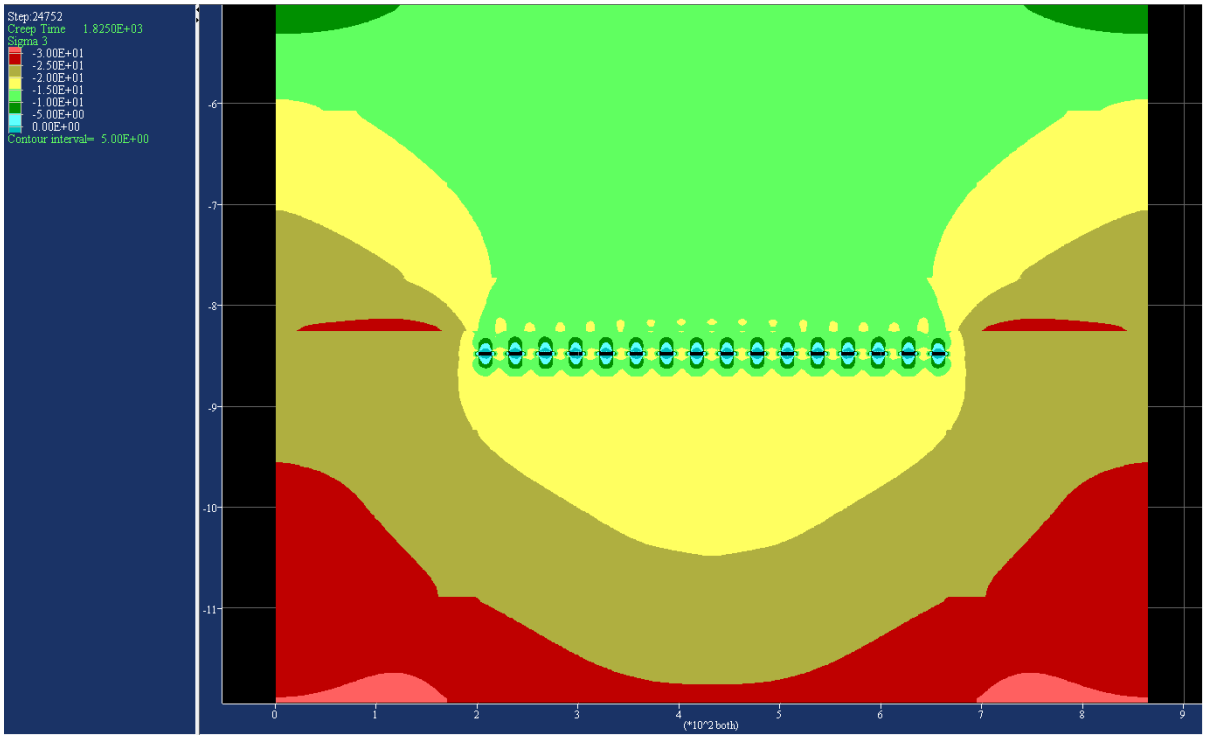

Figure B-3 Distribution of minor principal stress component σ_3, at the end of five years

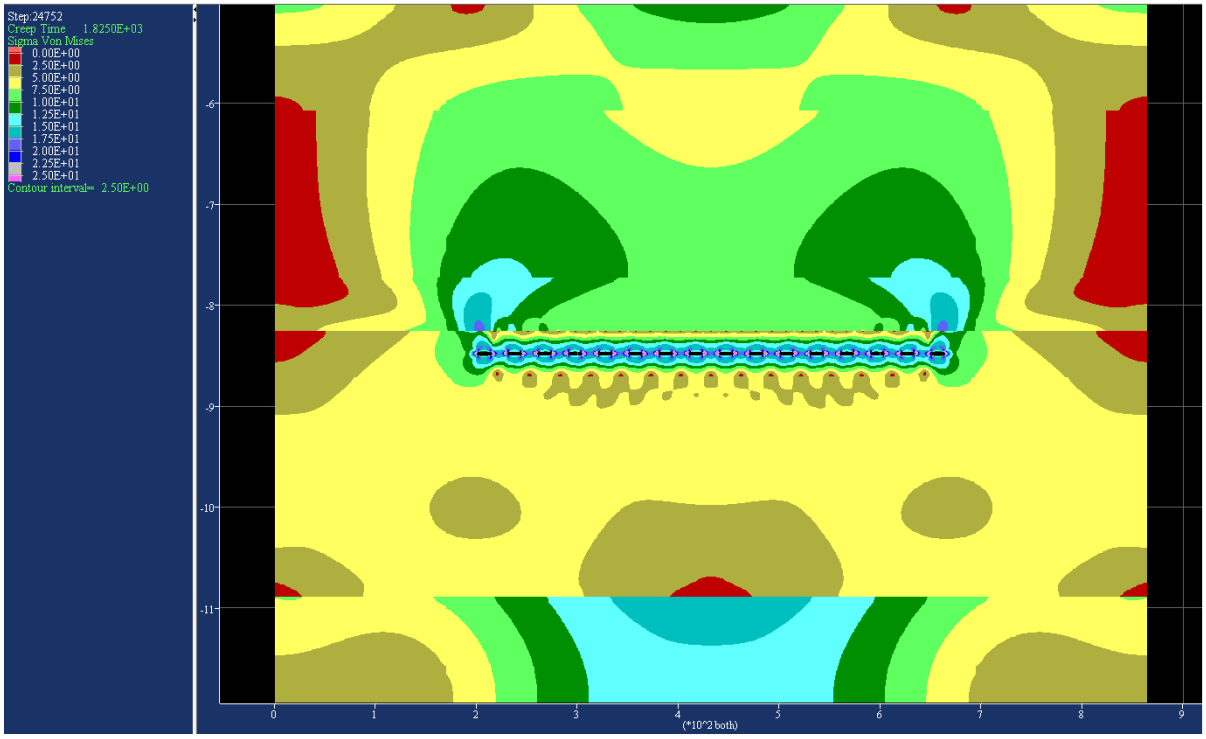

Figure B-4 Distribution of Von Mises stress component σ_{vm}, at the end of five years

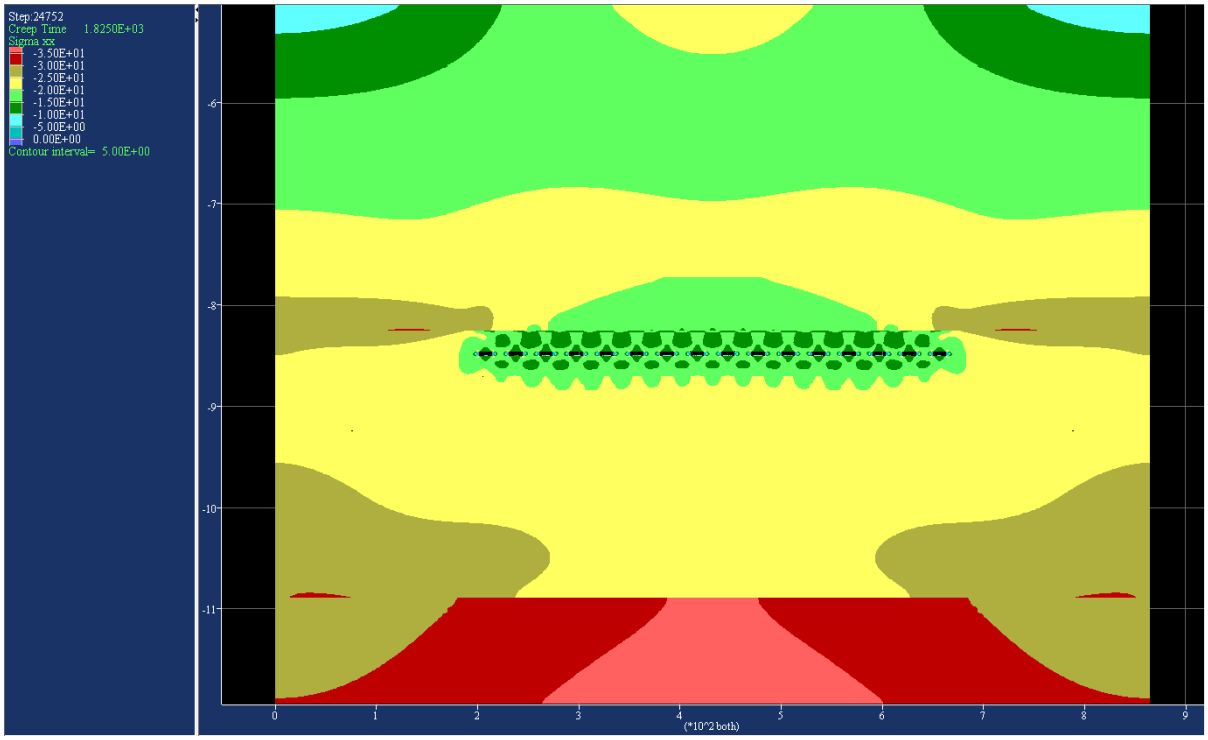

Figure B-5 Distribution of horizontal stress component σ_{xx}, at the end of five years

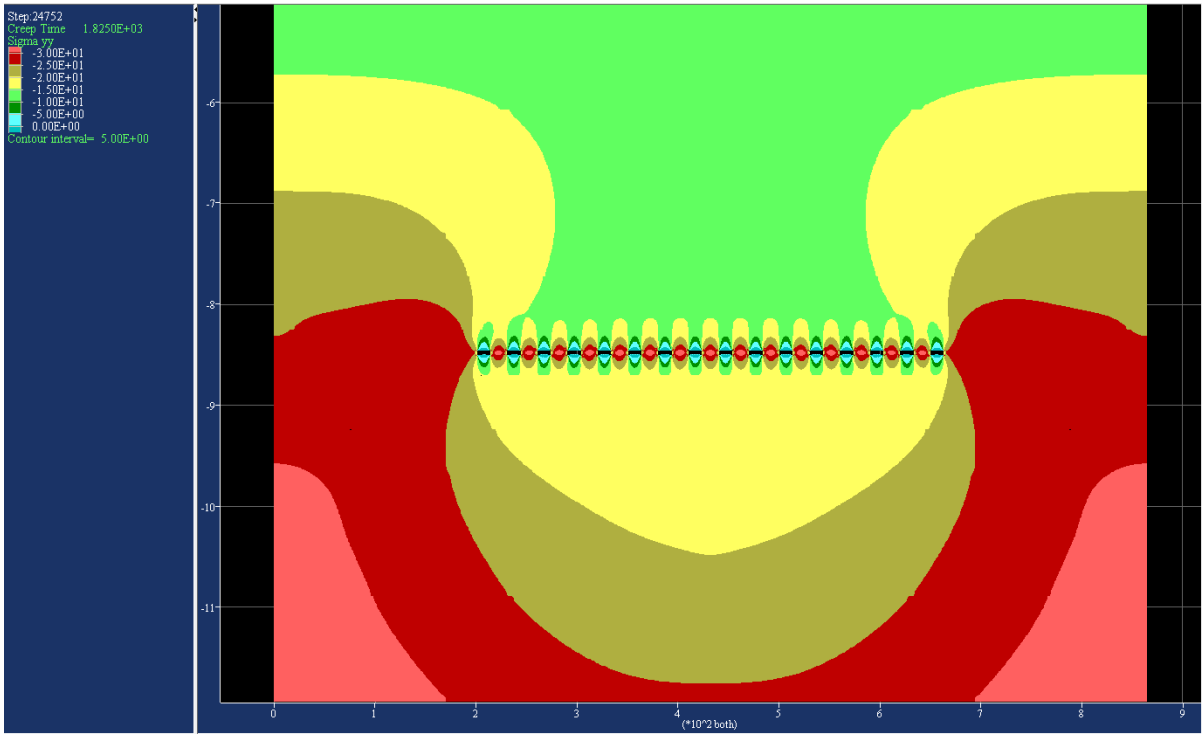

Figure B-6 Distribution of vertical stress component σ_{yy}, at the end of five years

Appendix C. Results of the finite difference analysis for the conditions corresponding to thirty years after the excavation of the rooms

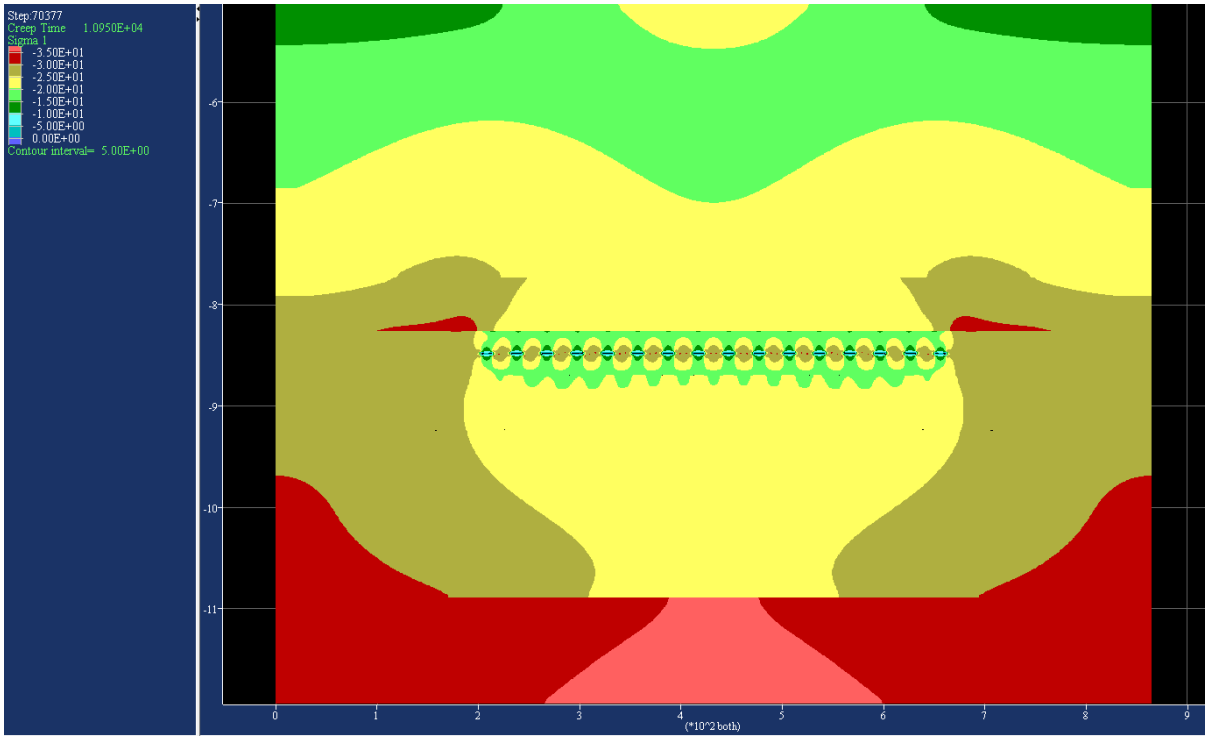

Figure C-1 Distribution of major principal stress component σ_1, at the end of 30 years

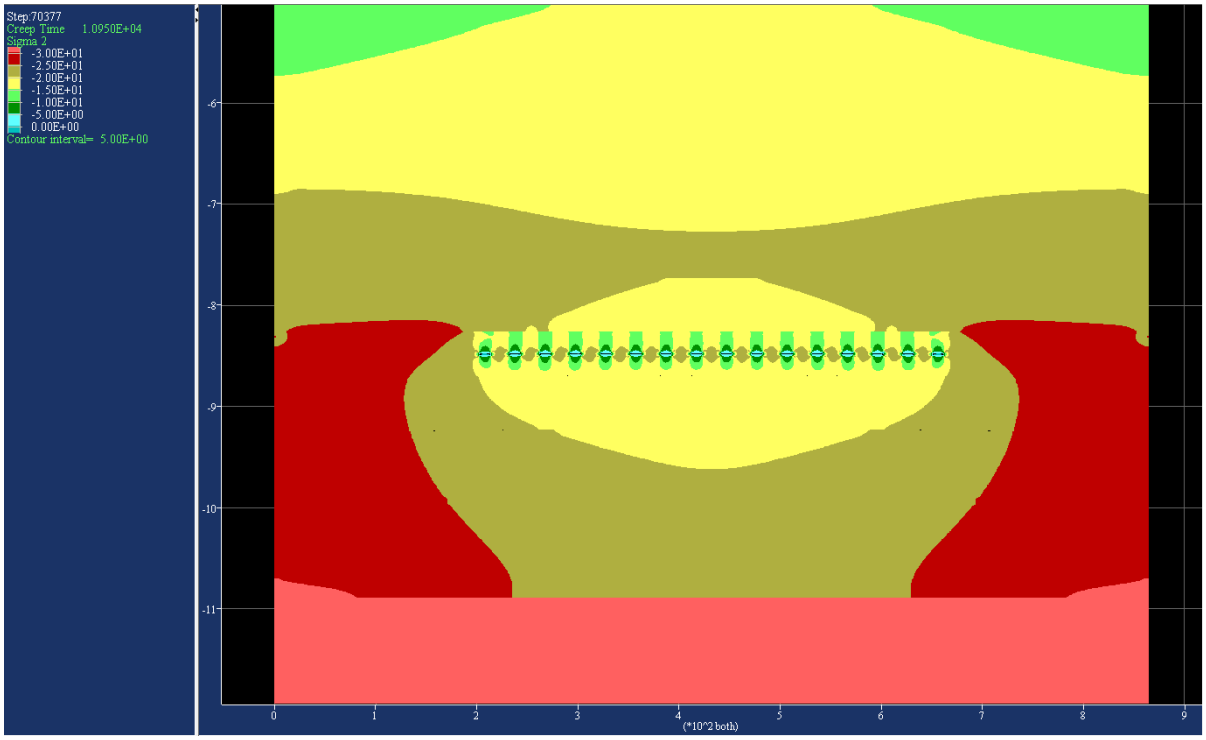

Figure C-2 Distribution of intermediate principal stress component σ_2, at the end of 30 years

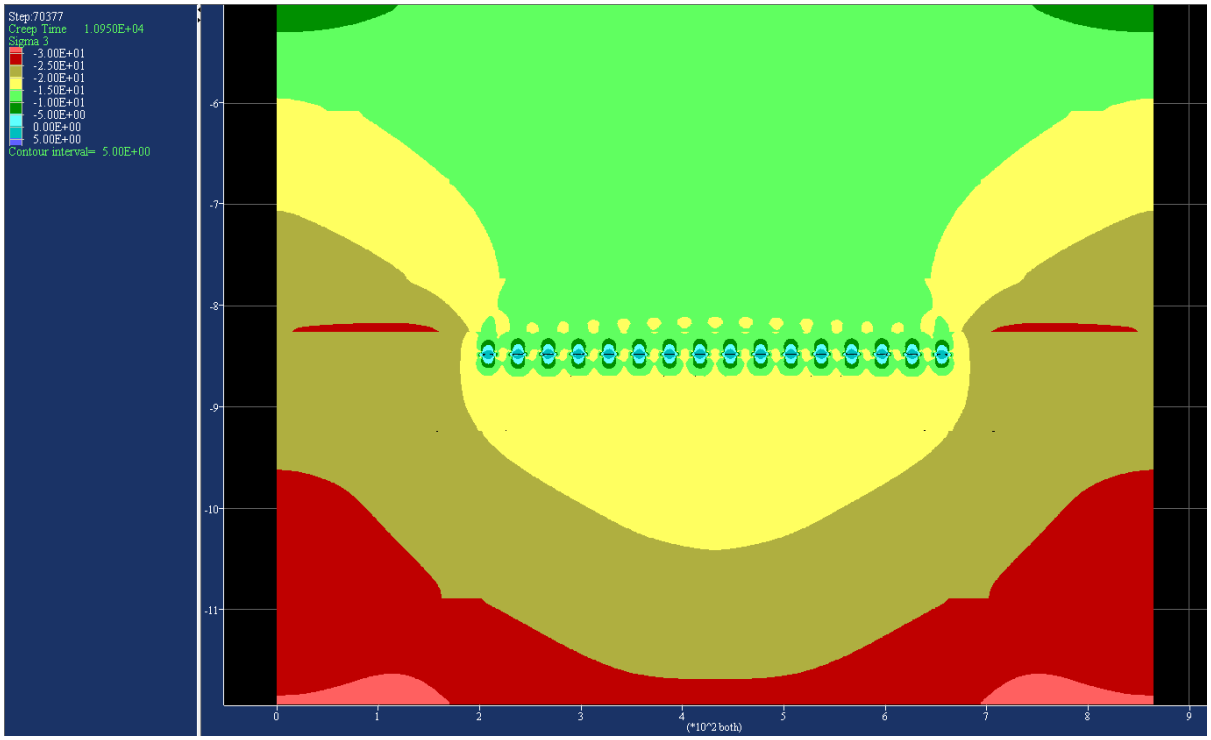

Figure C-3 Distribution of minor principal stress component σ_3, at the end of 30 years

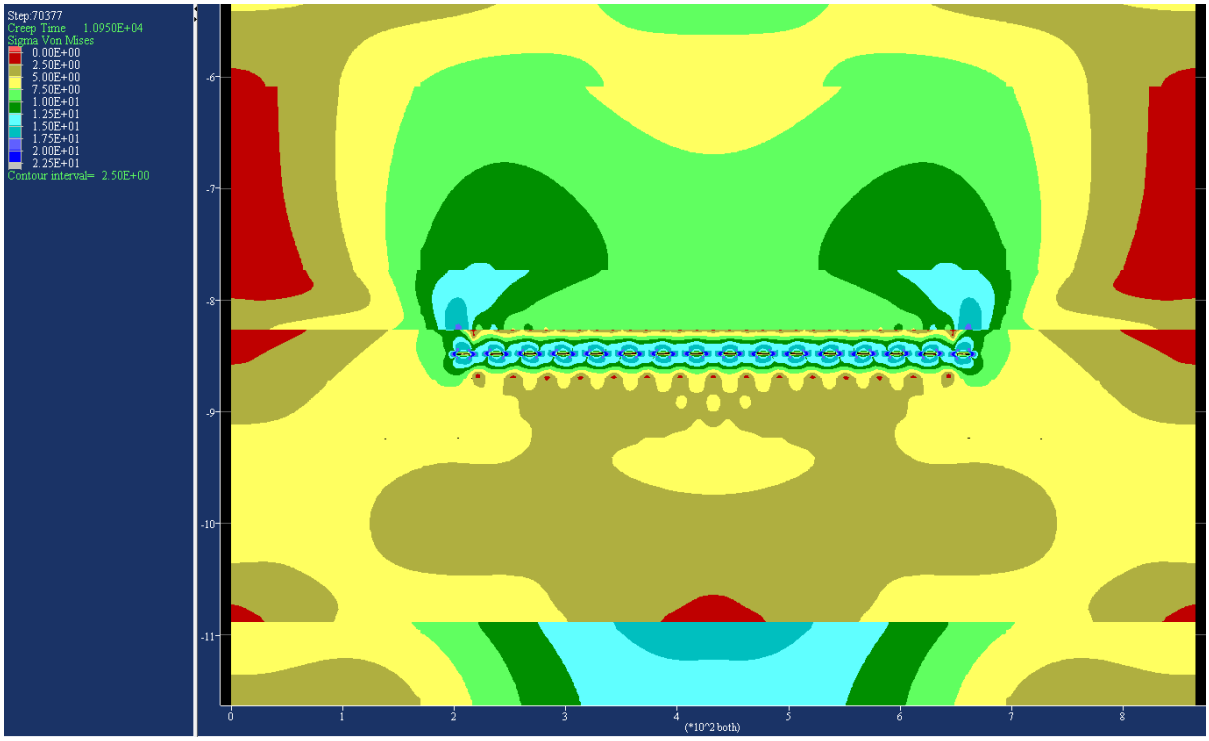

Figure C-4 Distribution of Von Mises stress component σ_{vm}, at the end of 30 years

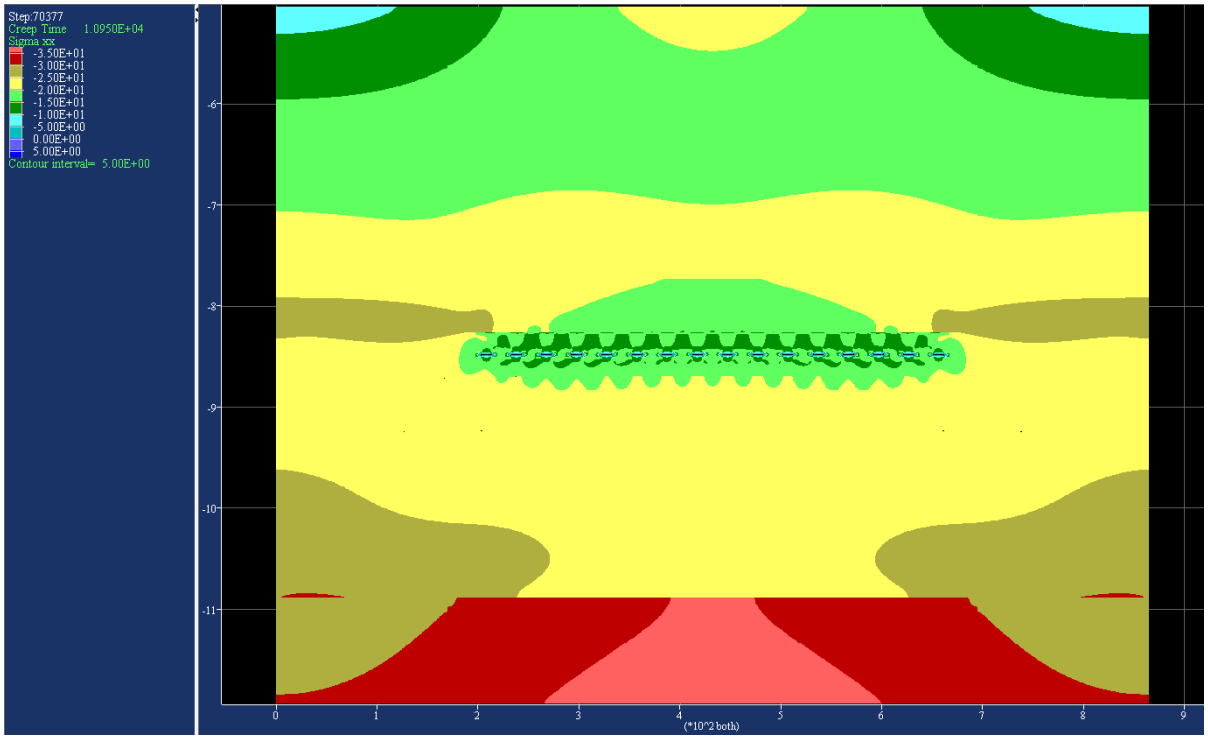

Figure C-5 Distribution of horizontal stress component σ_{yy}, at the end of 30 years

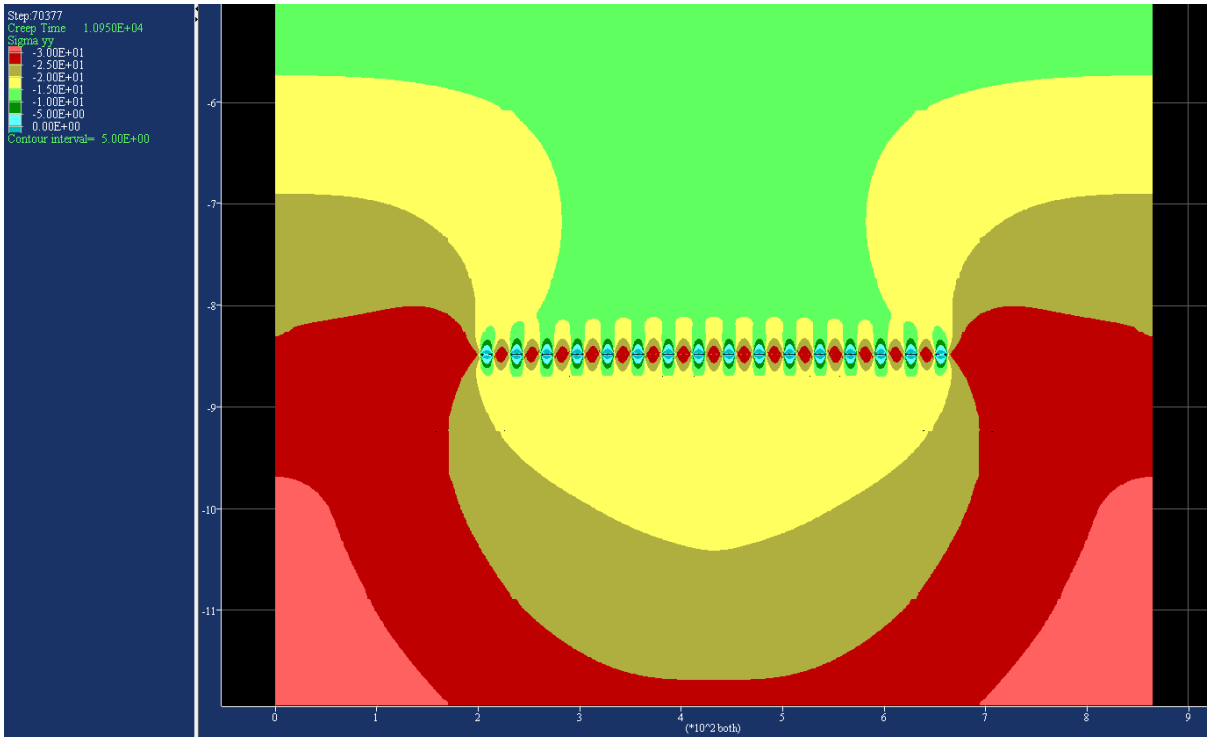

Figure C-6 Distribution of vertical stress component σ_{yy}, at the end of 30 years

Appendix D. Plan of the general arrangement of the Chandler mining site (after Douglas, 2016)

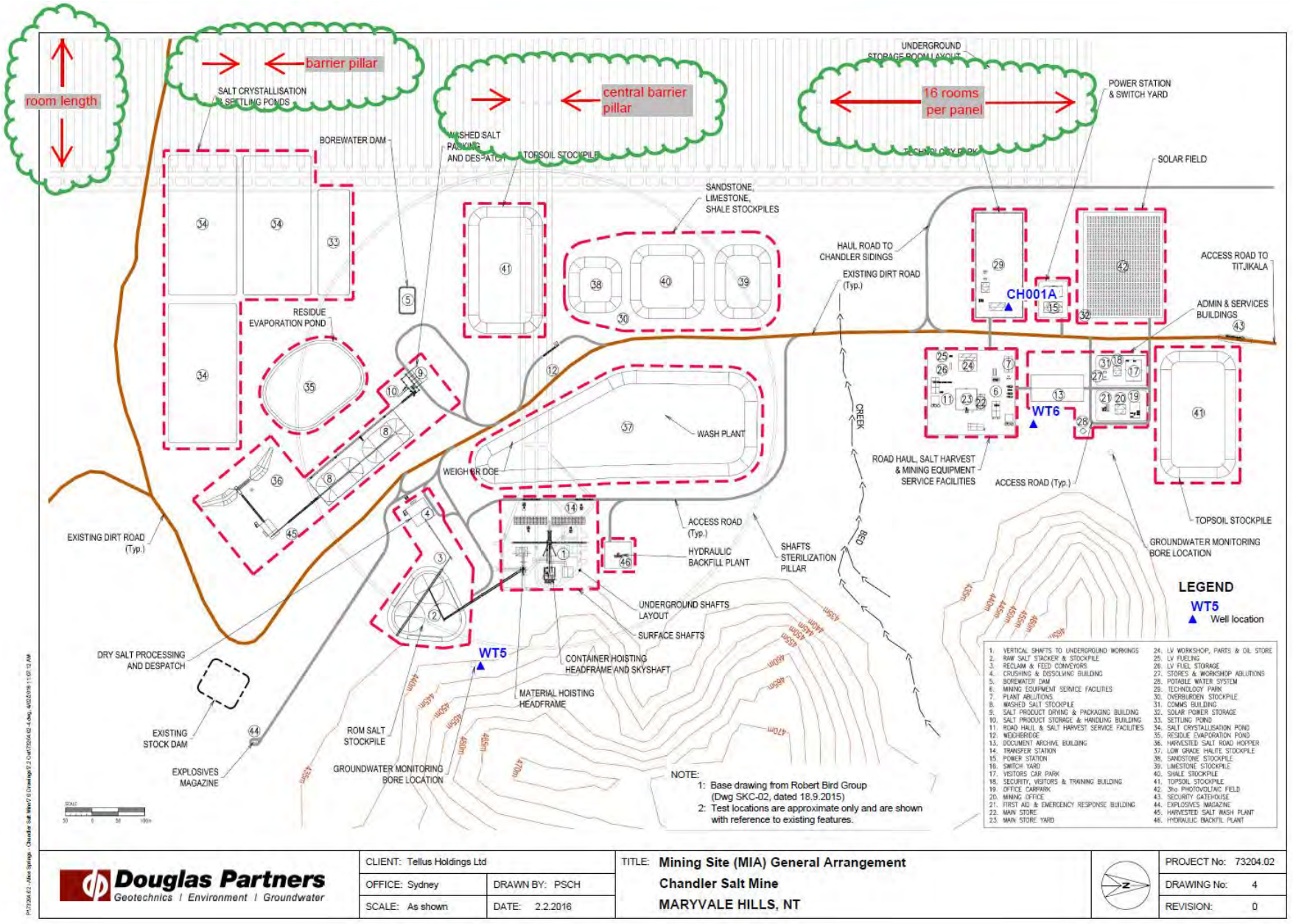
room length
barrier pillar
central barrier pillar
16 rooms per panel
UNDERGROUND STORAGE ROOM LAYOUT
SALT CRYSTALLISATION & SETTLING PONDS
BOREWATER DAM
WASHED SALT PACKING AND DES-PATCH
TOPSOIL STOCKPILE
SANDSTONE, LIMESTONE, SHALE STOCKPILES
POWER STATION & SWITCH YARD
SOLAR FIELD
HAUL ROAD TO CHANDLER SIDINGS
EXISTING DIRT ROAD (Typ.)
ACCESS ROAD TO TITJIKALA
ADMIN & SERVICES BUILDINGS
CH001A
RESIDUE EVAPORATION POND
WASH PLANT
WEIGHBRIDGE
CREEK
WT6
ROAD HAUL, SALT HARVEST & MINING EQUIPMENT SERVICE FACILITIES
ACCESS ROAD (Typ.)
TOPSOIL STOCKPILE
GROUNDWATER MONITORING BORE LOCATION
EXISTING DIRT ROAD (Typ.)
ACCESS ROAD (Typ.)
HYDRAULIC BACKFILL PLANT
SHAFTS STERILIZATION PILLAR
BCO
UNDERGROUND SHAFTS LAYOUT
SURFACE SHAFTS
WT5
CONTAINER HOISTING HEADFRAME AND SKYSHAFT
MATERIAL HOISTING HEADFRAME
DRY SALT PROCESSING AND DESPATCH
EXISTING STOCK DAM
ROM SALT STOCKPILE
EXPLOSIVES MAGAZINE
GROUNDWATER MONITORING BORE LOCATION
LEGEND
WT5
Well location
NOTE:
1: Base drawing from Robert Bird Group (Dwg SKC-02, dated 18.9.2015)
2: Test locations are approximate only and are shown with reference to existing features.
Douglas Partners
Geotechnics | Environment | Groundwater
CLIENT: Tellus Holdings Ltd
OFFICE: Sydney
DRAWN BY: PSCH
SCALE: As shown
DATE: 2.2.2016
TITLE: Mining Site (MIA) General Arrangement
Chandler Salt Mine
MARYVALE HILLS, NT
PROJECT No: 73204.02
DRAWING No: 4
REVISION: 0

Appendix E. Empirical salt pillar design equations

The average vertical stress (σ_p) for a rib pillar, when the conditions are met for tributary loading, is given by Obert & Duvall (1967) as:

$$\sigma_p = \sigma_v \left(\frac{W_p + W_o}{W_p}\right) \quad \textbf{Equation E1}$$

where, for the Chandler mine, W_p is the width of the rib pillars (equal to 15 m), W_o is the width of the rooms (equal to 15 m) and the vertical geostatic stress (σ_v), for the investigated room and pillar layout, may be calculated using Equation 1 as being equal to:

$$\sigma_v = - 0.025 \times 845 = - 21.125 \text{ MPa} \quad \textbf{Equation E2}$$

Consequently, σ_p is equal to -42.25 MPa.

One of the earliest investigations into the design of hard-rock pillars was carried out by Salamon & Munro (1967). They concluded that the pillar strength could be adequately predicted by:

$$\sigma_{ps} = K_p \frac{W_p^a}{H_p^b} \quad \textbf{Equation E3}$$

where σ_{ps} (expressed in MPa) is the pillar strength, K_p is the strength of a unit volume of rock (expressed in MPa for 1 m^3), and W_p and H_p are the pillar width and height in m, respectively. The parameters a and b are empirical constants and a review of available data from coal pillars (Greenwald et al., 1939, Steart, 1954, Holland & Gaddy, 1957, Salamon & Munro, 1967 & Bieniawski, 1968) indicated that the average values for the constants a and b are 0.405 and 0.765 respectively.

Equation E3 with a = 0.5 and b = 0.75 was used by Hedley & Grant (1972) to design pillars in the Elliot Lake uranium mines in Canada until their closure in the late 1990's and similarly, Passaris (1982) used the same equation with a = 0.461 and b = 0.658 for the design of bauxite pillars in the 51KM Parnassus bauxite mine in Greece.

However, empirical pillar formulas, such as Equation E3, which were developed from back-analysis of failed hard-rock pillars in operating mines, are not applicable in salt mines where the time-dependent deformational behaviour of salt makes the task of salt mine pillar design more complex.

For this reason, when dealing with salt pillars, the pillar-design equation that calculates the average stresses in salt rib pillars that was developed by Van Sambeek (1996) provides, in the first instance, a more appropriate methodology:

$$\bar{\sigma}_{vmp} = -\frac{\sqrt{3}}{2}\left[1 - exp\left(-2.94\ \frac{H_p}{W_p}\right)\right] \times \sigma_v \quad \textbf{Equation E4}$$

Where, $\bar{\sigma}_{vmp}$ is the average Von Mises (or effective) stress acting on the salt pillar.

The derivation of Equation E4 was based on a series of plane-strain numerical modelling analyses and although it adequately reproduced the results of extensive modelling efforts, the comprehensive evaluation of the pillar equation was limited by the two-dimensional nature of the analyses.

The limitations of Equation E4 were addressed by Frayne & Van Sambeek (1999) by conducting a series of three-dimensional numerical modelling analyses to examine the behaviour of salt pillars. The results of their three-dimensional modelling confirmed the applicability of the following pillar-design equation:

$$\bar{\sigma}_{vmp} = -\left[1 - 0.9\ exp\left[-1.862\left(\frac{H_p}{W_p}\right)\right] \times exp\left[-1.5\left(\frac{H_p}{L_p}\right)\right]\right] \times \sigma_v \quad \textbf{Equation E5}$$

Where L_p is the length of the pillar.

By substituting in Equation E5 the dimensions of the Chandler mine rib pillars, i.e. W_p = 15 m, W_o = 15 m and L_p = 240 m, we get:

$$\bar{\sigma}_{vmp} = 12.43 \text{ MPa}$$

which, when combined with Equations 10 and 13, results in a *Strength Factor* equal with:

$$Strength\ Factor = \frac{\sqrt{3}\left(k_\varphi + q_\varphi \frac{I_1}{3}\right)}{\bar{\sigma}_{vmp}} = 2.35$$

Marco Clemente
Atkins
200 Broomielaw
Glasgow
G1 4RU

marco.clemente@atkinsglobal.com